FIELD IONIZATION AND ION CURRENT GENERATION IN THE FIELD ION MICROSCOPE

Hiroshi Iwasaki

DEPARTMENT OF ELECTRONIC ENGINEERING,
FACULTY OF ENGINEERING,
OSAKA UNIVERSITY,
SUITA, OSAKA
JAPAN

March 1975

Abstract

The image formation in the field ion microscope was studied theoretically by calculating both the ionization probability and the current-voltage characteristics. The model was extended to include the field adsorption effects on the imaging process.

In Chap.1, a general introduction was given to the experimental results and the existing theory of field ionization and ion current generation, giving particular attention to points which were revised and extended in the present investigation. The aim of the present work was made clear.

In Chap.2, field ionization probability of a gas atom above a clean metal surface was calculated. The comparison and criticism of various methods of calculation were given. The effect of the orbitals of metal atoms on field ionization was investigated approximating the metallic state by the tight-binding method, and formation of the point image contrast was discussed. The energy distribution of the field ionized atoms was also obtained. The result was in agreement with the experimental observations.

In Chap.3, field ionization probability above a metal surface with various adsorbed atoms was calculated. A one-dimensional model calculation of the electronic transmission coefficient of the field ionizing system was carried out; this predicts that the ionization probability would be enhanced and suppressed by the adsorption of the atoms with small ionization potential, and by the field adsorption of the inert gas atoms respectively. The latter effect was verified in case of the three-dimensional calculation, which disagrees with the previous investigator's prediction of the extremely high

enhancement of the field ionization by field adsorption.

In Chap.4, the dynamic approach to calculation of the field-ion current was discussed. The velocity distribution functions of the gas particles, attracted to the spherical emitter, were derived. The dependence of the ion current on the emitter temperature and the gas temperature was discussed.

In Chap.5, the field-ion current, based on the balance equation for the velocity distribution function of the concentrated gas particles in the emitter region, was calculated. The expression for the ion current in terms of equilibrium quantities, such as the supply function and rate constants for ionization and escape, was derived and used to discuss the calculated results. The field adsorption effect on the ion current was then investigated, based on the adsorption effects on both the electronic transition probability obtained in Chap.3 and the gas-surface interaction.

In Chap.6, the conclusions of the present investigation were given.

CONTENTS

CHAPTER 1

INTRODUCTION

1.1 General

The field ion microscope (FIM) invented by Müller[1] is one of the powerful devices for the surface science capable of imaging the metal surfaces in atomic detail. The detailed interpretation of the image is now becoming increasingly important as experimental techniques continue to develop and to be applied to wider fields[2,3]. The recent discovery of field-adsorption of an inert gas[4,5] necessitates a refinement of the theory of the field ionization process.

The present study is an attempt to improve the understanding of the imaging process and image interpretation by both quantum mechanical calculations of the field ionization probability and theoretical considerations of the ion current generation.

The detailed investigation of the ion current generation will provide fine demonstrations of the theory of the field ionization by intermediating between the theory of the microscopic process and the experimentally observable behaviour of the ion current.

1.2 Field Ionization

1.2.1 The Hamiltonian of the Field Ionizing System

The process of field ionization may be viewed as a rearrangement-type collision of an atom with a metal surface[6]. As a gas atom approaches the metal surface (shown in fig.1), the electrons and nucleus of the free atom begin to interact with the N electrons of the metal, and the constitutive atomic cores of the metal lattice[7]. For the time being, we consider

field ionization of a monovalent atom (e.g. hydrogen). Also, the independent-electron model[8], in which the interaction potential V_i , is replaced by an external (one-electron) potential, is considered. A specific expression for V_i was given by Cutler and Davis[9], and by Boudreaux and Cutler[10], analytically as

$$V_i = V_e(r, R) - e^2/4Z \ , \tag{1}$$

where

$$V_e(r, R) = -\frac{e^2}{4z}[1 - \exp(-V_0 z/8 \times 10^{-10})] + e^2/|R + r|, \quad z > 0, \ Z > Z_c \ , \tag{2}$$

$$= -V_0 \ , \quad z < 0, \ Z > Z_c \ . \tag{3}$$

Where z and Z are the components of the position r of the atomic electron and the position R of the nucleus respectively, all in A units (see fig.1). The quantity V_0 is the depth of the potential well in the Sommerfeld-Hartree model of the metal in eV. The plane z = 0 is the metal surface and Z_c is the cut-off distance for field ionization discussed later. In eq.(2), the first term is the image potential of the electron which includes exchange and correlation effects[9] and the second term is the interaction of the electron with the image of the nucleus.

The total Hamiltonian of an atom near the metal surface under the electric field F is

$$H_t = -\frac{\hbar^2}{2m}\nabla_r^2 - \frac{\hbar^2}{2M}\nabla_R^2 + eFz - eFZ + V_i - e^2/|r - R| \ , \tag{4}$$

where m and M are the mass of an electron and a nucleus respectively. In the rearrangement collision formalism, we

assume that the separated parts of the system can exist, in the initial and the final states, in two different arrangements ("channels") corresponding to the "original" and "rearranged" systems. Namely,

$$H_t = H_i + V_i = H_f + V_f \quad , \tag{5}$$

where V_f is the interaction potential of the ion with the metal. The probability that the total system, initially in a state, Ψ_i , will rearrange itself into the final state Ψ_f in unit time, has been shown to be given by[12]

$$P = \left(\frac{2\pi}{\hbar}\right) \delta(E_i - E_f) \left| \langle \Psi_f | V_f | \Psi_i \rangle \right|^2 \tag{6}$$

within the first Born approximation, where

$$H_i \Psi_i = E_i \Psi_i \quad , \tag{7}$$

$$H_f \Psi_f = E_f \Psi_f \quad . \tag{8}$$

The rearrangement collision formalism has, however, some difficulties, one of which is the lack of orthogonality between the initial and final states of the system. Mittleman[11] pointed out that even in lowest order the Born approximation must be changed from eq.(6) to

$$P = \left(\frac{2\pi}{\hbar}\right) \delta(E_i - E_f) \left| \langle \Psi_f | V_f (1 - \Pi_f) | \Psi_i \rangle \right|^2 \quad , \tag{9}$$

where Π_f projects onto the final state of the system.

Since the motion of the nucleus is much slower than that of the electron, the standard adiabatic assumptions are justified. The Schrödinger equation of the electron that transfers from the gas atom to the metal tip at the fixed position of the

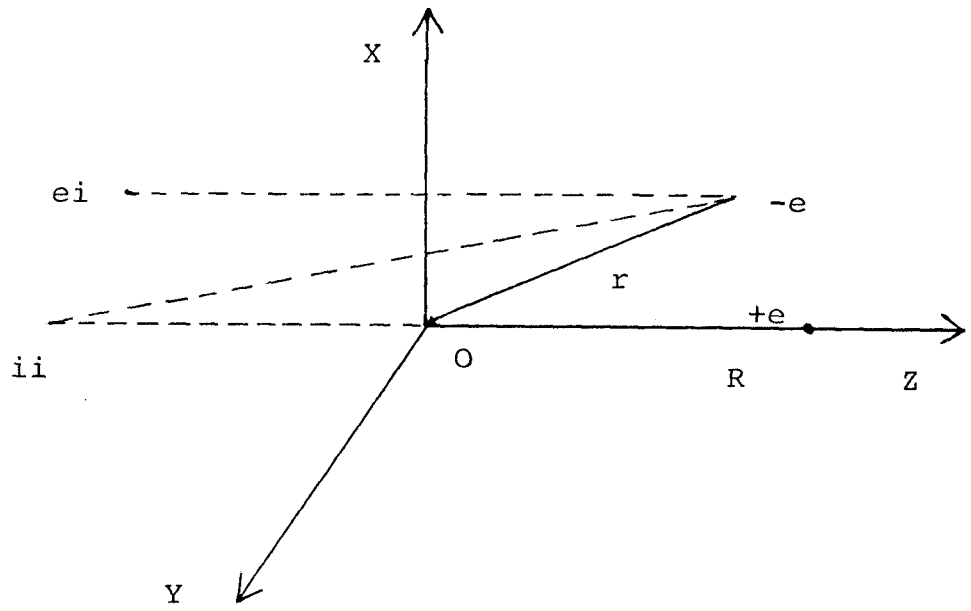

Fig. 1-1. Coordinate system of a metal and a monovalent atom.

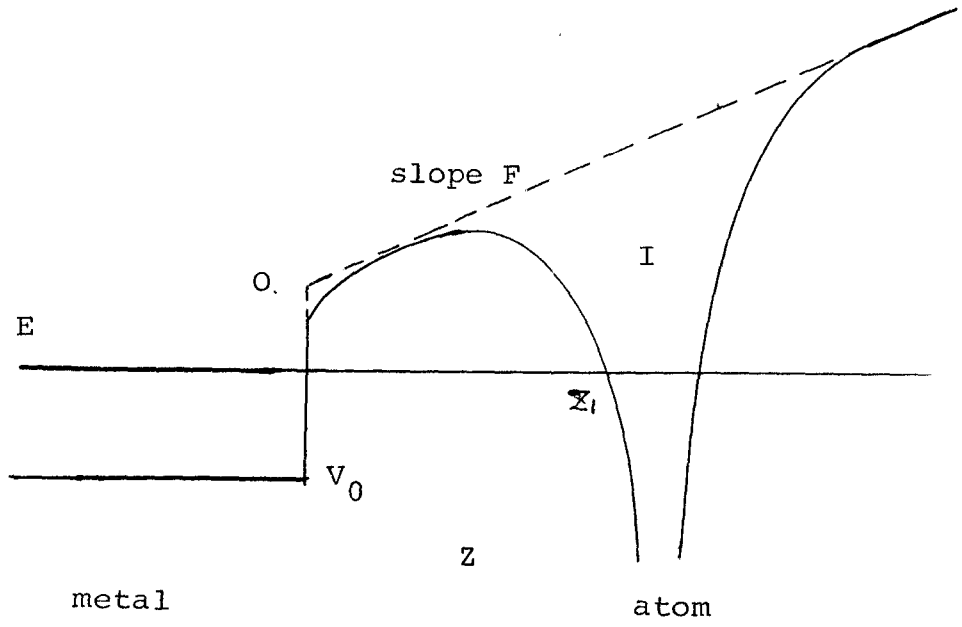

Fig. 1-2. Potential diagram for an electron in field-ionization.

nucleus is given by[9]

$$\left(-\hbar^2 / 2m \cdot \nabla_r^2 + V(r,R) \right) \Psi_e = E(R) \Psi_e \quad , \tag{10a}$$

$$V(r,R) = V_e(r,R) + eFz - e^2 / |r-R| \quad . \tag{10b}$$

The electronic potential V (r, R) is shown schematically in fig.2. Then, field ionization consists in the tunneling of electrons through the potential barrier which contains the position R of the nucleus of the free gas atom as a parameter.

1.2.2 The Interpretation of the Field Ionization

Our discussion below follows that of Duke[8]. The idea of tunneling can be formulated either as a time-dependent initial-value problem or as a stationary-state problem. In the former, one constructs a wave packet from the one-electron eigen-states approximately localized in the interior region and calculates that the integrated probability density in the interior region decays exponentially for an initial period of time. This formulation, although conceptually simple, suffers from two defects. First, the initial wave packet can never be completely localized in the interior region if constructed from eigenstates of the full Schrödinger equation. Second, the time-dependent picture is cumbersome to use in actual calculations.

To circumvent the first defect, Oppenheimer[13] devised a simpler time dependent formulation. In this method, the initial and the final states are taken to be eigenstates of different Hamiltonians. The actual problem is regarded as a combination of the two others with coupling and the process of field ionization interpreted as consisting of transitions between almost orthogonal states of the same energy. Thus, writing

$$H = H_L + H_L' = H_R + H_R' \quad , \tag{11}$$

Oppenheimer gives the transition probability per unit time, P, from the initial Ψ_0 to a continuum of final states Ψ_ν by

$$P = \left(\frac{2\pi}{\hbar}\right) \sum_\nu |\langle \nu | H - H_R | 0 \rangle|^2 \, \delta(E_\nu - E_0) \quad , \tag{12}$$

where

$$H_R \, \Psi_0 = E_0 \, \Psi_0 \quad , \tag{13}$$

$$H_L \, \Psi_\nu = E_\nu \, \Psi_\nu \quad . \tag{14}$$

Following Duke, we consider the relation between the transfer-Hamiltonian model and Oppenheimer's formalism of tunneling. The transfer-Hamiltonian model consists of writing the Hamiltonian of the system in the form

$$H = H_L + H_R + H_T \quad . \tag{15}$$

H_L and H_R are the Hamiltonians of the two classically allowed regions of configuration space, and H_T is an operator describing transitions between them. The existence and uniqueness of a simple form such as eq.(15) for the given Hamiltonian is not obvious. P is given by

$$P = \left(\frac{2\pi}{\hbar}\right) \sum_\nu |\langle \nu | H_T | 0 \rangle|^2 \, \delta(E_\nu - E_0) \quad . \tag{16}$$

Duke pointed out that a decomposition of the form specified by eq.(15) can be performed only in the sense of writing the transition probability given by eq.(12) in terms of the matrix elements of a transition operator, H_T , with matrix elements defined by $\langle \nu | H_T | 0 \rangle \equiv \langle \nu | H - H_L | 0 \rangle$. The transfer-Hamiltonian model is in current use for the many-body

description of tunneling, despite the weakness of its conceptual foundations. As Feuchtwang[14] pointed out, it therefore remains an open question whether the formalism does provide a reliable procedure for handling tunneling.

The simplest, and most easily utilized, interpretation of the single-particle tunneling process is the stationary-state theory of weakly quantized[15] (or quasi-stationary) "bound-state in the continuum". A state whose energy eigen value E is larger than $-V_0$ is non-degenerate and has a continuous spectrum. For energy E near $E_0 = V_e(Z, Z) + eFZ - I$, the amplitude of the wave function in the nucleus potential is large compared with that outside the atom or in the metal. These states are called resonance or virtual states. From the quasi-classical point of view, the problem reduces to obtain the transmission coefficient of an electron through the potential barrier. The probability that electrons tunnel from the atom to the metal is commonly taken to be

$$P = \left| \Psi_{E_0}(0) / \Psi_{E_0}(z_1) \right|^2 . \qquad (17)$$

It often is calculated using the WKB method.

From the quantum-mechanical point of view, Kemble[15] has given more rigorious discussion. He decomposed the resonance states into the incident streams of particles on the barrier and the corresponding reflected and transmitted streams. By physical intuition, Kemble has shown that the wave form of the waves trapped inside the atom must be nearly constant in time and the transmission coefficient for the outgoing waves incident on the barrier must be at all times very nearly equal to the transmission coefficient for a train of waves of uniform

amplitude and energy incident on the barrier. The stationary state wave function and the transmission coefficient are obtained by the matching wave function method[16].

The local or atomic density of states N(E) is defined as

$$N(E) = \sum_i |\langle \psi_i | \psi_A \rangle|^2 \, \delta(E - E_i) \, , \qquad (18)$$

where ψ_A is the isolated atomic wave function and summation is over all eigen states ψ_i that are normalized to constant current in the metal region. The energy distribution of N(E) reflects the energy uncertainty of the weakly quantized state. The width of the peaks on the resonance curve also gives the ionization probability by the Heisenberg uncertainty principle[15].

Now, the minimum value Z_c of Z at which the atom will be ionized exists as the final state must be empty in Oppenheimer's formalism. In the stationary state model, critical distance Z_c exists because if ion core comes up to the metal beyond the critical distance, the resonance energy of the ion core potential is below the Fermi-level of the metal and so it has one electron and ionization does not occur.

1.2.3 Calculations of the Field Ionization Probability

Reviews of the calculations of field ionization probability have been given by Sharma, Fonash and Schrenk[7] and by Müller and Tsong[2,12]. Some parts of the discussion below follow those of them.

Subsequently to Müller's first observation of the field ionization near a metal surface[17], Inghram and Gomer[18] initiated the one-dimensional WKB treatment of field ionization in FIM, and some refinements were brought forward by Müller and Bahadur[19]. The one-dimensional calculation provides many of

the basic concepts such as the critical distance for ionization.

The kinetic energies of field ions, that correspond to acceleration voltage, distribute correspondingly to the distribution of locations of the origin of the ionization. Tsong and Müller[20] observed that the half-width of this energy distribution of ions (field ion energy distribution) is so narrow that the zone, in which almost all ions are produced (defined as the ionization zone), is less than 0.2 A in width. The one-dimensional WKB calculations using square well models for both the atom and the metal yield a half-width of about 0.4 A [20], and the calculations with more rigorious one-dimensional barrier yield that of 0.7 A [21]. Boudreaux and Cutler[10] performed the three dimensional calculations of the ionization probability using the time-dependent perturbation theory. They took a state, that is given by a plane wave inside the metal and by an exponentially decreasing function outside the metal in the absence of the field, for the final state and found the half-width of the ionization zone for an atomic hydrogen on tungsten to be 0.11 A. Their formulation of field ionization by the time-dependent perturbation theory is criticized from Oppenheimer's points of view in section 2.1. There, suitable choices of the initial and the final states are discussed for the total Hamiltonian given by Boudreaux and Cutler[10].

Boudreaux and Cutler[6] also calculated the ionization probability by the rearrangement-type collision theory, and obtained the narrow half-width of 0.12 A for atomic hydrogen at a field of 2.3 V/A. Fonash and Schrenk[22] investigated, by this formalism, the effects of the Fermi surface on field ionization,

concluding that the anisotropy of the Fermi surface produce a regional image contrast[2,12]. Sharma and Schrenk[23] also investigated, by the rearrangement collision formalism, the effects of the surface potential periodicity from which they conclude that the point image contrast of a FIM image is shown to arise. Müller and Tsong[12] concluded that the effects[22,23] they investigated are of secondary importance in explaining the regional and point image contrasts. Sharma, Fonash and Schrenk[7] claim that the rearrangement collision formalism does not suffer from the ambiguity of the transfer Hamiltonian approach. However, in the three calculations[6,22,23] by the rearrangement collision theory, eq.(6) was used, instead of eq.(9). This approximation may yield nonsensical results[11].

In contrast with the previous investigators, we take the tight-binding Bloch states for the final metallic states in section 2.2 and investigate the contributions of the s and d orbitals to the total field ionization probability by the Oppenheimer's theory. The regional image contrast and point image contrast are qualitatively discussed. This calculation may be regarded as the first attempt to quantify the extended-orbital concept of Knor and Müller[24]. The calculated widths of the ionization zone (0.32 ~ 0.42 A) are qualitatively in good agreement with the recent experimental observations by Utsumi[25] and by Müller and Sakurai[26].

Let us consider the effects of field adsorption[4,5] on field ionization probability. There are a few experimental observations that a field-adsorbed inert atom increases the field-ion current[27-30]. Alferieff and Duke[31] have considered one-dimensional model in which a neutral adsorbate is

represented by a delta function with its strength given by the ionization potential (equals to 15 eV). The transmission probabilities they obtained by the matching wave method with and without an adsorbate are essentially unchanged. Duke and Alferieff[32] discussed that negative values of ionization potenital correspond to pseudopotentials associated with neutral adsorbates which are repulsive in the delta-potential limit. Alferieff and Duke were interested in the effects of adsorption on the lower energy Jason peaks[33], not on the main peaks of the ion energy distribution. The argument above urges us to reconsider the problem in more detail. The model calculations similar to those of Alferieff and Duke[31] are presented in section 3.1. The potential of a field-adsorbed inert gas atom is represented by a potential well, in the strong potential model[32]. The effects of the chemisorption or metallic adsorption as well as those of the field adsorption are investigated. In contrast with the WKB point of view[12,34], calculated ionization probabilities often are reduced by the field adsorption.

Nolan and Herman[35] first pointed out that not the resonance effects or the transition with the aids of virtual intermediate states, but exchange effects owing to the overlap with the adsorbate orbitals constitute the major effect in the enhancement of the ionization probability. Their formalism is quite similar to eq.(9) where the initial and the final states are Slater determinantal states[36]. The enhancement factor, which is the ratio of ionization rates with and without the adsorbed atom, is evaluated by them. The values seem to be rather too high such that 3$\sim$5 for helium as the adsorbate,

$30 \sim 90$ for neon and 10^4 for argon, probably due to the omission of the field term from the perturbation potential (see section 3.2). Indeed, in the modified calculations, Nolan and Herman[37] obtained small enhancement factor: $1 \sim 0.4$ for helium and $2 \sim 10$ for neon.

For the purpose of getting at the truth of the extremely large enhancement factor given in the former paper of Nolan and Herman[35], we also calculate the ionization probability when there are a field adsorbed atom on the apex of the metal atom in the manner of the many body tunneling. A limited basis consisting of the isolated orbitals of imaging inert gas atom, Ψ_{He} and of adsorbed atom, Ψ_A and plane wave metal states which exponentially decays outside the metal surface in the presence of the field, Ψ_k are adapted. If all the basis states are orthogonal to each other, the off diagonal terms, which arise from the presence of the adsorbed atom, are composed of only exchange integrals, $V_{AkAHe} = \int \Psi_A^*(r_1)\ \Psi_k^*(r_2) \cdot e^2/r_{12} \cdot \Psi_A(r_2)\ \Psi_{He}(r_1)\ d\tau_1 d\tau_2$. We formulate the ionization probability that it will contain the terms discussed above in the orthogonal limit. Thus, the initial and the final states are defined by properly orthogonalizing the limited basis, and then ionization probability may be given by the Fermi-Golden rule, regarding the off-diagonal terms as perturbation. Our calculations lead to the considerable reduction of the ionization probability for helium as the adsorbate, small reduction for neon and small enhancement for argon. The ratios of the ionization probabilities, with and without the adsorbed atom are 0.06, 0.7 and 4.0 for helium, neon and argon, respectively.

1.3 Ion Current Generation

The present section will comprise a brief introduction of the contributions of previous authors, following a survey of Southon[38]. The first theoretical calculations of ion currents were formulated in terms of a supply function, S, equal to the number of gas atoms striking the emitter in unit time, and an ionization probability, Q, describing the probability that an impinging gas atom will be ionized in passing through the ionization zone once. The relation between Q and P defined in section 1.2 is given by[2]

$$Q = 1 - \exp[-\int_{Z_c}^{Z_c+d} P(Z)/v(Z)\ dZ] \ , \qquad (19)$$

where d is the depth of the ionization zone and v(Z) is a radial velocity of a gas atom. If $d \ll 1$, we obtain

$$Q = 1 - e^{-t/\tau} \ , \qquad (20)$$

where $t = d/v(Z_c)$ and $\tau = P(Z_c)^{-1}$ and t and τ are a time duration of a gas atom and ionization lifetime respectively.

Good and Müller[39] first pointed out that S exceeds the supply function in zero field, S_0, due to the polarization attraction (see appendix I). Correct analytical expressions of the supply function S are available for ideal tip shapes, such as the expression for a spherical tip[38], for a cylindrical emitter[38], and for a hyperboloid shape[40]. We derive the expressions of dS/dv_n and dS/dv_t for a spherical tip in chapter 4 where they are called $N_n(v_n)$ and $N_t(v_t)$. The quantities v_n and v_t are the velocity components normal and parallel to the emitter surface respectively.

Müller and Bahadur[19] have derived an expression for the

total ion current on the assumptions that a gas atom approaches the emitter along a surface normal, strikes it only once and rebounds with half the incoming velocity. The expression was then given by

$$I = 3SQ_{in} \quad , \tag{21}$$

where Q_{in} is the probability of ionization during the inward journey. The calculated current initially rises steeply with increasing field as Q_{in} increases, whilst at high fields ion current depends on the supply function alone since $3Q_{in}$ is equal to unity, in general agreement with measurements at room temperature.

Müller[41] pointed out first that an atom will be unable to escape from the tip region, if the kinetic energy of the atom after collision with the emitter is less than the polarization energy, E_p , and it will eventually make a series of random hops before being ionized. Gomer[42] has outlined a theory of the field-ion current which takes account of this behaviour.

Gomer[42] has considered three regimes relevant to the field-ionization process. At very low fields, the equilibrium concentration of gas at the emitter, which exceeds ambient gas concentration n by the Boltzmann factor $\exp(E_p/kT)$, will be scarcely depleted. Thus, I is expressed, at very low fields

$$I \approx nQ \exp(E_p/kT)\ \Delta V \quad , \tag{22}$$

where ΔV is the volume of the ionization zone . This expression will be confirmed to exist by our detailed analysis discussed later. The ion current rises steeply with increasing field due to the strong field dependence of Q and the Boltzmann factor.

The expression (21) derived by Müller and Bahadur[19] takes no account of the latter field dependence. At high fields, when any gas reaching the emitter is certain to be ionized and therefore no trapped atoms exist, the field ion current is simply given by the supply function. At intermediate field strengths, Gomer[42] has shown that the balance of the rates of escape by ionization, k_i , and by diffusion to the shank of an emitter, k_d , determines the steady state concentration of gas at the emitter, N. Later, Southon[38] pointed out that gas atoms are prevented from diffusing towards shank by the polarization potential, but will escape by thermally activated processes. He also introduced the probability of capture, P_c , that a gas atom striking an emitter surface is subsequently unable to escape to a region of a zero polarization potential energy, and the supply of gas atoms from the shank to the emitting area. Gomer[42], Southon[38], and Müller and Tsong[2] discussed in detail the field ionization processes, estimating the rate constants, k_i and k_d on the basis of the assumed somewhat ambiguous energy (or velocity) distribution of trapped atoms. We will present, in chapter 4, a thoroughly dynamical calculation of ion current by simulating trajectories of gas atoms, without invoking the distribution function.

Recently, Van Eekelen[40] introduced somewhat different distribution function, N(v) : the rate, at which gas atoms strike a surface, as a function of velocity component normal to the surface. He formulated a balance equation for N(v), and computed a number of properties of FIM, such as the field and the temperature dependence of the total ion current. The computed results, obtained without having to invoke a "deus

ex machina", such as an unknown contribution from the shanks, appear to be in good agreement with the experimental observations[2,12,38].

We define the rate constants for ionization, k_i and for escape without ionization, k_e , as functionals of $N(v_n)$, and the capture probability , P_c , as a functional of $N_n(v_n)$. Making use of the balance equation for N(v) developed by Van Eekelen[40], we reformulated the expressions of the total-ion current in terms of quantities defined above and the supply function. These formulations enable us to discuss the computed results physically. Then, we compute the field ion current versus other parameters of interest, following Van Eekelen[40], with slight modifications. One of them is the extension of the , in a sense, one-dimensional model to the three-dimensional one, which is accomplished by the use of the velocity distribution function, $N_n(v_n)$. The dependence of ion current on the tip temperature T_s and the gas temperature T_g is extensively investigated. Finally, the effects of field adsorption on the ion current are investigated. The procedure reveal that ion current is indeed increased by the field adsorption as observed experimentally [29], even if ionization probability itself were suppressed correspondingly to our theoretical predictions.

Finally, we refer to the author's stanspoint, in which field adsorption is regarded to perturb the field ionization process above a clean metal surface and not to change it drastically. Thus, we investigate the mechanism of the ion current generation above a clean surface at first and then the effects of the field adsorption are investigated as the extended version of the problem. Fortunately, the procedure is revealed to be a suitable one.

CHAPTER 2

FIELD IONIZATION ABOVE CLEAN METAL SURFACE

It is important to calculate the field ionization probability when there is no adsorbate on the metal surface, because the procedure may give the fundamental step to understand the field ionization process when there are adsorbate of various species between the ionizable gas atom and the metal surface. Moreover, field ionization on the clean metal surface actually takes place, for example on the (110) plane of tungsten under the usual experimental condition of FIM[1] and over all planes at high tip temperatures.

In this chapter we present two calculations of ionization probability on the basis of Oppenheimer's approximation. In the first calculation how to choose the initial and the final states on this approximation is shown assuming the metallic wave function as plane waves[2]. The tight-binding Bloch wave function is used as a metallic state in the second calculation.

The usual time dependent perturbation theory is a description of a transition between orthogonal states which are eigen-states of the same Hamiltonian. In the treatment of the field ionization process by this method, one must make certain of the orthogonality between the initial and the final states or define them which describe the electron transfer process reasonably. Then, the transition probability is calculated by the Fermi Golden rule, regarding off-diagonal parts of the total Hamiltonian as

a perturbation. It will be shown in section 2.1 that a lack of the orthogonality between the initial and the final states leads to a nonsensical results.

2.1 Ionization Probability Calculations Using Plane Waves as Metallic States

2.1.1 Formulation

First, we follow Oppenheimer's formalism[3]. Oppenheimer has presented the approximate method of describing the time dependence of the wave function $|\psi\rangle$ under the total Hamiltonian H_t which is given as

$$H_t = H + H_0 + H_1 \quad . \tag{1}$$

He expanded $|\psi\rangle$ as

$$|\psi\rangle = |0\rangle \exp(-2\pi i\nu_0 t) + \int C(\nu' t)|\nu'\rangle \exp(-2\pi i\nu' t)\, d\nu' \quad , \tag{2}$$

where

$$(H + H_0 - E_0)\,|0\rangle = 0 \quad , \tag{3}$$

$$(H + H_1 - E_\nu)\,|\nu\rangle = 0 \quad , \tag{4}$$

$$E_\nu = h\nu \quad , \tag{5}$$

and we change the original expression $\exp(2\pi i\nu t)$ to $\exp(-2\pi i\nu t)$. Then we obtain

$$\frac{ih}{2\pi}\frac{\partial C(\nu t)}{\partial t} = \langle \nu | H_1(t) | 0\rangle + \int C(\nu' t)\langle \nu | H_0(t) | \nu'\rangle\, d\nu' , \tag{6}$$

where

$$H_1(t) = \exp[2\pi i(H + H_1)t/h]H_1 \exp[-2\pi i(H + H_0)t/h], \quad (7)$$

$$H_0(t) = \exp[2\pi i(H + H_1)t/h]H_0 \exp[-2\pi i(H + H_1)t/h], \quad (8)$$

Integrating and iterating eq. (6), we obtain

$$C(\nu t) = \langle \nu | \tilde{U}(t, 0) | 0 \rangle \quad , \quad (9)$$

$$\tilde{U}(t, t') = -i\frac{2\pi}{h}\int_{t'}^{t} H_1(\tau)d\tau + \sum_{n=2}^{\infty}(-i\frac{2\pi}{h})^n \int_{t'}^{t} d\tau_1 \int_{t'}^{\tau_1} d\tau_2 \cdots \int_{t'}^{\tau_{n-1}} d\tau_n$$

$$\times H_0(\tau_1)H_0(\tau_2) \cdots H_1(\tau_n) \quad . \quad (10)$$

We can get the usual time evolution operator $U(t, t')$[4] in the time dependent perturbation theory by changing $H_1(t)$ to $H_0(t)$ in eq. (10).

2.1.2 Field Ionization Probability in FIM

The total Hamiltonian of the system which consists of an atom (e.g., hydrogen) near the metal surface under high electric field is given by

$$H_t = H + H_0 + H_1$$

$$= T + V(r) \quad , \quad (11)$$

where T is the kinetic energy and V(r) is given by (1-10b), the expression of which is given first by Boudreaux and Cutler[5] .

Oppenheimer has shown that the transition matrix element to the second order is

$$M = \langle \nu_0 | M_1 + M_2 | 0 \rangle \quad , \quad (12)$$

where

$$M_1 = H_1 \quad , \tag{13}$$

$$M_2 = [1/h(\nu_0 - \bar{\nu})]\ H_0 H_1 \quad , \tag{14}$$

$$\nu_0 = E_0/h \quad , \tag{15}$$

and $\langle \nu | H_0 | \nu_0 \rangle \langle 0 | H_1 | \nu \rangle$ has a maximum for $\nu = \bar{\nu}$.

There is some choice of H, H_0 and H_1 for the total Hamiltonian H_t. We discuss the three cases shown in Table 1. The schematic diagram of the potential and the wave function for the final state of the cases 1 and 2, and of the case 3 in Table 1, are shown in Fig.1a and Fig.1b, respectively.

The eigenfunction of the initial state $|0\rangle$ is the hydrogen 1s wave function U_0 in case 1 and $N_0 U_0 [1 + (F/I)(z-Z)]^6$ in cases 2 and 3, where N_0 is the normalization constant, F is the field strength and I is the ionization energy of the atom. The eigenfunction of the final state $|\nu\rangle$ in the classically forbidden region is approximated by

$$|\nu\rangle = N_f \exp[-k(\nu, z)], \tag{16}$$

where for cases 1 and 2 :

$$k(\nu, z) = \int_0^{\bar{z}} [(2m/\hbar^2)(-E_\nu + eFz' + V_e)]^{1/2}\, dz' \tag{17}$$

and for case 3 :

$$k(\nu, z) = \int_0^{\bar{z}} [(2m/\hbar^2)(-E_\nu + V_e)]^{1/2}\, dz' \tag{18}$$

N_f is the normalization constant and E_ν is measured from the vacuum level. Eqs.(16), (17) and (18) are obtained on the basis of a WKB approximation. Moreover, in the calculation of

Table 2-1

Three Cases for Ionization Probability Calculations

	H	H_o	H_1	$\lvert R\cdot h(\bar{\nu}-\nu_0)\rvert$ (eV)
case 1	T	$-e^2/\lvert r-R\rvert$	$V_e(r,R)^*+eFz$	11.7
case 2	T+eFz	$-e^2/\lvert r-R\rvert$	$V_e(r,R)$	11.9
case 3	T	$eFz-e^2/\lvert r-R\rvert$	$V_e(r,R)$	7.07

* $V_e(r,R)$ is given by eqs. (1-2) and (1-3).

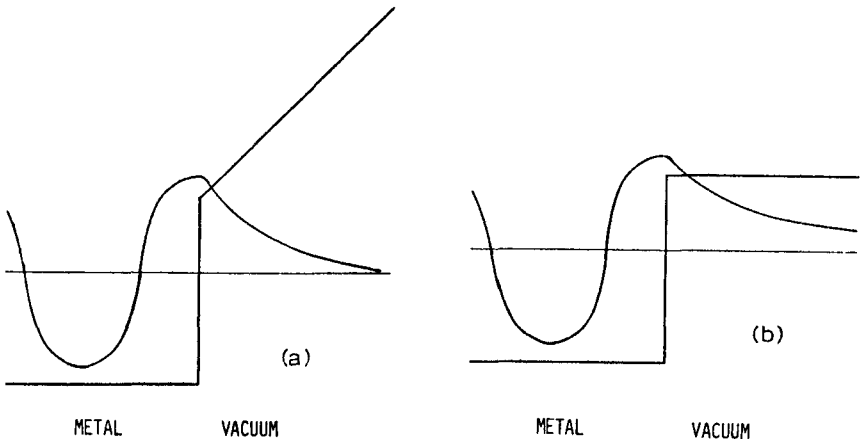

Fig. 2-1. Schematic diagram showing the potential and the wave function for the final state of cases 1 and 2 (a) and 3 (b).

the matrix elements below, $V_e(r,R)$ in eqs.(17) and (18) is neglected and specifically $k(\nu, z)$ of eq.(18) becomes

$$k(\nu, z) = k(\nu)z \quad , \tag{19}$$

$$k(\nu) = (-2mE_\nu/\hbar^2)^{1/2} \quad . \tag{20}$$

The favorable choice of the initial state and the final state may be deduced by comparison of the ratio R of the second order matrix element $\langle \nu_0 \mid M_2 \mid 0 \rangle$ to the first order matrix element $\langle \nu_0 \mid M_1 \mid 0 \rangle$ with each other case :

$$R = \frac{\langle \nu_0 \mid H_0 H_1/h(\nu_0 - \bar{\nu}) \mid 0 \rangle}{\langle \nu_0 \mid H_1 \mid 0 \rangle} \quad . \tag{21}$$

The ratio $\langle \nu_0 \mid H_0 H_1 \mid 0 \rangle / \langle \nu_0 \mid H_1 \mid 0 \rangle$ is calculated for each case and shown in Table 1, where F = 2.3 V/A, I = 13.6 eV and the Fermi energy of the metal is 4.5 eV. The energy $h\bar{\nu}$ may be estimated to be such an energy that an electron of the metal of this energy can arrive at the hydrogen atom without exponential decay. In case 3, $H + H_1$ has no field term and $h(\bar{\nu} - \nu_0)$ is around the Fermi energy of the metal plus potential energy V_{e-m}, about 5.5 eV. In cases 1 or 2, $H + H_1$ has a field term eFz, and $h(\bar{\nu} - \nu_0)$ may be greater than the ionization energy of 13.6 eV.

As H_1 contains a field term in case 1, $h(\bar{\nu} - \nu_0)$ in case 1 may be greater than that in case 2.

The most favorable case may be case 1 from the convergence discussed above and because in this case we can use the exact eigenfunction for the initial state.

Now, the transition matrix element on the basis of Oppenheimer's approximation to the first order is given by

$$M = \langle \nu_0 | V_e + eFz\,\theta(z) | 0 \rangle \quad , \tag{22}$$

where the final state $|\nu_0\rangle$ is defined by eqs.(16) and (17). The expression (22) is quite similar to the one found from the time dependent perturbation theory[5] in which instead of eqs.(16) and (17), eqs.(16) and (18) or the final state of case 3 are used for $|\nu_0\rangle$. It must be noticed that M is a function of the separation distance R between the atom and the metal not only because of the dependence of the integral (22) on the position of the atom, but also because of the dependence of the final wave function $|\nu_0\rangle$ on the position of the atom.

The transition matrix element calculations by the two methods are compared in Fig. 2. The matrix element by the time dependent perturbation theory does not decrease as the distance of the hydrogen atom from the surface increases, since E_ν and the exponential decay constant $k(\nu)$ in eq.(20) decrease as the separation of the hydrogen atom and the metal becomes large by the condition $|E_\nu| = |I| - eFR$, which is necessitated by the energy conservation of the initial and the final state. E_ν or $k(\nu)$ do not depend on the position of the electron but depend on the position of the nucleus of the gas atom.

The defects of the time dependent perturbation theory on the basis of non-orthogonal eigenstates or ambiguous choice of the transfer Hamiltonian[6,7] may be reduced by using the formalism on the basis of Oppenheimer's approximation.

2.2 Detailed Calculation of the Ionization Probability Using Tight-Binding Bloch States as Metallic States[8]

2.2.1 Introduction

The advanced quantum mechanical treatments of field

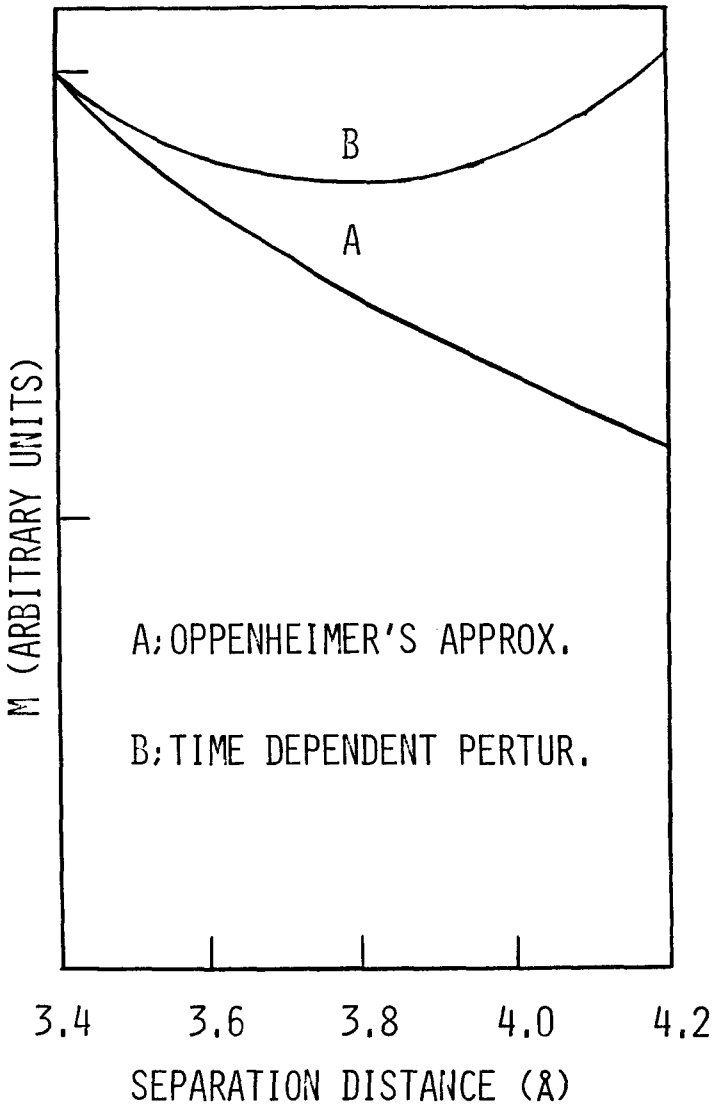

Fig. 2-2. The transition matrix element on the basis of Oppenheimer's approximation and the time dependent perturbation theory.

ionization processes of FIM must explain experimental results that an image of FIM shows directly an atomic structure of a metal surface as many spots, each of which corresponds to each an individual atom of the metal surface. Knor and Müller[9] have presented the qualitative interpretation of field ion images as projections of regions where the fully occupied orbitals of inert gas atoms can easily overlap with the partially occupied single or hybridized orbitals of surface metal atoms.

Boudreaux and Cutler[5,6] have presented two different approaches to the problem of the narrow field ionization zone, using the rearrangement collision theory and the time dependent perturbation theory. They claimed that their three dimensional analysis gave extremely narrow half widths of ion energy distribution of 0.11 A and 0.12 A in qualitative agreement with the experiments by Tsong and Müller[10]. Recent experiments, however, show wider half widths as will be discussed in detail in Section 2.3. The final state of the tunneling electron was assumed to be a plane wave state in a metal in their work.

To date, Sharma and Schrenk[11] showed that the non-uniform ionization probability at the critical distance is not the result of field fluctuations, but is the result of the distortion of the tail of the plane wave outside the surface by a periodic surface potential.

The high resolution of an atomic scale in the FIM image suggests that the configuration of electrons on metal surface are very similar to those of the atoms in the bulk metal as Knor and Müller[9] noticed. Also, in consideration of the band structure of a transition metal, it is important to consider the tight-binding d-band electronic state in addition to the free

s-like band electronic state to construct a model of electronic configuration of the metal surface[12].

In this chapter, the field ionization probability is calculated by the method discussed in Section 2.1 assuming the metallic state as the tight-binding Bloch wave function. It is examined whether the ionization probability shows the atomic resolution of the (001) crystallographic plane for example or not and how the s-state and d-state contribute to the total ionization probability.

2.2.2 Theoretical Discussion

An electron localized at a hydrogen atom is assumed to be characterized by a hydrogen 1-s state wave function :

$$U_0 = N_0 \exp(-r'/a_0) \tag{23}$$

The coordinate system is shown in Fig.3. The metal surface is considered as a plane where the electron gas has decayed to some appropriate value of its density in the bulk and lying 2 A above the lattice plane determined by the ion cores. For simplicity only the case that the vector R lies on the XZ plane is considered.

Let Φ_{jk} represent a k state of the j-th energy band in the metal. For example, j is 1, 2, ... for Δ_1, Δ_2, ... on the Δ axis[13]. Φ_{jk} is assumed to be given by the linear combination of the atomic type wave function :

$$\Phi_{jk} = \frac{1}{\sqrt{N}} \sum_{\ell, n} B_{njk} \phi_n(\vec{r} - \vec{R}_\ell) \exp(i\vec{k} \cdot \vec{R}_\ell) \quad , \tag{24}$$

where the sum is over all N lattice sites of the metal and

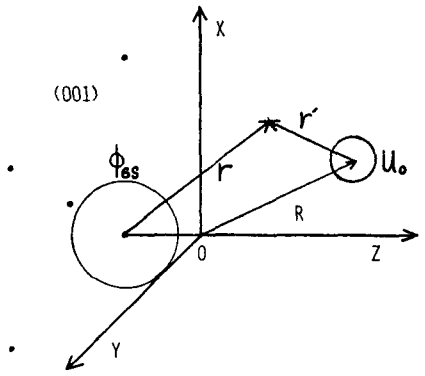

Fig. 2-3. The metal surface is defined as lying 2 Å above the lattice plane of ion cores. The origin O is chosen as shown in this figure. $\boldsymbol{R}$ is the vector from O to the hydrogen nucleus. The metal surface is the (001) crystallographic plane with an interatomic spacing of 3.16 Å. The [110], [1$\bar{1}$0], and [001] axes are parallel to the X, Y and Z axes, respectively.

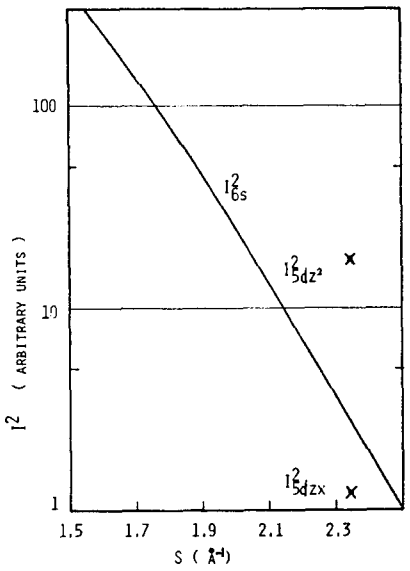

Fig. 2-4. The value of $I^2(6s)$ ($X = Y = 0$, $Z = Z_c$) as a function of S. Z_c is obtained as 3.52 Å for assumed Fermi energy E_F of 5.5 eV measured from the bottom of the band and V_0 of 10.0 eV. The values of $I^2(5d_{Z^2})$ ($X = Y = 0$, $Z = Z_c$) and $I^2(5d_{ZX})$ ($X = 1.7$, $Y = 0$, $Z = Z_c$) are shown for $Sd = 2.34$ Å.

$\phi_n(r)$ is the atomic wave function of the metal atom. For special k vector as symmetry (001) direction (Δ axis), B_{njk} is zero except for j = Δ_2', n = $5d_{XY}$; j = Δ_5, n = $5d_{ZX}$ and $5d_{YZ}$; j = Δ_1, n = 6s or n = $5d_{Z2}$ and j = Δ_2, n = $5d_{X2-Y2}$. When the atom comes near enough to the metal surface, the electron experiences perturbations due to $F+V_e(r,R)$ which can induce a transition of the electron from the atomic state U_0 into the metal state Φ_{jk}.

The probability of such a transition per unit time is given by

$$P(R) = \frac{2\pi}{\hbar} \frac{\Omega}{(2\pi)^3} \sum_j \int_j |\langle \Phi_{jk}|V|\, U_0\rangle|^2 \frac{1}{|\nabla_k E|}\, dS \quad , \qquad (25)$$

where E is the energy of the Φ_{jk} state measured from the bottom of the band, Ω is the volume of the metal, and V(Z) is the interaction potential given by[5]

$$V(Z) = -\frac{e^2}{4Z}[1 - \exp(-\lambda Z)] + \frac{e^2}{r_1}\left(1 - \frac{\Delta}{2Z} + \frac{\Delta^2}{4Z^2}\right) + eFZ, \quad Z \geq 0 \qquad (26a)$$

$$= -V_0\left\{1 + \frac{A}{Z}[1 - \exp(\lambda Z)]\cos(kZ + \delta)\right\} , \qquad Z < 0 \qquad (26b)$$

where r_1 is the distance between an electron of the hydrogen and an image of the hydrogen ion, Δ is the dipole length of the polarized hydrogen atom, and V_0 is the energy of the vacuum measured from the bottom of the band. Values of the five parameters in eq. (26b) are chosen as follows[5] : k = 10.0 A^{-1}, λ = 1.24 A^{-1}, δ = 0.085 and A = 0.44 A for V_0 = 10.0 eV. The second term in eq. (26b) represents the interaction potential

energy of the electron with the image of the ion in the metal.

The surface integral (25) is performed on the equi-energy surface of

$$E = V_0 - [I - V(Z)], \tag{27}$$

where I is the ionization energy of the hydrogen atom. By the Pauli principle, $P(R) = 0$ for $Z < Z_c$, where the critical distance Z_c is determined by introducing the Fermi energy to E in eq.(27).

Of the atomic wave functions in the sum of eq.(24), only the 6s, $5d_{Z^2}$ and $5d_{ZX}$ orbitals are considered, as they stick out from the surface. Some j state may be constructed mainly by the 6s or 5d atomic wave function and the so-called s-like band or d-like band.

Now the atomic wave function ϕ_n is assumed to be a Slater function[14] as follows :

$$\phi(6s) = N_s r^3 \exp(-S_s r) , \tag{28a}$$

$$\phi(5d_{Z^2}) = N_d r^{n_d^* - 1} \exp(-S_d r) \frac{\sqrt{5}}{4\sqrt{\pi}} [3(Z - d)^2 - r^2] \frac{1}{r^2} , \tag{28b}$$

$$\phi(5d_{ZX}) = N_d r^{n_d^* - 1} \exp(-S_d r) \frac{\sqrt{15}}{\sqrt{2\pi}} X(Z - d) \frac{1}{r^2} , \tag{28c}$$

where d is the Z coordinate of the metal ion core and taken as -2 A. From the Slater rule, $S_s = 1.55\ A^{-1}$, $S_d = 2.34\ A^{-1}$ and $n_d^* = 4.2$ for tungsten. For simplicity, $n_d^* = 4$ is used. Consider the integral

$$\langle \Phi_{jk} | V | U_0 \rangle = \frac{1}{\sqrt{N}} \sum_{l,n} B_{njk} \langle \phi_n(r - R_l) | V | U_0(R) \rangle \exp(i\vec{k} \cdot \vec{R}_l)$$

$$= \frac{1}{\sqrt{N}} \sum_{l,n} B_{njk} L_n(\vec{R}, \vec{R}_l) \exp(i\vec{k} \cdot \vec{R}_l) , \tag{29}$$

where

$$L_n(\vec{R}, \vec{R}_\ell) = \langle \phi_n(r - R_\ell) \,|V|\, U_0 \rangle \quad . \tag{30}$$

Since the hydrogen wave function U_0 decreases exponentially as $\exp(-r/a_0)$, it is enough to consider only the integrals $L_n(\vec{R}, \vec{R}_\ell)$ where $\vec{R}_\ell$ varies among the surface lattice points. The origin of $\vec{R}_\ell$ is chosen to be the nearest surface atom core to the hydrogen atom and the integral I_n is defined as

$$I_n(\vec{R}) \equiv L_n(\vec{R}, 0). \tag{31}$$

So,

$$L_n(\vec{R}, \vec{R}_\ell) = I_n(\vec{R} - \vec{R}_\ell) \quad , \tag{32}$$

$$\langle \Phi_{jk} |V|\, U_0 \rangle = \frac{1}{\sqrt{N}} \sum_{\ell,n} B_{njk} I_n(\vec{R} - \vec{R}_\ell) \exp(i\vec{k} \cdot \vec{R}_\ell) \quad . \tag{33}$$

Now, the integral $I_n(\vec{R})$ is to be calculated.

2.2.3 Evaluation and Results

Now we have

$$I(6s) = \int N_s r^3 \exp(-S_s r) V(Z) N_0 \exp(-\frac{r'}{a_0}) \, d\tau \quad , \tag{34a}$$

$$I(5d_{Z2}) = \int N_d r^3 \exp(-S_d r) \frac{\sqrt{5}}{4\sqrt{\pi}} [3(Z - d)^2 - r^2] \frac{1}{r^2} \times V(Z) N_0 \exp(-\frac{r'}{a_0}) \, d\tau \quad , \tag{34b}$$

$$I(5d_{ZX}) = \int N_d r^3 \exp(-S_d r) \frac{\sqrt{15}}{2\sqrt{\pi}} X(Z - d) \frac{1}{r^2} \times V(Z) N_0 \exp(-\frac{r'}{a_0}) \, d\tau \quad . \tag{34c}$$

The three-fold integral was carried out on an NEAC 700 to an accuracy of no less than one part in 10^3. The integration (34) can be carried out analytically when we use V = eFZ and d = 0 A. The nature of the function $I_n(R)$ obtained analytically under the above special conditions, is quite similar to that obtained by the numerical integration of eq.(34). This shows that the field term may be dominant in the interaction potential and that the numerical calculation of eq.(34) may be accurate.

The values of $I^2(6s)$ $(X = Y = 0, Z = Z_c)$, $I^2(5d_{Z^2})$ $(X = Y = 0, Z = Z_c)$ and $I^2(5d_{ZX})$ $(X = 1.7, Y = 0, Z = Z_c)$ are sensitive to the choice of S_s and S_d (see Fig.4). The parameter S is a measure of how tightly bound the electron is with smaller S implying less tightly bound electrons. The radius r_m where the wave function of the metal atom has its maximum value is $(n^* - 1)/S$. For S_s and S_d from the Slater rule, r_m is 1.9 A and 1.3 A, respectively. The more expanded wave function $\phi(6s)$ at the metal surface may suffer from the electric field penetration. The hydrogen atom separated about 5.5 A from the metal ion core sees the "6s" wave function as the compressed sphere in the normal direction of the surface. So, it may be reasonable to use the "6s" wave function of the S_s values which are larger than S_s from Slater's rule in the calculation of $I^2(6s)$ $(Z = Z_c)$ and its Z dependence. On the other hand, in the calculation of the X dependence of $I^2(R)(6s)$, the 6s wave function of S_s equal to 1.55 A^{-1} may be used. The result (Fig.4) shows that for values of S_s of about 2.0 A^{-1} and S_d from the Slater rule, $I^2(6s) \approx I^2(5d_{Z^2})$ and both the s-band and the d-band contribution to the ionization process must be considered.

The strong dependence of the value of the transition matrix

element on the expansion of the wave function is in good agreement with the experimental result of FIM images of SiC by J. Kudo et al.[15]. The images show that Si atoms ($r_{m\ 3p}$= 1.06 A) are much brighter than carbon atoms ($r_{m\ 2p}$= 0.66 A) such as the second layer edge Si atoms constitute the image contrast of ($\bar{1}\bar{1}\bar{1}$) plane of SiC where the top layer is constructed by carbon atoms.

Now, the X dependence of $I_n^2(\vec{R})$ at the critical distance is shown in Fig.5. Let ΔX_n represent the half width of I_n^2 (X, Y = 0, Z = Z_c). As $\Phi(5d_{Z^2})$ has a big lobe extending in the Z-direction, $\Delta X(5d_{Z^2})$ is smaller than $\Delta X(6s)$:

$$\Delta X(5d_{Z^2}) = 1.5 \text{ A}, \qquad \Delta X(6s) = 2.1 \text{ A}. \tag{35}$$

On the other hand, $I^2(5d_{ZX})$ has a maximum at X = 1.7 A.

The value of I_n^2(X, Y = 0, Z) decreases slowly from the value of Z = Z_c as Z increases by a nearly equal rate for some X values. The half widths of $I^2(5d_{Z^2})$, $I^2(5d_{ZX})$ and $I^2(6s)$ are 0.32 A, 0.30 A and 0.42 A, respectively (see Fig.6).

Now, consider the ionization probability $P(\vec{R})$

$$P(\vec{R}) = \frac{2\pi}{\hbar} \frac{\Omega}{(2\pi)^3} \sum_j \int_j |\langle \Phi_{jk} | V | U_0 \rangle|^2 \frac{1}{|\nabla_k E|} dS$$

$$= \frac{1}{\sqrt{N}} \frac{2\pi}{\hbar} \frac{\Omega}{(2\pi)^3} \sum_j \int_j \left| \sum_{n,l} B_{njk} I_n(\vec{R} - \vec{R}_l) \exp(i\vec{k} \cdot \vec{R}_l) \right|^2 \frac{1}{|\nabla_k E|} dS. \tag{36}$$

To obtain $P(\vec{R})$ itself, the knowledge of B_{njk} and the k-E relation is necessary for each j state. The energy band calculation of body-centered cubic tungsten by the non-relativistic augmented

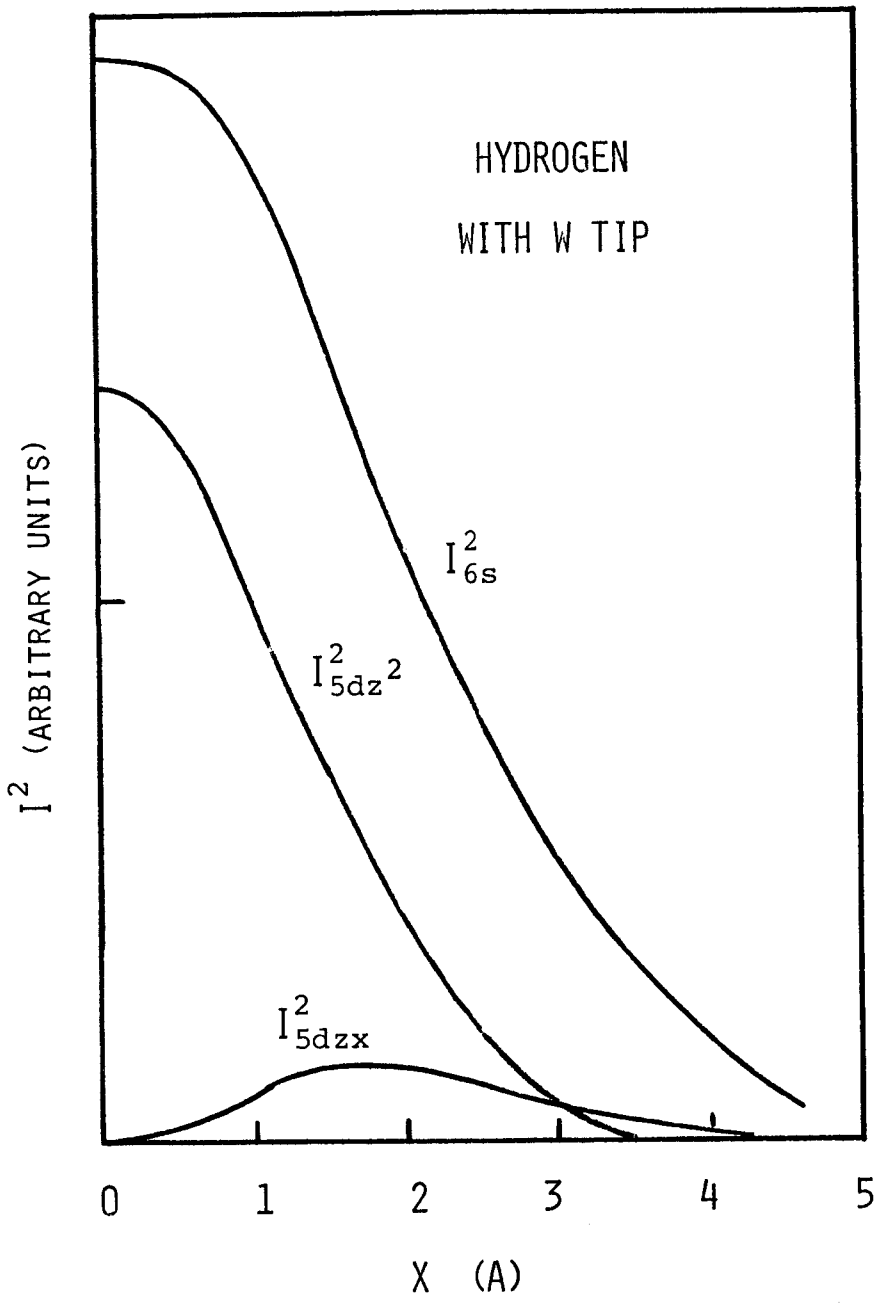

Fig. 2-5. The value of $I^2(6s)(X,Y=0,Z=Z_c)$, $I^2(5d_{z2})(X,Y=0,Z=Z_c)$ and $I^2(5d_{zx})(X,Y=0,Z=Z_c)$ as a function of X.

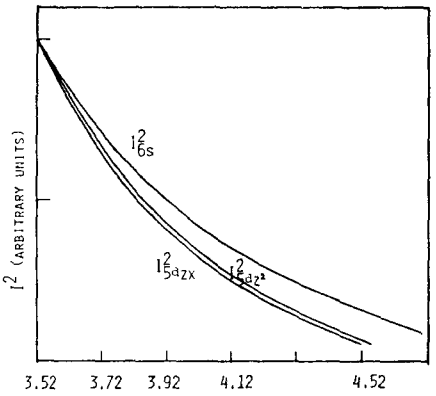

Fig. 2-6.

The value of $I^2(6s)$ ($X = Y = 0, Z$), $I^2(5dz^2)$ ($X = Y = 0, Z$) and $I^2(5dzx)$ ($X = 1.7$, $Y = 0, Z$) as a function of Z. The ratio of $[I^2(5dzx)/I^2(5dz^2)]_{z=z_c}$ is 0.07. S_s is taken as 2.0 Å^{-1}.
The ratio of $[I^2(5dz^2)/I^2(6s)]_{X=0}$ is 0.7.

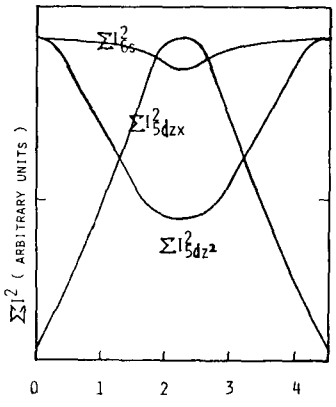

Fig. 2-7.

The ionization probability as a function of X for the assumed most simple case. The X axis is chosen as in fig. 3. The separation distance of the two atoms along the X axis is 4.47 Å.

plane wave method has been reported by Mattheiss[16]. The calculation of $P(\vec{R})$ by using the results of Mattheiss is not performed in this paper because of its complexity.

Knor and Müller[9] have assumed that the atomic orbitals directing the nearest neighbor atoms are dominant in the ionization process. In bcc tungsten, these orbitals are $5d_{ZX}$ and $5d_{YZ}$ for the plane which is being discussed. From the calculated energy band structure by Mattheiss, there is no evidence that only these atomic orbitals are dominant in the sum of the atomic orbitals $\sum_n B_{njk}$, or in the surface integration process.

So, the contribution of all atomic orbitals to the ionization probability $P(\vec{R})$ must be considered. To see how $P(\vec{R})$ depends on the position vector $\vec{R}$, a calculation is performed for the very simple case. At first, $\vec{R}$ varies under the condition that Z is constant ($Z = Z_c$). The assumption is that the j state has only one type of atomic orbital and the total ionization probability is the sum of each non-interacting band, called 6s, $5d_{Z^2}$, etc. Then,

$$P(\vec{R}) = \frac{1}{\sqrt{N}} \frac{2\pi}{\hbar} \frac{\Omega}{(2\pi)^3} \sum_j \int \left| \sum_n I_n(\vec{R} - \vec{R}_l) \exp(i\vec{k} \cdot \vec{R}_l) \right|^2 \frac{1}{|\nabla_k E|} dS, \quad (37)$$

$$\left| \sum_l I_n(\vec{R} - \vec{R}_l) \exp(i\vec{k} \cdot \vec{R}_l) \right|^2 = \sum_l I_n^2(\vec{R} - \vec{R}_l) + 2 \sum_{l \neq l'} I_n(\vec{R} - \vec{R}_l) \times I_n(\vec{R} - \vec{R}_{l'}) \cos[\vec{k} \cdot (\vec{R}_l - \vec{R}_{l'})]. \quad (38)$$

The summation is over the second nearest neighbor lattice site in the surface, as $I_n^2(R) \ll I_n^2(0)$ for large $|R|$;

$$\int_n \left| \sum_l I_n(\vec{R} - \vec{R}_l) \exp(i\vec{k} \cdot \vec{R}_l) \right|^2 \frac{1}{|\nabla_k E|} dS$$

$$= N_n(E) \left[\sum_l I_n^2(\vec{R} - \vec{R}_l) + 2 \sum_{l,l'} A_{l-l'} I_n(\vec{R} - \vec{R}_l) I_n(\vec{R} - \vec{R}_{l'}) \right], \quad (39)$$

where

$$N_n(E) = \int \frac{1}{|\nabla_k E|} dS , \quad (39a)$$

and

$$A_{l-l'} \equiv \int_n \cos[\vec{k} \cdot (\vec{R}_l - \vec{R}_{l'})] \frac{dS}{|\nabla_k E|} \left(\int \frac{dS}{|\nabla_k E|} \right)^{-1} . \quad (39b)$$

In general, $|A_{l-l'}| \ll 1$, as the integrands cancel each other in the surface integration. So, finally $P(\vec{R})$ is approximated by

$$P(\vec{R}) = \frac{2\pi}{\hbar} \frac{1}{\sqrt{N}} \frac{\Omega}{(2\pi)^3} \sum_n N_n(E) \sum_l I_n^2(\vec{R} - \vec{R}_l) . \quad (40)$$

For each atomic orbital, $\sum_l I^2(\vec{R} - \vec{R}_l)$ is shown as a function of X (see Fig.7). From the result, in this simple case it depends on the relative magnitude of $N_n(E)$ whether the ionization probability has a maximum at the point immediately above the atoms or between the atoms.

Next, consider the Z dependence of $P(\vec{R})$ for the simple case mentioned above. The Z dependence of $I_n^2(R)$ has nearly the same half width for some X values. The Z dependence of $P(\vec{R})$ is obtained multiplying that of $N_n(\vec{R})$ by that of $I_n^2(\vec{R})$. The energy E depends on R by eq.(27). From the calculated result of the energy band by Mattheiss, $N_n(E)$ is not expected to make the half width of $P(\vec{R})$ as narrow as 0.2 A (see Section 2.3).

2.2.4 Summary

In the case of ionization from the (001) plane of tungsten, the interaction of metallic 6s, $5d_{Z2}$, $5d_{ZX}$ and $5d_{YZ}$ orbitals with the hydrogen gas atom are important.

The overlap integrals of the $5d_{Z2}$ and 6s orbitals with the hydrogen wave function have a maximum immediately above the surface atoms and those of $5d_{ZX}$ and $5d_{YZ}$ have a maximum at the intermediate region of the surface atoms. It depends on the relative magnitude of these contributions to the ionization probability, whether the total ionization probability has a maximum immediately above the atoms, or intermediate of the atoms. The point image contrast may arise from field adsorption of imaging gases, as will be discussed in the later Sections.

In this treatment, the change of the value of $I_n^2(R)$ from plane to plane, caused by the directional change of the atomic orbitals $\phi_n(r)$ or by considering another atomic orbital, e.g., $5d_{X^2-Y^2}$ and $5d_{XY}$, is one cause of the dependence of the ionization probability $P(\vec{R})$ from plane to plane.

2.3 Ion Energy Distribution of Field Ionized Gas Atoms

The experimental and theoretical results of the half-widths of ion energy distribution are summarized in Table 2. Recent experimental studies by Utsumi[17] and Müller and Sakurai[18] show that the half widths of the ion energy distribution are not so extremely narrow as Boudreaux and Cutler obtained theoretically[5,6]. The calculated values of ours are in good agreement with the recent experimental results.

Table 2-2

Summary of Half-width of the Ion Energy Distribution

Half-width	Method, site	Reference
0.2A	Experiment	Tsong & Muller (10)
0.67A(2eV)	D_2 on (011) W	Sakurai (1)
1.0eV	Above protruding atom	
o.26A	He on (110) W	
o.48A	zone decoration	Utsumi (17)
o.42A	on (121) W	
o.29A	H on (110) W	
0.4A	Theory WKB	Tsong & Muller (10)
0.7A	WKB	Boudreaux (Ph. D. thesis)
0.11A	Time dependent perturbation theory	Boudreaux & Cutler (5)
0.12A	Rearrangement collision Theory	Boudreaux & Cutler (6)
0.38A	Matching wave function method	present work (section 3.1)
0.38A	Oppenheimer's method	Iwasaki & Nakamura (2)
0.32~0.42A 0.7eV	Tight-binding wave metal state	Iwasaki & Nakamura (8)

CHAPTER 3

FIELD IONIZATION PROBABILITY ABOVE ADSORBED SURFACE

To interpret the images of FIM , it is very important to understand how the images are formed when there are metallic or chemisorbed atoms such as Ir and Mo or O_2 and H_2 on a metal surface. Moreover, recent atom-probe experiments by Muller et. al. definitely established the field adsorption of imaging gas atoms such as He, Ne and Ar even above 150K[1]. This apex-adsorbed atom may have a significant effect on the field ionization process. So, the general theory of the field ionization process must take account of this effects.

In section 3.1, field ionization probability on the adsorbed surface is investigated in general, by calculating the transmission coefficient of an electron by matching wave functions in one dimension.

Section 3.2 is devoted for the more detailed calculation of the ionization probability when there are field adsorbed inert gas atoms on the metal surface.

A simple square-well potential, which is parameterized by its depth and the value of its lowest energy bound state, is employed to represent the adsorbate potential, as the low-energy scattering of electrons from finite-range potentials is insensitive to the details of the potential , in section 3.1. The validity and difficalties of a one-dimensional potential model have been extensively discussed by Duke and Alferieff[2].

A detailed introduction to the problems studied in section 3.2 will be given at the biggining of that section.

3.1 One Dimensional Model Calculations of the Transmission Coefficient

Alferieff and Duke[3] has presented the calculation of the ionization probability when there is an adsorbate by deriving the one dimensional transmission coefficient for an electron. Their interest was, however, in the effects of the adsorbate represented by the delta potential, not on the main peak of the ion energy distribution but in the lower energy Jason peaks[4].

Here we study the change of the ionization probability at the main peak due to the adsorption represented by the potential well as shown schematically in fig. 1. Transmission coefficients for an electron are calculated by matching the wave function in each region to construct the state which behaves as the propagating wave into the metal in the metal region[2,5]. The wave functionis expressed in each region R_i (see fig. 1) as follows.

$$\exp(-ik_1x)+ C_1\exp(ik_1x), \qquad (R_1) \quad (1)$$

$$C_2\sqrt{y}\, J_{\frac{1}{3}}(\tfrac{2}{3}\sqrt{\alpha}y^{\frac{3}{2}})+C_3\sqrt{y}\, J_{-\frac{1}{3}}(\tfrac{2}{3}\sqrt{\alpha}y^{\frac{3}{2}}), \qquad (R_2) \quad (2)$$

$$C_4\exp(-ik_3x)+C_5\exp(ik_3x), \qquad (R_3) \quad (3)$$

$$C_6\sqrt{y}\, J_{\frac{1}{3}}(\tfrac{2}{3}\sqrt{\alpha}y^{\frac{3}{2}})+C_7\sqrt{y}\, J_{-\frac{1}{3}}(\tfrac{2}{3}\sqrt{\alpha}y^{\frac{3}{2}}), \qquad (R_4) \quad (4)$$

$$C_8\exp(-ik_5x), \qquad (R_5) \quad (5)$$

where

$$y=Fz-E, \qquad (6)$$

$$\alpha= -(h^2F^2/2m)^{-1}, \qquad (7)$$

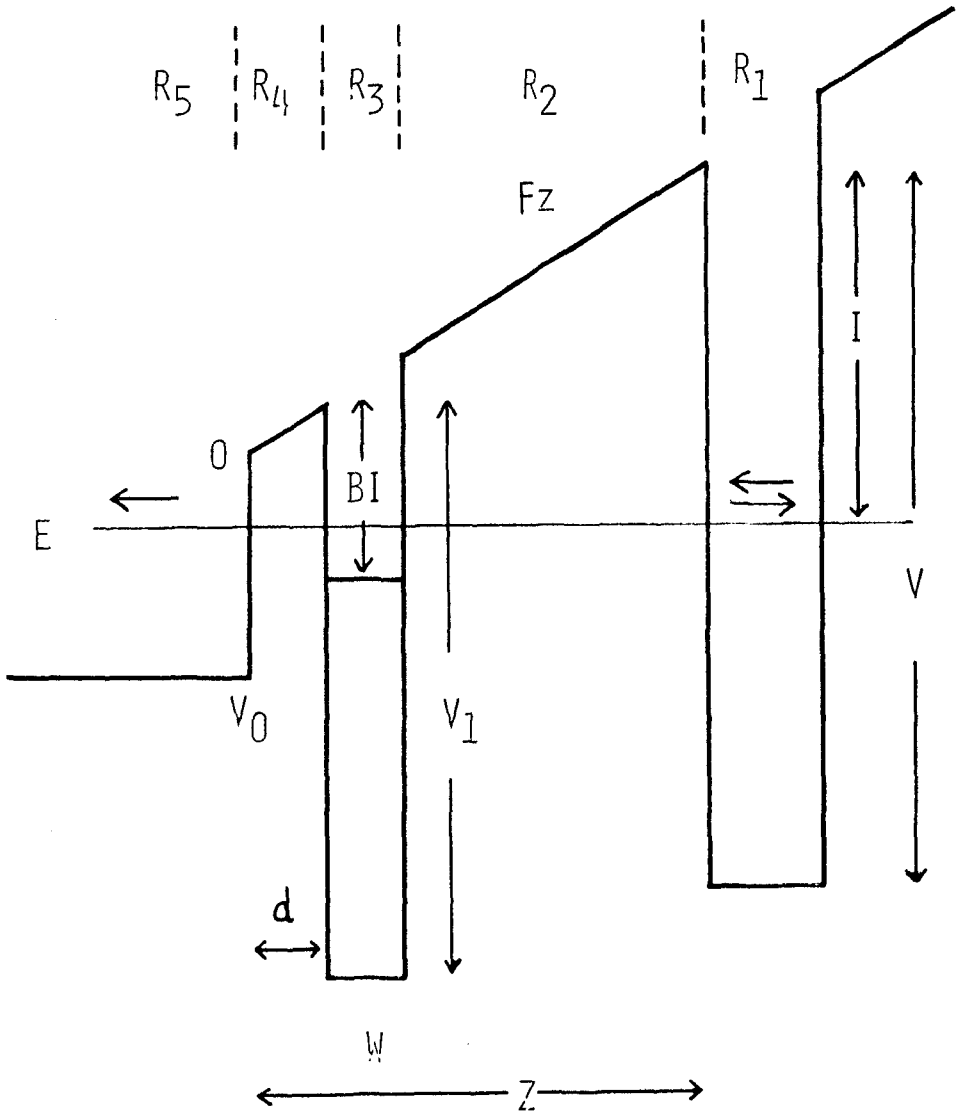

Fig. 3-1. One-dimensional potential energy diagram for an electron in the presence of an adsorbed atom in FIM.

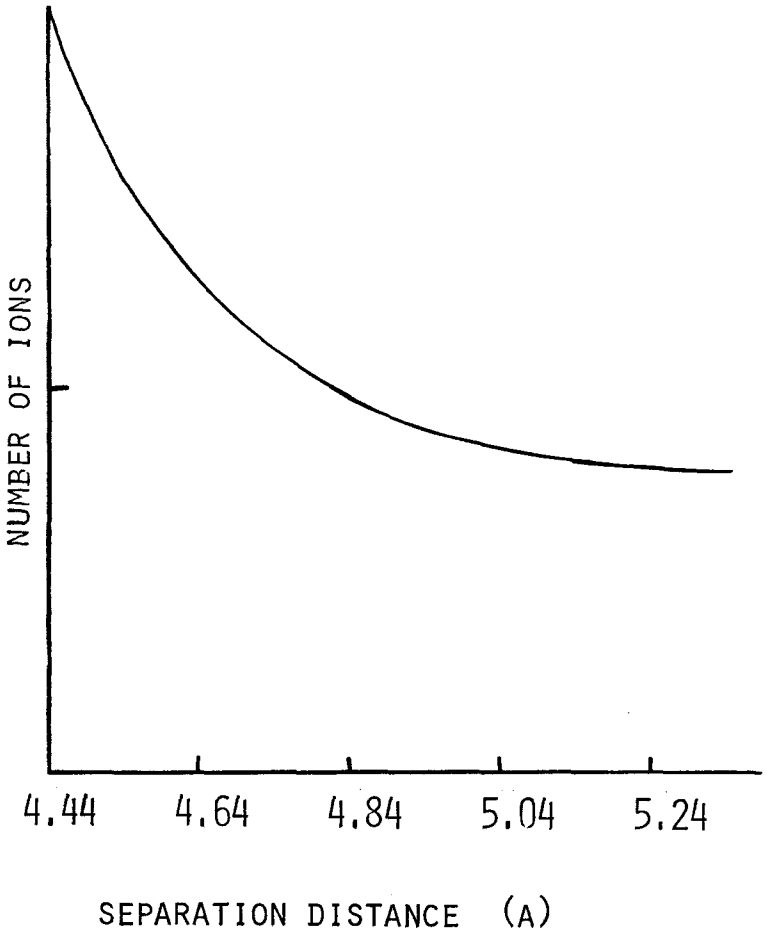

Fig. 3-2a. Ion energy distribution of helium on clean tungsten. F=4.5V/A, I=24.5eV.

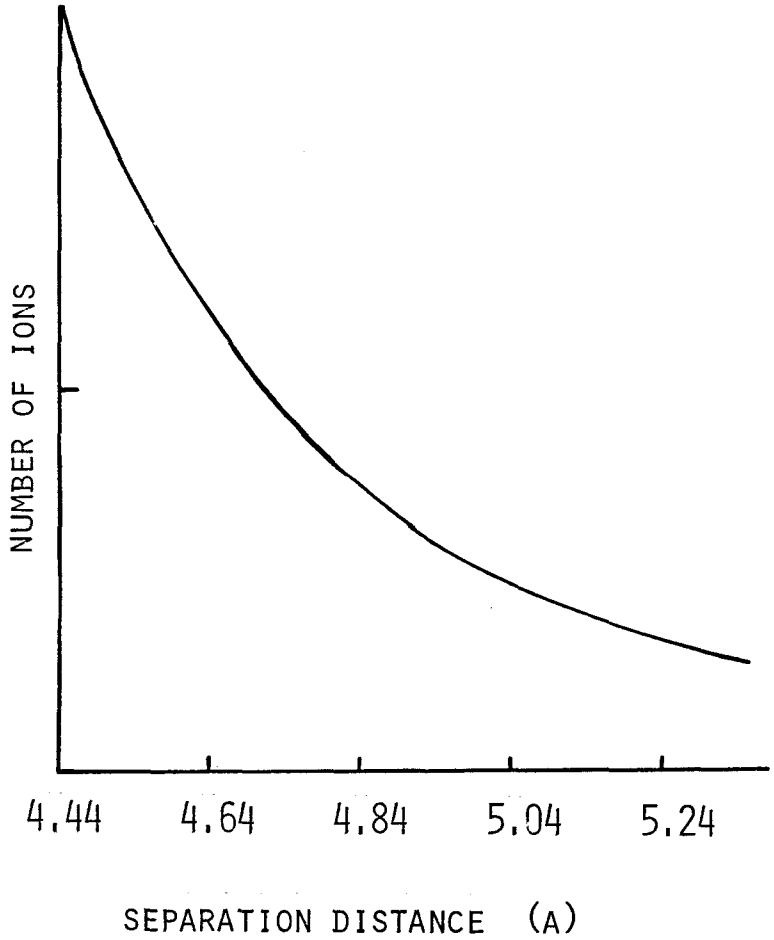

Fig. 3-2b. Ion energy distribution of H_2 on clean tungsten. F=2.5V/A, I=15.6eV.

$$k_i = 2m(E-V_i)/h, \tag{8}$$

$$E=I-FZ, \tag{9}$$

and $J_{\pm\frac{1}{3}}$ are Bessel functions of the indicated order, $F/|e|$ is the field-strength, E is the energy of an tunneling electron measured from the vacume level when field is zero, I is the ionization energy of the gas atom and Z is the distance of it from the metal surface. The matching condisions bring up the simultaneous linear equations for C_i. $|C_8|^2$ gives the transmission coefficient for an electron.

Ion energy distribution of helium and hydrogen on clean tungsten calculated by this method is shown in figs. 2a and b respectively. The relative values of the transmission coefficient when there is an adsorbate to that when surface is clean are summarized in table 1 for various depth V_1, width W and position d of the potential well that represents the adsorbate. W is given by,

$$W=\tan^{-1}(BI/(V_1-BI))^{1/2}/k_3, \tag{10}$$

where BI is the ionization energy of an adsorbate. The ratios as a function of ion energy E are depicted in fig. 3.

The results are summarized as follows.

First, it is shown that the ionization probability is enhanced by the adsorption of small depth and wide width potential well "atom". So, it may be suggested that by the adsorption of atoms with small ionization potential such as alkali atoms and atoms whoes electron affinity are large, bright spots are formed in the FIM image.

It must be noticed, however, that this enhancement does not show the resonance in the ion energy distribution as fig. 3 in

contrast with the case of the field emission[2] . This is due to the fact that in FIM the "size resonance" of the transmission coefficient where E equals BI, can occur but the "symmetry resonance" of it due to the symmetry of the barrier[2] can not by the following reasons. The distance between the adsorbate and the ionizable gas atom is larger than that between the adsorbate and the metal surface as the gas atom must be separated from the metal than the critical distance (see fig.1. A gas atom has one electron when its ground state energy E is smaller than the Fermi energy of the metal.). Moreover, the ionization potential of the gas atom is much greater than the work function of the metal.

So, one should not expect that the enhancement of the ionization probability by the adsorption necessarily add a peak or shoulder in the ion energy distribution. This speculation is consistent with a recent paper by Sakurai et al.[6] . They have shown that a field-adsorbed hydrogen promote field ionization with neither a shift in the peak nor a broadening of the width of the energy distribution of helium ions.

Next, it is shown that the ionization probability is sometimes reduced by the adsorption of an atom represented by the deep depth and narrow width potential well (see table 1 and fig.3). This potential well may be associated with the inert gas in the point of view of the strong pseudopotential model[2] . Duke and Alferieff [2] have investigated the influence of the shape of the potential on the transmission coefficient by computing it for potentials with a fixed BI and well depths V_1=

Table 3-1

Enhancement factor of the ionization probability at the main peak for helium on tungsten. The position of the potential well d is chosen to be 1.0A.

V_1 \ BI(eV)	5.0	15.0	25.0
BI x 2.5	5.55 (0.48)*	2.16 (0.28)	1.24 (0.22)
x 5	1.99 (0.20)	1.07 (0.12)	0.75 (0.09)
x 7.5	1.47 (0.13)	0.89 (0.07)	0.66 (0.06)
x10	1.27 (0.09)	0.82 (0.05)	0.62 (0.04)
x12.5	1.17 (0.07)	0.78 (0.04)	0.60 (0.03)

* The number in the parentheses indicate the width of the potential well W in A units.

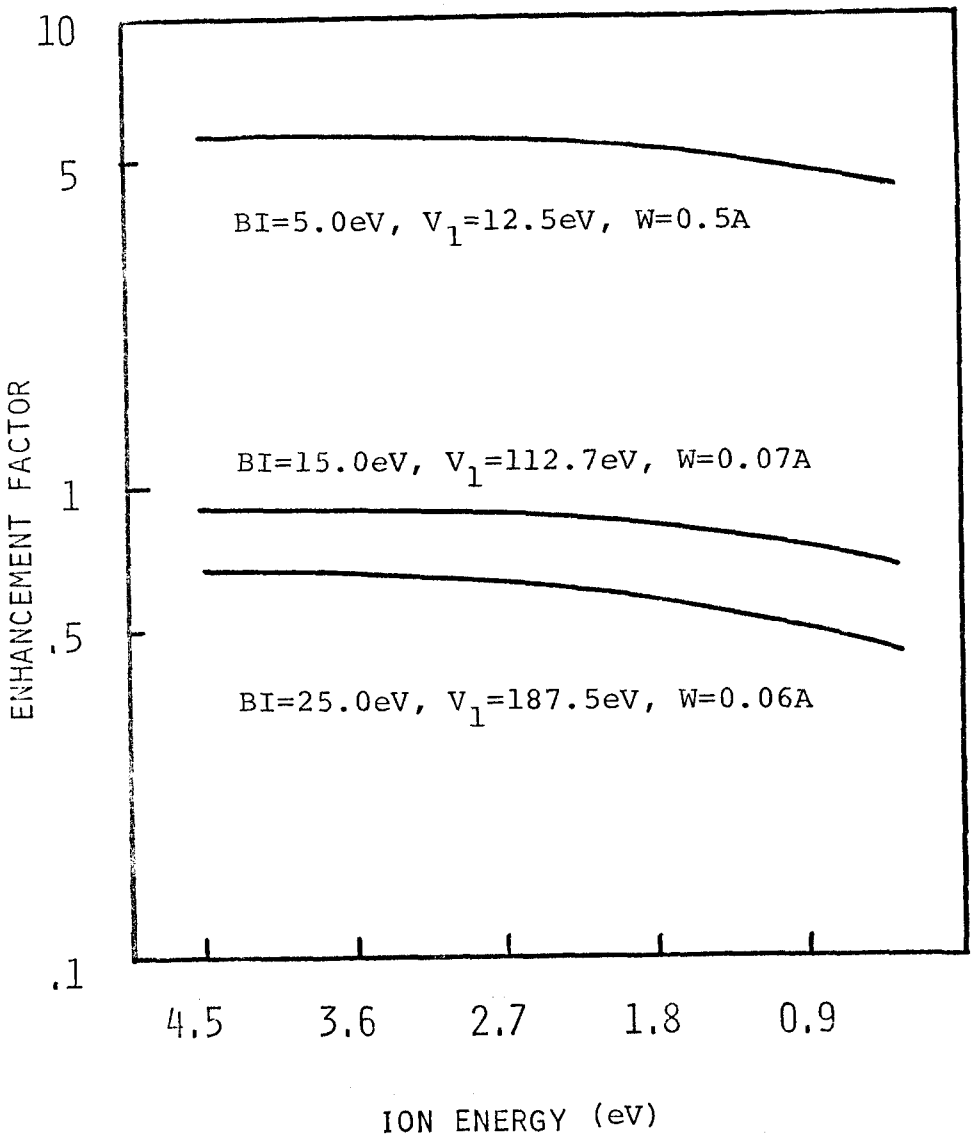

Fig. 3-3. Enhancement factor of ionization probability of helium by field adsorption.

2BI, 5BI, 10BI and 100BI. They pointed out that the increasing of the transmission coefficient in the strong-pseudopotential model of neutral adsorbates for small V_1 (or for large W) may by reinterpreted as an increase in the transmissivity of the barrier because a wider " hole " has been cut out of the barrier. Therefore, we may conclude that the possibility of a reduction in the transmission coefficient by neutral adsorbates is a general feauture of the model, omitting the result for BI=25.0eV and V_1=2.5 BI in table 1.

This is the result of the exact calculation of the one-dimensional problem of the transmission probability and does not result from the WKB treatments of it. This result is similar to that of the field emission[2] . Namely, only the exact calculation agreed to the fact that by the adsorption of nitrogen on tungsten, the emission current is reduced. So, one should not expect the increase of the ionization probability from the point of view of the WKB approximation as Tsong[7] did.

This reduction of the ionization probability is consistent with the more detailed study of the field adsorption effects on the field ionization probability[8,9] . The experimental observation that ion current is increased by the field adsorption[10] may be explained by both the increase of the capture probability for incident supply and the decrease of the escape probability for trapped particles by the field adsorption discussed in later chapters.

3.2 Three Dimensional Calculation of the Field Adsorption Effects on the Field Ionization Probability

3.2.1 Introduction

Tsong and Müller[11,12] have shown that the noble gas atom adsorbes at the apex of the individual surface atom of the field ion microscope (FIM) tip by the field-induced dipole-dipole interaction, after the experimental establishment of the field adsorption by Müller[13]. A few experiments have shown that these field adsorbed noble atoms increase the field ion current[10,14-16].

We develop here the theory of the effects of the field adsorption on the ionization probability [8] in detail as the field adsorption takes place under normal conditions.

Many body effects of electrons such as the exchange and the correlation effects may play an important role on the process as a tunneling electron passes through the closed-shell systems of a field adsorbed inert gas atom and so they must be properly included in the theory.

Recently Nolan and Herman have reported that the time-dependent perturbation calculation which includes exchange effects between the adsorbate electronic orbitals and the ionizable He atomic orbitals shows the enhancement of the ionization rate of the He gas atoms by a factor of 3 to 5 for helium as the adsorbate, 30 to 90 for neon and 10^4 for argon[17]. In their treatment, the interaction potential does not contain the field term as the atomic state of the imaging gas atom in the initial state and the metallic states in the final states are assumed to be those in the presence of the field. However, the actual wave function of the gas atom used in the calculation is

that for no field. As a result the field term is neglected in the interaction potential to which ionization rate is very sensitive. This decomposition of the total Hamiltonian may be regarded as that of case 1 in section 2.1 and on the other hand, the perturbation potential H' which they used is composed of only $V_e(r,R)$, instead of $V_e(r,R) + eFz$. Probably, the rather high enhancement factor may be due to the perturbation potential which is largest in the region between the adsorbed atom and the metal because it does not contain uniform-field-type terms. Indeed in the later modified calculations Nolan and Herman used the distorted electronic wave function of gas atom by the field and obtained small enhancement factor for He (1-0.4) and Ne (2-10)[9]. In this case, their choise of the initial and the final states may be regarded as that of case 2 in table 1 of chapter 2.

We start by orthogonalizing the limited basis. On the basis of these new defined orthonormal set, the expression of the ionization probability is derived which include not only the similar term discussed by Nolan and Herman i. e. the product of the overlap integral and one body hopping matrix elements, but also those terms which represents the transition of an electron by Coulomb interaction.

3.2.2 Theoretical Considerations

The systems of the helium gas imaging a tungsten tip with helium, neon and argon as the adsorbate are considered. A limited basis consisting of the isolated self-consistent He-atom orbitals denoted by ϕ_{He}, the isolated self-consistent adsorbed-atom orbitals ϕ_A and the self-consistent eigenstates ϕ_k of the semi-infinite metal under the electric field and under the

presence of the ion core of the gas atom will be adopted.

Now let us introduce a new orthogonal set $\{\psi_\lambda\}$ made by nonorthogonal set $\{\phi_\lambda\}$ and define creation and destruction operators C_μ^+ and C_μ for every spin orbitals ψ_μ.

Then the Hamiltonian operator for the system is written as[18]

$$H = \sum_{rs\sigma} C_{r\sigma}^+ \tilde{V}_{rs} C_{s\sigma} + \frac{1}{2} \sum_{ijkl} \tilde{V}_{ijkl} C_i^+ C_j^+ C_k C_l \quad , \tag{11}$$

where $\tilde{V}_{rs}$ is matrix elements of the one body operator H_0 of the system in the ψ representation and

$$\tilde{V}_{ijkl} = \int \psi_i^*(r_1) \psi_j^*(r_2) \frac{e^2}{r_{12}} \psi_k(r_2) \psi_l(r_1) d\tau_1 d\tau_2 . \tag{12}$$

For the system discussion H_0 is

$$H_0 = P^2/2m + V_m(r) + V_{He}(r) + V_A(r) + eFZ \quad , \tag{13}$$

$$V_m(r) = \sum_{\text{metal}} \frac{-Z_m e^2}{|r - R_m|} \quad , \tag{13a}$$

$$V_{He}(r) = \frac{-2e^2}{|r - R_{He}|} \quad , \tag{13a}$$

$$V_A(r) = \frac{-Z_A e^2}{|r - R_A|} \quad . \tag{13b}$$

where the coordinate system is shown in Fig. 4 and Z_m and Z_A is the atomic number of the metal atom and adsorbate respectively and the last term represents the effects of the uniform field.

We can obtain another expression of H[18] where the operators b_r^+ and b_r create and destroy electrons in the basis state ϕ_r as

$$H=\sum_{\substack{rstu\\ \sigma}} b_{r\sigma}^{+}\chi_{rs}^{+}V_{st}\chi_{tu}b_{u\sigma}+\frac{1}{2}\sum_{ijlm}b_i^{+}b_j^{+}\Big(\sum_{rstu}\chi_{ir}\chi_{js}\,V_{rstu}\chi_{ul}\chi_{tm}\Big)b_l b_m, \tag{14}$$

where each matrix element V_{st} and V_{rstu} is ϕ representation and χ is inverse matrix of overlap matrix of basis set $\{\phi_\lambda\}$.

The transition probability between $\Phi_i=b_{He\uparrow}^{+}b_{He\downarrow}^{+}\prod b_A^{+}\prod b_k^{+}|V\rangle$ and $\Phi_f=b_{k\uparrow}^{+}b_{He\downarrow}^{+}\prod b_A^{+}\prod b_k^{+}|V\rangle$ may be calculated by using H expressed in eq.(14). Although the initial and the final state is defined straightforwardly, it may be too complicated to calculate the transition probability between the states defined above, because the expressions of the matrix elements are complicated and the usual Fermi-Golden rule can not be used as b_r^{+} and b_r does not obey the usual Fermion anti-commutation rules.

To avoid the difficulty discussed above, we can use the expression of Hamiltonian shown in eq.(11). The calculation of the transition probability may be straightforward on the basis of the Hamiltonian expressed in eq. (11)but we must take care in the definition of the new basis set $\{\psi_\lambda\}$, the initial and the final states, that they describe well the physical process that an electron transits from the He gas atom to the metal.

After the definition of $\{\psi_\lambda\}$, the total Hamiltonian of the system may be devided into the diagonal part H_d and the off-diagonal part H_{od}.

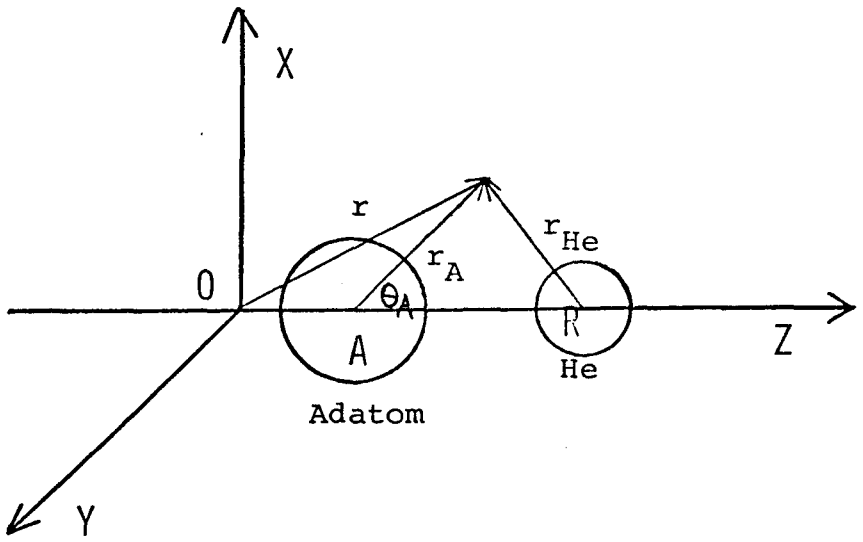

Fig. 3-4. The diagram of the system. The XY plane is defined as the metalic surface and the coordinate system is shown.

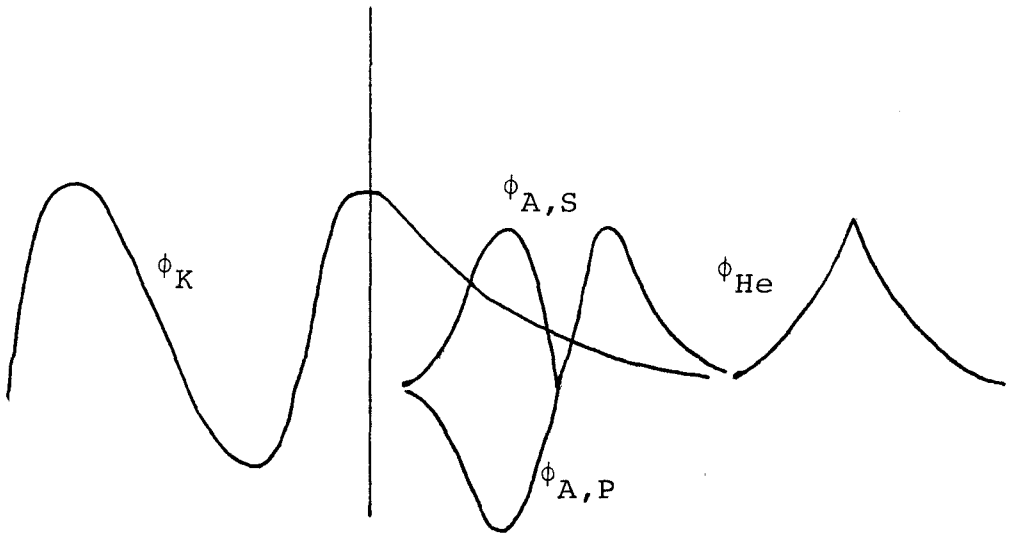

Fig. 3-5. Schematic diagram of wave functions used in Coulomb term V_{AKAHe},

$$V_{AKAHe}=\int\phi_A^*(r_1)\phi_K^*(r_2)\frac{e^2}{r_{12}}\phi_A(r_2)\phi_{He}(r_1)d\tau_1 d\tau_2 .$$

$$H_{od}=(\sum_{\sigma k'}V_{k'He}C^{+}_{k'\sigma}C_{He\sigma}+\sum_{A\sigma}\tilde{V}_{AHe}C^{+}_{A\sigma}C_{He\sigma}$$
$$+\sum_{Ak'\sigma}V_{Ak'}C^{+}_{A\sigma}C_{k'\sigma})+\text{(h. c.)}$$
$$+1/2\sum{}'\tilde{V}_{ijlm}C^{+}_{i\sigma}C^{+}_{j\sigma'}C_{l\sigma'}C_{m\sigma}, \qquad (15)$$

where the summation of the last term exclude those terms which lead to the product of the number operators and so are included in H_d.

Then, the transition probability between the initial state $\Psi_i=C^{+}_{He\uparrow}C^{+}_{He\downarrow}\prod C^{+}_{A}\prod C^{+}_{k'}|V\rangle$ and the final state $\Psi_f=C^{+}_{k\uparrow}C^{+}_{He\downarrow}\prod C^{+}_{A}\prod C^{+}_{k'}|V\rangle$ is expressed as follows,

$$P=(2\pi)^{2}\hbar^{-1}N(\epsilon_k)|\langle\Psi_f|H_{od}|\Psi_i\rangle|^{2}, \qquad (16)$$

where $N(\epsilon_k)$ is the density of states.

According to eq.(15), the transition matrix element is

$$M\equiv\langle\Psi_f|H_{od}|\Psi_i\rangle=\tilde{V}_{kHe}+\tilde{V}_{HekHeHe}$$
$$+\sum_{A\sigma}\tilde{V}_{A\sigma kHeA\sigma}+\sum_{k'\sigma}\tilde{V}_{kk'\sigma k'\sigma He}$$
$$-\sum_{A}\tilde{V}_{AkAHe}-\sum_{k'(\text{occup.})}\tilde{V}_{k'kk'He}. \qquad (17)$$

Now we define Ψ_λ as follows.

$$\Psi_A = \phi_A \ ,$$

$$\Psi_{He} = \phi_{He} - \sum_{A'} \phi_{A'} \langle A' | He \rangle \ ,$$

$$\Psi_K = \phi_K - \sum_{A'} \phi_{A'} \langle A' | K \rangle - \phi_{He} \langle He | K \rangle \ , \quad (18)$$

where hereafter each bra and ket vector means corresponding state.

The set $\{\Psi_\lambda\}$ defined above may be regarded orthonormal to the order of the square of the overlap integrals.

The transition matrix elements M is calculated by introducing eq.(12), (13) and (18) to eq.(17). The details of the derivation of the transition matrix elements are described in Appendix 2.

Finally one obtains the transition matrix elements M as

$$\begin{aligned} M = {} & \langle K | eFZ\ \Theta(z) + U | He \rangle - \langle K | He \rangle \langle He | eFZ\ \Theta(z) + U | He \rangle \\ & - \sum_{A'A''} \langle K | \{ eFZ\ \Theta(z) + U + V_{HF,He} \\ & - |A''\rangle\langle A''| eFZ\ \Theta(z) + U + V_{HF,He} \} | A' \rangle \langle A' | He \rangle \\ & - \sum \langle K | A' \rangle \langle A' | eFZ\ \Theta(z) + U - |E_{He}| | He \rangle \\ & - \sum_{A'} V_{A'KA'He} + \sum_{A'A''} \langle K | A' \rangle V_{A''A'A''He} \ , \end{aligned} \quad (19)$$

where U(r) and $V_{HF,He}$ is the Hartree-Fock potential of the metal and helium respectively and E_{He} is the first ionization energy of helium.

In the above expression, the one body interactions in each

terms are formulated and the matrix elements representing the transition by Coulomb interaction are shown. The other terms than the first two terms represent the field adsorption effects on the transition probability.

Now, the level width function $\Gamma(\epsilon)$ of the net level density of the imaging gas atom $\rho_{He}(\epsilon)$ without adsorbate is derived following Grimley[18] as

$$\Gamma(\epsilon_K) = \pi \sum_{K'} \left| \epsilon_K S_{HeK'} - V_{HeK'} \right|^2 \delta(\epsilon_K - \epsilon_{K'})$$

$$\doteqdot \pi \left| \epsilon_K S_{HeK} - V_{HeK} \right|^2 \quad N(\epsilon_K) \qquad , \qquad (20)$$

if imaging gas interacts with S electron of the metal and $N(\epsilon)$ is a slowly varying function. The transition matrix element derived from this level width is equivalent to the first two terms in eq.(19). The second term assures that the transition probability converge to that of space ionization when imaging gas is far apart from the metal surface.

3.2.3 Discussion and Results

The potential U(r) + eFZ Θ(Z) is assumed to have the form given by Boudreaux and Cutler(eqs.(2-26a,b)). The metal wave function used is givenby(2-16,17)The adatom wave functions are approximated by the Slater-type orbitals. The inner core orbitals and the P_x and P_y orbitals are neglected as their contributions to M are very small. The distance of the adsorbed atom from the metal surface is 1.0 A for He, 1.2 A for Ne and 1.4 A for Ar and $|E_{He}|$ = 24.46 eV. For F = 5.0 V/A and at helium metal separation distance 4 A, the transition matrix element M is calculated on a computer and each term of eq. (19)

is shown in Table 2 indicated by the number in the parentheses. Enhancement factor means |total transition matrix element / direct transition matrix element|^2.

If the basis set $\{\Phi_\lambda\}$ are orthogonal to each other, M contains only the first term and the 5th Coulomb interaction term of eq.(19). V_{AKAHe} is positive for S orbital of Φ_A and negative for p orbitals (see Fig. 5). As the former term is positive and absolute value of the two terms are same order of magnitude the S state of the adsorbate suppress the transition probability and the p state enhance it. As a result, in this case of the approximation of orthogonal basis $\{\Phi_\lambda\}$, the ionization probability is suppressed by the helium field adsorption and may be a little changed by the Ne or Ar field adsorption.

In general, S orbital contribution of adsorbate of eq.(19) is the opposite sign to the direct term but that of p orbital is the same sign to it in the same way as V_{AKAHe}. As a result the transition probability is suppressed by the field adsorption of He considerably. For the case of Ne adsorption, the contribution of S and p orbital cancel each other and the transition probability is somewhat decreased by the field adsorption. For the case of Ar adsorption, p orbital contribution is superior to S orbital contribution and the transition is somewhat enhanced.

Each term of the matrix element shown in Table 4 shows the sharp decrease as the separation of the gas atom from the metal surface becomes large but the total ionization matrix element obtained by the cancellation of each term show rather slow decrease.

The ion current may be increased by the field adsorption of helium by the increase of the population of ionizable gas atom

in the ionization zone in spite of the decrease of the ionization probability of the imaging gas atom itself. This situation will be clarified in later Chapters on the basis of gas kinetical theory of FIM.

Table 3-2

Calculated values of the each term of the transition matrix element M

Adsorbate	He	Ne	Ar
Direct transition (1+2)	-1.163	-1.163	-1.163
Transition due to overlap $\langle A \mid He \rangle$ (3)	0.110	-0.022	-0.687
Transition due to overlap $\langle K \mid A \rangle$ (4)	1.018	0.203	-0.455
Transition due to Coulomb interaction (5+6)	0.329	0.034	0.014
Total transition matrix element	0.294	-0.948	-2.291
Enhancement factor	0.064	0.664	3.88

Calculated values for F = 5.0 V/Å at R_{He} = 4.0 Å in arbitrary units. The number in the parentheses indicate the term in eq.(19).

CHAPTER 4

ION CURRENT GENERATION IN THE FIELD ION MICROSCOPE: I DYNAMIC APPROACH

Notation used in this chapter

ρ closest approach to the tip center for a particle

v velocity of a particle far from the emitter

v_p dipole attraction velocity

$E_p = mv_p^2/2 = \alpha F^2/2$, where m and α are the mass and polarizability of a particle, respectively and F is field strength

v_n, v_t normal and tangential velocity components of a particle at the emitter surface

$N_n(v_n)$, $N_t(v_t)$ rates at which particles strike unit emitter surface per unit time, with velocity components

$Pe(v_n', v_t')$ probability for a particle, which hit the emitter with velocity (v_n', v_t'), to escape from the emitter

$N(v, T_g)$ rates, at which particles strike unit emitter surface per unit time, as a function of v and gas temp. T_g

$K_e(v, T_s)$ probability for particles to escape after the first impact or in their few hops as a function of v and tip temperature T_s

4.1 Introduction

The ion current generation in the field ion microscope (FIM) has been studied by Müller[1], Gomer[2] and Southon[3] dynamically. In the treatises, the total gas supply to the field-ion emitter surface is found. The rate constants for ionization and escaping from the tip region without ionization are calculated and finally the total ion current is obtained.

Really, the supply of captured atoms must be used instead of the total supply as Southon[3] has indicated. Both rate constants and the probability of capture[3] are the quantities averaged over the velocity distribution of the particles at the tip region in equilibrium and so are the functionals of the distribution function .

In this paper, instead of calculating the averaged quantities such as effective ionization rate constant on the basis of assumed somewhat ambiguous velocity distribution, ion current is shown to be able to calculate thoroughly dynamically. The incident trajectories and rebounds of all particles are tracked and the ionized fractions generated in passing through the ionization zone are summed up. The simplification that the particles scattered from an emitter surface have the average velocity is employed. It enabled us to get easily the information on the influence of the many variables such as the tip temperature and the gas temperature, in the field range where particles are ionized in a few hops.

In tbe succeding chapter[4], the velocity distribution of the particles at the tip region is derived by the quasi-static approach.

4.2 The Supply Function

In analyzing the hopping process of gas particles, it will be assumed for simplicity that the emitter is spherical. Then, the magnitude of the electric field F is given by

$$F(r) = F_t(R_t/r)^2 , \qquad (1)$$

where F_t is the electric field at the tip surface, r is the

distance to the center of the tip and R_t the tip radius.

A particle approaching the tip with, v, its velocity when very far from the tip, and ρ, the distance of closest approach to the tip center if the electric field were zero, has radial and tangential velocity, $v_n(r)$ and $v_t(r)$. Those are found assuming the conservation of energy and angular momentum as follows.

$$v_n(r) = v\left\{1 - (\rho/r)^2 + (v_p/v)^2 \cdot (R_t/r)^4\right\}^{1/2} , \tag{2a}$$

$$v_t(r) = v\rho/r , \tag{2b}$$

where

$$mv_p^2/2 = E_p = \alpha F_t^2/2 , \tag{2c}$$

and v_p is a dipole attraction velocity, E_p is the polarization energy of a gas atom, α is its polarizability and m its mass.

The number of gas particles that pass through a certain plane far from the tip in unit time with v between v and v + dv and ρ between ρ and $\rho + d\rho$ is called $N(v,\rho)dvd\rho$. As the velocity distribution is Maxwellian far from the tip, $N(v,\rho)dvd\rho$ is given by

$$N(v,\rho)dvd\rho = n(m/2\pi kT_g)^{3/2} v^3 \exp(-mv^2/2kT_g) \cdot 2\pi\rho\, d\rho\, dv , \tag{3}$$

where n and T_g are the density and the temperature of the ambient gas respectively and k is the Boltzmann constant. From eqs.(2a) and (2b)

$$\rho\, d\rho = -(R_t/v)^2 v_n dv_n , \tag{4a}$$

$$\rho\, d\rho = (R_t/v)^2 v_t dv_t , \tag{4b}$$

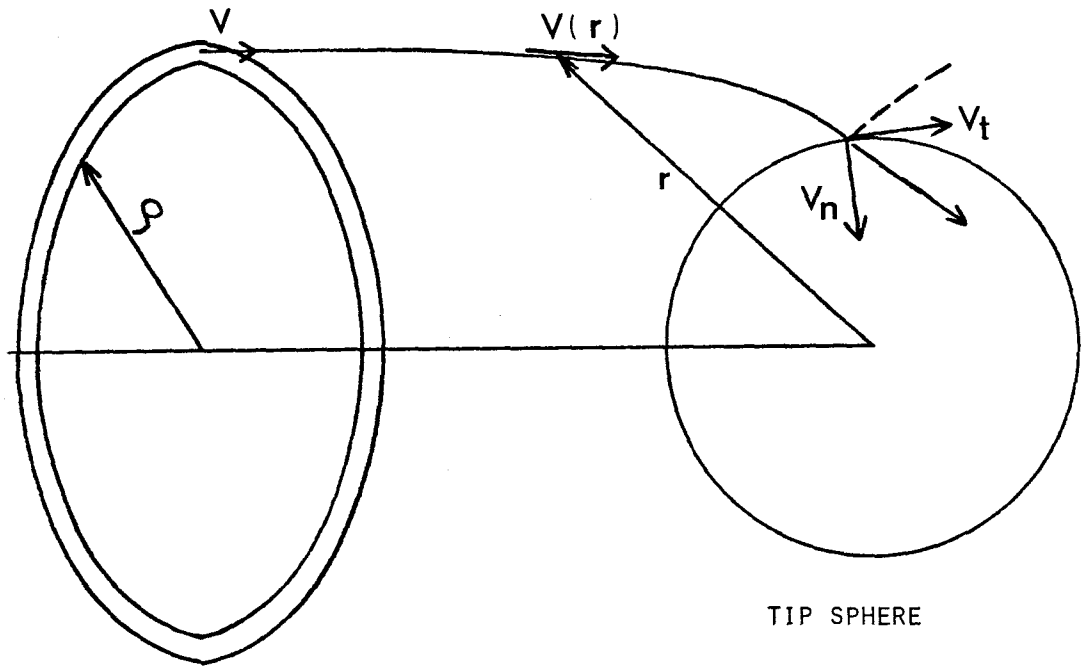

Fig. 4-1. A trajectory of a gas particle from field free region to the tip surface. v_n and v_t are the velocity components at the tip surface.

where v_n and v_t are equal to $v_n(R_t)$ and $v_t(R_t)$, respectively. The numbers of particles that approach the tip from a given direction with v between v and v + dv and hit the tip surface in unit time with v_n between v_n and $v_n + dv_n$ and with v_t between v_t and $v_t + dv_t$ are called $N(v,v_n)dvdv_n$ and $N(v,v_t)dvdv_t$, respectively. We obtain from eq.(3) and eqs.(4a) and (4b)

$$N(v, v_n)dvdv_n = n(m/2\pi kT_g)^{3/2} \, v \exp(-mv^2/2kT_g) \, 2\pi R_t^2 v_n dvdv_n \, , \tag{5a}$$

$$N(v, v_t)dvdv_t = n(m/2\pi kT_g)^{3/2} \, v \exp(-mv^2/2kT_g) \, 2\pi R_t^2 v_t dvdv_t \, . \tag{5b}$$

For a given value of v, the maximum value $\rho_{max}(v)$ of ρ, at which the particle will reach the tip, exists[5]. So, there exist minimum values $v_{min}(v_n)$ and $v_{min}(v_t)$ of v at which the particle will hit the tip surface with a given v_n and v_t, respectively.

$$v_{min}(v_n) = \begin{cases} v_p - v_n & \text{for } v_n < v_p \, , \\ (v_n^2 - v_p^2)^{1/2} & \text{for } v_n > v_p \, , \end{cases} \tag{6a}$$

$$v_{min}(v_t) = \begin{cases} v_t^2/(2v_p) & \text{for } v_t < \sqrt{2}\, v_p \, , \\ (v_t^2 - v_p^2)^{1/2} & \text{for } v_t > \sqrt{2}\, v_p \, . \end{cases} \tag{6b}$$

The numbers of gas particles that hit unit tip surface in unit time with v_n between v_n and $v_n + dv_n$ and with v_t between v_t and $v_t + dv_t$ are called $N_n(v_n)dv_n$ and $N_t(v_t)dv_t$, respectively. We obtain from eqs.(5a) and (5b) and eqs.(6a) and (6b)

$$N_n(v_n) = \int d\Omega \int_{v_{min}(v_n)}^{\infty} dv\, N(v, v_n)/4\pi R_t^2$$

$$= S_0(m/kT_g) \cdot \begin{cases} v_n \exp[-m(v_p - v_n)^2/2kT_g] & \text{for } v_n < v_p \,, \\ \exp(E_p/kT_g)\, v_n \exp(-mv_n^2/2kT_g) & \text{for } v_n > v_p \,, \end{cases} \qquad (7a)$$

$$N_t(v_t) = \int d\Omega \int_{v_{min}(v_t)}^{\infty} dv\, N(v, v_t)/4\pi R_t^2$$

$$= S_0(m/kT_g) \cdot \begin{cases} v_t \exp[-(mv_t^2/2)^2/(4E_p\, kT_g)] & \text{for } v_t < \sqrt{2}\, v_p \,, \\ \exp(E_p/kT_g)\, v_t \exp(-mv_t^2/2kT_g) & \text{for } v_t > \sqrt{2}\, v_p \,, \end{cases} \qquad (7b)$$

$$S_0 = n(kT_g/2\pi m)^{1/2} \,, \qquad (7c)$$

and S_0 is the supply function in the absence of the electric field and Ω is the solid angle. The distributions, $N_n(v_n)$ and $N_t(v_t)$, for helium, at F_t = 4.5 V/A are depicted in fig.2. The thermal velocity, $v_{th} = (kT_g/m)^{1/2}$ is also indicated in fig.2. The numerical value of velocity is expressed by the value of the reduced velocity defined as $\sqrt{mv^2/2}$ in $[eV]^{1/2}$.

The incident particle characterized by ρ near $\rho_{max}(v)$ will be accelerated by the dipole attraction force to have a large value of v_t. As can be seen from fig.2, no small fraction of particles arrive at the tip surface with large tangential velocities. Differentiating $N_t(v_t)$ with respect to v_t, we obtain the most probable tangential velocity, v_{tm}.

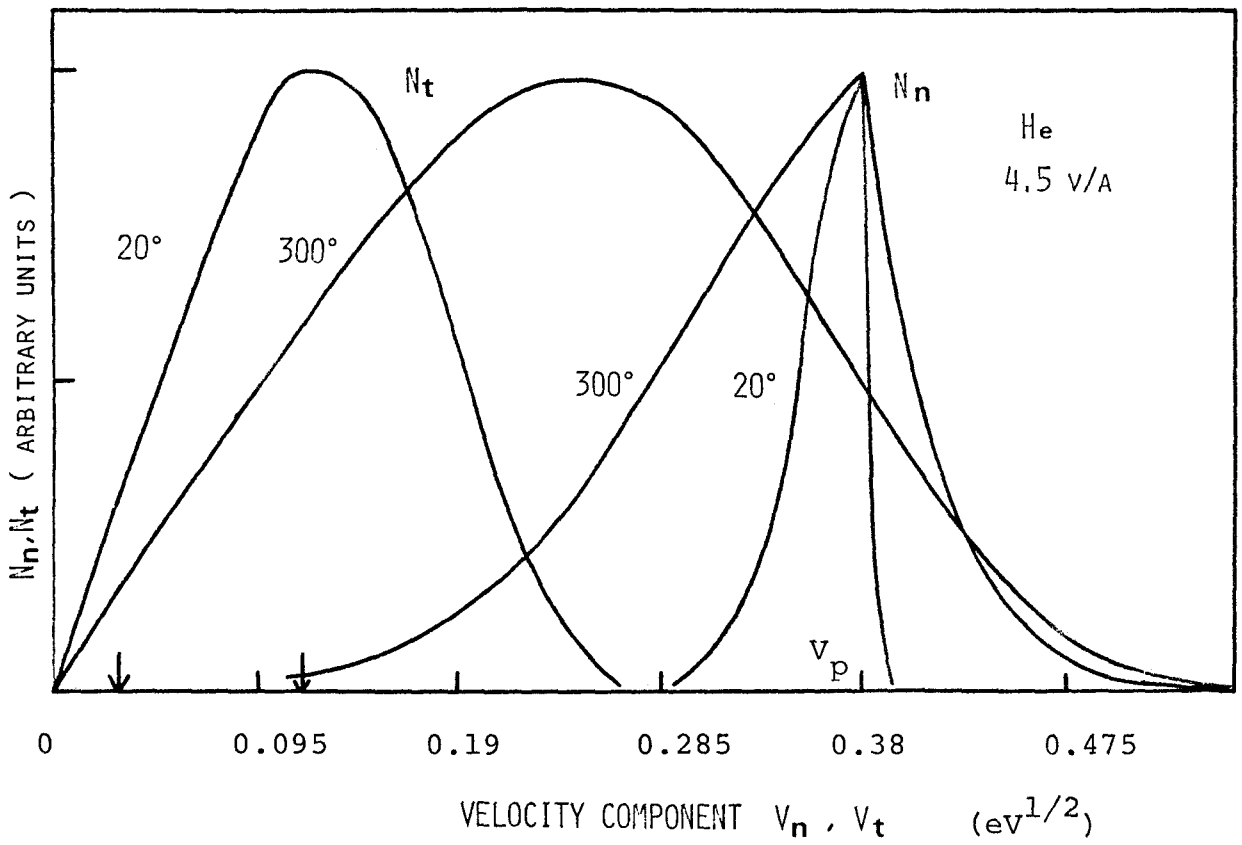

Fig.4-2. Distributions of supplied particles, $N_n(v_n)$ and $N_t(v_t)$ for helium, at a field strength of 4.5 V/A. v_p (eq.(2c)) is 0.38 $eV^{1/2}$. The ratios of the maximum values N_n (300°)/N_n (20°) and N_t (300°)/N_t(20°) are 0.017 and 0.034, respectively. Values of thermal velocity, v_{th} are shown by the arrows.

$$v_{tm} = (2/m)^{1/2} \ (kT_g \cdot E_p)^{1/4} \ . \qquad (8)$$

We obtain the supply function S by integration as follows.

$$S = \int_0^{\infty} dv \int_0^{\rho_{max}(v)} d\rho \ N(v, \rho)$$

$$= \int_0^{\infty} dv_n \ N_n(v_n)$$

$$= S_0 \left\{ (\pi \ E_p/kT_g)^{1/2} \ \mathrm{erf}[(E_p/kT_g)^{1/2}] + \exp(-E_p/kT_g) \right\} \ . \qquad (9)$$

This is the formula for S as derived by Southon[3] .

4.3 Ion Current Generation

Now we introduce the collision matrix following Van Eekelen[5] : particles that have hit the surface with velocity (v_n', v_t') rebound with a velocity distribution $W(v_n , v_t)$ $= b(v_n , v_t , v_n', v_t')$. The collision matrix is derived on the basis of classical "hard cube model"[6] (see appendix 3). A particle that left the surface with velocity (v_n , v_t) has a radial kinetic energy E(r) at distance r from the center of the tip as follows.

$$E(r) = mv_n^2(r)/2$$

$$= mv_n^2/2 + mv_t^2/2 \ [1 - (R_t/r)^2] - E_p[1 - (R_t/r)^4] \ . \qquad (10)$$

A particle will escape if its kinetic energy E(r) is positive for any r and otherwise it will return to the tip and hit the surface again. There exists the minimum value v_{nc} of v_n at

which E(r) has no zeros and so a particle can escape.

$$v_{nc} = v_p(1 - mv_t^2/4E_p) \quad . \tag{11}$$

Then, an incident particle with initial velocity v will be eventually trapped if it looses kinetic energy, by collision with the surface, more than $mv^2/2 - (mv_t^2/2)^2/4E_p$ instead of $mv^2/2$.

When a particle, which has velocity (v_n , v_t) at the surface, passes through the ionization zone, it is ionized with the probability $Q(v_n , v_t)$. The probability Q is given by

$$Q(v_n , v_t) = 1 - \exp[-t(v_n , v_t)/\tau \ ] \ , \tag{12}$$

where

$$t(v_n , v_t) = \int_{R_t+Z_c}^{R_t+Z_c+d} \frac{dr}{|v_n(r)|} \ , \tag{13}$$

and τ is the ionization lifetime of a particle in the ionization zone which is Z_c above the surface and whose depth is d. $v_n(r)$ in eq.(13) are given by eq.(2a) and by eq.(10) for a newly arriving particle from field free region and for a rebounding particle, respectively. We use the formula for τ given by Gomer[2] .

$$\tau = \nu^{-1} \exp[0.68(I - \Phi) \ (I - 7.6 \ F_t^{1/2})^{1/2}/F_t], \tag{14}$$

with the ionization energy I and the work function Φ in eV, and F_t in V/A; ν is the orbital frequency of the tunneling electron in the gas atom.

Particles that have arrived at the tip surface at a certain instant of time drop off from the tip region during their many hops by the thermal activation and field ionization, if they are captured after the first impacts. The procedure is repeated

by a computer till the number of particles $N(v,\varphi)$ converge to a very small fraction for each incidence characterized by v and φ. The total ion current is obtained by summing up the numbers of generated ions.

It is impracticable to perform the whole process discussed above by a computer and we simplify the rebound process as follows. It is assumed that a fraction P_e of rebounding particles that have hit the surface with velocity (v_n', v_t') will escape with velocity (v_{ne}, v_t) and the remainder of them go on trajectories returning to the surface with velocity (v_{nr}, v_t), where P_e, v_{ne} and v_{nr} are defined as follows.

$$P_e = \int_{v_{nc}}^{\infty} b(v_n, v_t, v_n', v_t')dv_n , \tag{15a}$$

$$v_{ne} = \int_{v_{nc}}^{\infty} v_n \cdot b(v_n, v_t, v_n', v_t')dv_n/P_e , \tag{15b}$$

$$v_{nr} = \int_{0}^{v_{nc}} v_n \cdot b(v_n, v_t, v_n', v_t')dv_n/(1 - P_e) . \tag{15c}$$

4.4 Results and Discussion

The total ion currents of helium on tungsten are calculated by repeating the hopping 200 times for each incidence on a NEAC 700, where R_t = 500 A, α = 0.205 A^3, Z_c = 3.5 A, d = 0.3 A, $\nu = 2.4 \times 10^{16} sec^{-1}$, I = 24.6 eV and Φ = 4.5 eV. Except for higher tip temperature than 300 K, almost the same results are obtained for different choice of the collision matrix, b and b_{LS} (see appendix 3). The tip temperature T_S has effects on the total ion current through the collision matrix. Only a fraction

10^{-7} of particles are supplied to the hopping states that do not reach the ionization zone, after 65 hops when F_t = 4.5 V/A and T_S = 80 K. For T_S = 20 K, the fraction increases to 10^{-3} and only 45 hops are needed to decrease the hopping height below Z_c.

The dynamic equilibrium between the gas ionization probability and the probability of escape without ionization from the tip region by thermal activation may play an important role in determining the amount of the ion current[7]. The number of particles that had velocity v, when very far from the tip and arrive at the unit tip surface in unit time, $N(v, T_g)$ is given by

$$N(v, T_g) = \int d\Omega \int_0^{\rho_{max}(v)} d\rho \; N(v, \rho)/4\pi R_t^2 \; . \qquad (16)$$

The fraction of $N(v, T_g)$, which escape without ionization after the first impact or in their few hops, is called $K_e(v, T_S)$. The temperature dependence of both quantities may be noticed. Some results of $K_e(v, T_S)$ for the collision matrix b, together with $N(v, T_g)$, are depicted in figs.(3a), (3b) and (3c). Figs. (3a) and (3b) show that incident particles having larger initial velocity than about 0.20 $eV^{1/2}$ almost escape from the tip region after few collisions. It is also shown that the probability of escape, K_e decreases as field strength increases (from fig.(3b)) and the mass ratio of the gas particle to the metal atom, μ increases (see fig.(3c)).

It can be seen from fig.(3c) that the trapped fraction of the total incident particles increase as the temperature of the gas in the field free region becomes low. This shows clearly

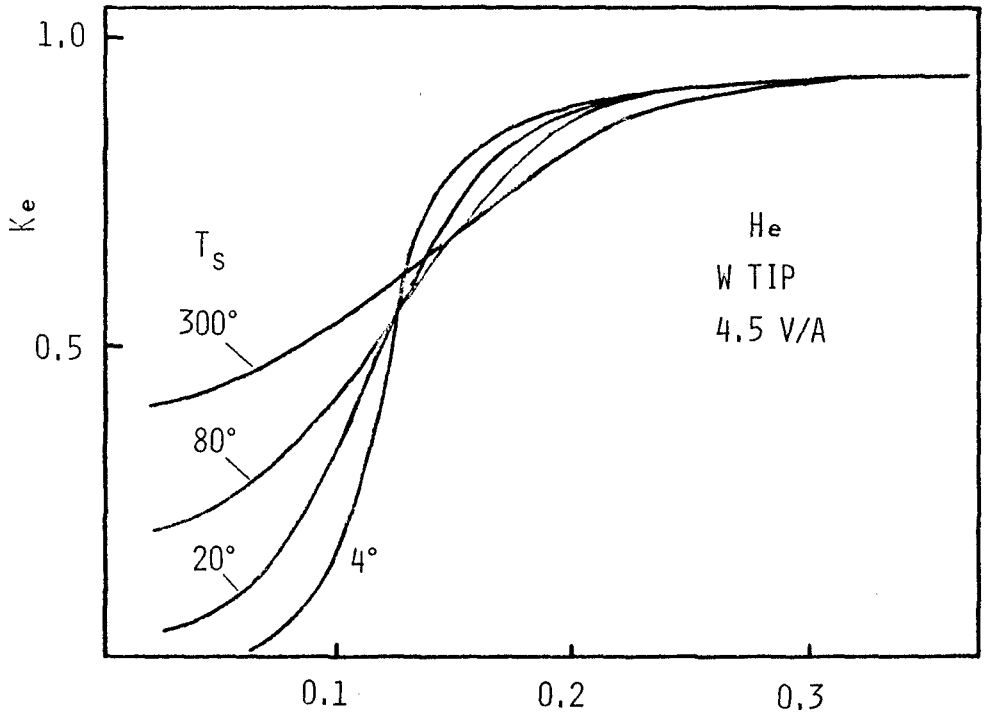

Fig. 4-3a.

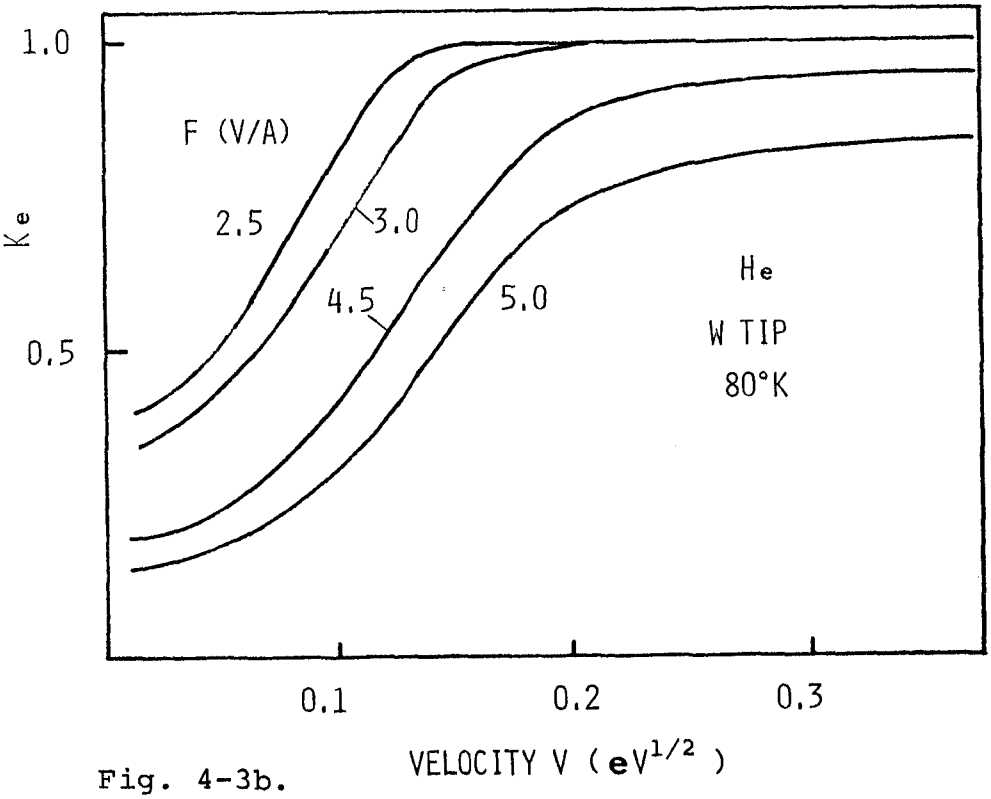

Fig. 4-3b.

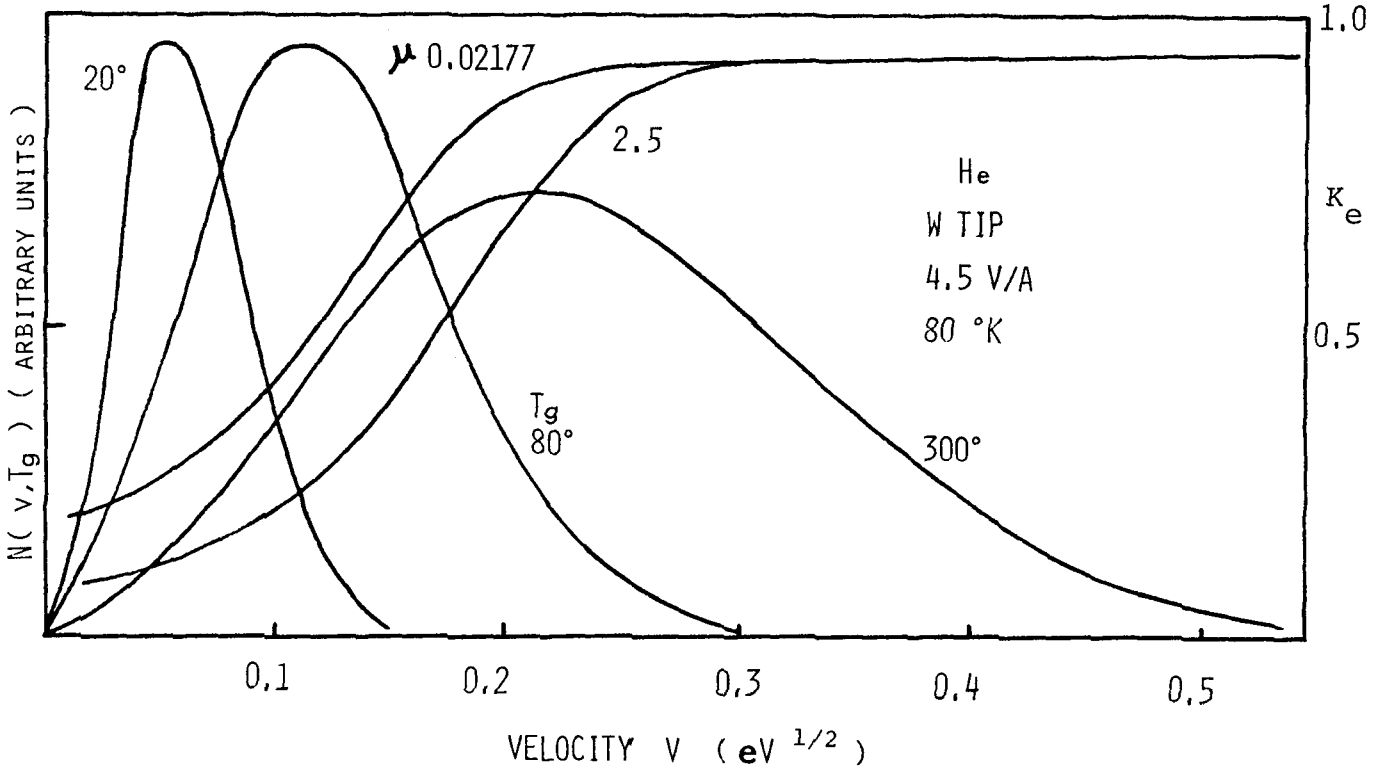

Fig. 4-3c.

Fig. 4-3.

The escape probability K_e versus velocity of an incident particle when very far from the tip, v, for helium with a tungsten tip, (a) at a field strength of 4.5 V/A, (b) at a surface temperature of 80 K, (c) at F = 4.5 V/A and T_S = 80 K, for μ equal to ordinary value of 0.02177 and 2.5, *together with* $N(v, T_g)$.

the large dependence of the ion current on the gas temperature and the importance of keeping the average gas temperature low by the metal electrode in contact with the cold finger of the conventional FIM design[8] .

The purely dynamical approach for calculating the total ion current which is shown in 4.3 may be performed by e. g. the Monte Calro method. However, the simplification employed by using eqs.(18a), (18b) and (18c) underestimates the probability of escape of particles after multiple collisions with the surface. So, the calculation of the ion current by the simplified procedure is valid in relatively high field region and high tip temperature region. The behaviour of the ion current for whole field and temperature range will be studied in the nexst chapter, making the results obtained here as a step.

CHAPTER 5

ION CURRENT GENERATION IN THE FIELD ION MICROSCOPE: II. QUASI STATIC APPROACH

Notation used in this chapter

v	radial velocity of a particle
v_c	maximum radial velocity, above which particles escape from tip region
$N'(v)$, $N(v)$	rates at which particles hit and leave unit tip surface per unit time with radial velocity v
I, I'	total ion current and contribution from bound particles in the tip region, respectively
N_t	supply of particles which are in bound states
k_i, k_e	rate constants for ionization and escape; the averaged out ionization and escape probability over distribution $N(v)$, respectively
P_c	capture probability defined by the averaged out trapping probability over distribution $N_n(v)$, where $N_n(v)$ is $N_n(v_n)$ in chapter 4

5.1 Introduction

Experimental measurements of field ion current versus other parameters of interest have been reported by a number of authors[1~5]. The increase of ion current by the field adsorption[6] of imaging-gas has also been reported by McLane et al.[7]. These experimental results afford data for the improvement of our understanding of the whole process of ion

current generation, which becomes of greater significance for the interpretation of the image.

There are two different ways for calculating field ion current, which are called by Müller and Tsong[8] , the dynamic and the quasi-static approach. The former one has been discussed in the previous chapter[9], henceforth referred to as I, in treating the purely dynamical calculation of ion current. The quasi-static approach developed in the paper of Van Eekelen[10] , henceforth referred to as VE, enabled us to calculate the velocity distribution function of gas particles and to explain many experimental features.

We follow Van Eekelen[10] to compute the field ion current with some modifications and extensions as follows. 1) The expression of the velocity distribution function of the supplied particles derived in I is used. 2) The tip temperature and the gas temperature are taken independently. 3) Field adsorption effects are demonstrated.

In the present study, equilibrium properties such as rate constants for ionization and for escape are formulated as functionals of distribution function. The expression of the total ion current by these terms[11,12] , which is familiar but not well founded, is reformulated on the basis of the balance equation derived in VE. The computed results are discussed in the light of these rate constants and the capture probability[12] .

5.2 The Balance Equation

It will be assumed for simplicity that the emitter is spherical. The local field variations at the tip are not taken into account. Also we disregard supply of gas particles from

the shank of the tip.

It is shown in I that velocities of the arriving particles at the tip surface from field free region should not be supposed to be purely radial as VE did. It is assumed that all newly incident particles on the tip surface have tangential velocity to the surface plane, v_t equal to the most probable tangential velocity v_{tm} given by eq. (4-8). A velocity distribution of particles that have hit the surface with velocity (v_n', v_t'), where v_n' is radial velocity, is described by the collision matrix $b(v_n, v_t, v_n', v_t')$[9,10]. We base the collision matrix on the hard cube model[13] (see appendix 3). As it conserves the tangential velocity of a particle, it may be justified to assume that tangential velocities of all particles are equal to v_{tm}. Hereafter, v means v_n in I and collision matrix is written as b(v, v').

Particles which left tip with radial velocity v smaller than v_c, which is given by eq. (4-11), go on trajectories returning to the surface. We obtain, for $v_t = v_{tm}$,

$$v_c = v_p - (kT_g/2m)^{1/2}, \tag{1}$$

where v_p is a dipole attraction velocity $(\alpha/m)^{1/2}F_t$, k is the Boltzmann constant, T_g is the temperature of the ambient gas, F_t is the electric field at the tip surface, α is a polarizability of a gas atom and m its mass.

Now, following VE, we call the numbers of gas particles that in unit time hit or leave unit tip surface with radial velocity between v and v + dv, in equilibrium, N'(v)dv and N(v)dv, respectively. Particles which hit tip with $v > v_c$ come

only from field free region. Particles which hit tip with $v < v_c$ on the other hand are composed of two components: particles arriving from field free region and particles which have previously hit the tip and return from a round trip passing through the ionization zone twice. The number of particles which arrive at unit tip surface in unit time from field free region with radial velocity v between v and v + dv, $N_n(v)$, is given by eq. (4-7a). Thus, in equilibrium we have

$$N'(v) = N_n(v)\{1 - Q(v)\} \quad \text{for } v > v_c ,$$

$$N'(v) = N_n(v)\{1 - Q(v)\} + N(v)\{1 - Q(v)\}^2 \quad \text{for } v < v_c , \tag{2}$$

where $Q(v)$ is the probability for a particle, which leaves the tip with velocity (v, v_{tm}), to be ionized in passing through the ionization zone once which is given by eqs. (4-11,12 and 13).

We have, by definition of a collision matrix

$$N(v) = \int_0^\infty N'(v')b(v, v')dv' . \tag{3}$$

By substituting (2) into (3), we obtain the balance equation for N(v) :

$$N(v) = \int_0^{v_c} N(v')\{1 - Q(v')\}^2 b(v, v')dv' + N_s(v) , \tag{4}$$

where

$$N_s(v) = \int_0^\infty N_n(v')\{1 - Q(v')\}b(v, v')dv' . \tag{5}$$

If we put $Q = 0$ in $N_s(v)$ and integrate over v using normalization condition of b, we get

$$\int_0^{\infty} N_s(v)dv = \int_0^{\infty} N_n(v)dv = S \ , \tag{6}$$

where S is the supply function and the second equation of (6) is given by eq. (4-9). For free particles, $v > v_c$, the ionization probability Q(v) is replaced by $Q_m = Q(v_c)$, following VE.

The derivation of the total ion current I as an example of the equilibrium quantities of the system has been shown in VE. There, the part of I due to the ionization of bound particles, $v < v_c$, was shown to be

$$I' = \int_0^{v_c} N(v) \left\{ 2Q(v) - Q(v)^2 \right\} dv \ . \tag{7}$$

We have, from eq.(4)

$$N(v) = \int_0^{v_c} N_t'(v')b(v, v')dv' + N_s(v) \ , \tag{8}$$

where

$$N_t'(v) = N(v) \left\{ 1 - Q(v) \right\}^2 \ . \tag{9}$$

$N_t'(v)$ gives the contribution to N'(v) from "bound" particles, after they have passed the ionization zone twice. We call the probability of escape and capture of a particle, which hit tip with radial velocity v', $P_e(v')$ and $P_t(v')$, respectively. They are given by the relation

$$P_e(v') = \int_{v_c}^{\infty} b(v, v')dv = 1 - P_t(v') \ . \tag{10}$$

If we integrate N(v) from 0 to v_c using eqs.(9) and (10), we get

$$\int_0^{v_c} N(v)dv = \int_0^{v_c} N_t'(v)\left\{1 - P_e(v)\right\} dv + \int_0^{\infty} N_n(v)\left\{1 - Q(v)\right\} P_t(v)dv \ . \qquad (11)$$

One finds, by transposition

$$\int_0^{v_c} \left\{N(v) - N_t'(v)\right\} dv + 2k_e N_t' = (1 - \langle Q \rangle_s) P_c S \ , \qquad (12)$$

where

$$N_t' = \int_0^{v_c} N_t'(v)dv \ , \qquad (13a)$$

$$2k_e = \int_0^{v_c} P_e(v) N_t'(v)dv/N_t' \ , \qquad (13b)$$

$$\langle Q \rangle_s = \int_0^{\infty} Q(v) N_n(v)dv/S \ , \qquad (13c)$$

$$P_c = \int_0^{\infty} N_n(v)\left\{1 - Q(v)\right\} P_t(v)dv/(1-\langle Q \rangle_s)S \ . \qquad (13d)$$

The brackets indicate an average and k_e gives the rate constant for escape and P_c gives the capture probability for the supply. From (9), we have

$$\int_0^{v_c} \left\{N(v) - N_t'(v)\right\} dv = N_t - N_t' = \int_0^{v_c} N(v)\left\{2Q(v) - Q(v)^2\right\} dv$$

$$= 2k_i N_t \ , \qquad (14)$$

where

$$N_t = \int_0^{v_c} N(v)dv \ , \tag{15a}$$

$$2k_i = \int_0^{v_c} N(v) \left\{ 2Q(v) - Q(v)^2 \right\} dv/N_t \ . \tag{15b}$$

K_i gives rate constant for ionization. We obtain, from eqs.(12) and (14)

$$\left\{ 2k_i + (1 - 2k_i)2k_e \right\} N_t = (1 - \langle Q \rangle_s) P_c S \ . \tag{16}$$

From eq.(7)

$$I' = 2k_i N_t = \frac{k_i(1 - \langle Q \rangle_s) \ P_c S}{k_i + (1 - 2k_i)k_e} \tag{17}$$

For $k_i \ll 1$, the number of bound particles that in unit time hit and leave unit tip surface, N, is given by

$$N = N_t + N_t' \sim 2N_t \ . \tag{18}$$

Then, for $k_i \ll 1$

$$I' = k_i N = \frac{k_i P_c S}{k_i + k_e} \ , \tag{19}$$

where

$$k_i = \int_0^{v_c} N(v)Q(v)dv/N_t \ , \tag{20a}$$

$$k_e = \frac{1}{2} \int_0^{v_c} N(v)P_e(v)dv/N_t \ , \tag{20b}$$

$$P_c = \int_0^{\infty} N_n(v)P_t(v)dv/S \ . \tag{20c}$$

Equation (19) is the formula given by Southon[12] . It may be

noticed that k_i and k_e are functionals of N(v).

The total ion current I is given by

$$I = I' + \langle Q \rangle_s S + Q_m(S - \langle Q \rangle_s S - I') \ . \qquad (21)$$

The second term and the third term give the contribution to I from incoming free particles and outgoing free particles, respectively.

5.3 The Collision Matrix

Let us define c(v, v') as the probability that normal velocity of a gas particle is changed, by the collision with the surface, from v' to v. On the basis of the classical hard cube model, c(v, v') is found from one-dimensional, head-on collision of a particle with the surface atoms that have a Maxwellian velocity distribution[13] . So, c(v, v') is identical with that derived by VE in one-dimensional model. We use the collision matrix b(v, v') that is constructed by VE from c(v, v') for higher value of v and from a Maxwell distribution at a partially accomodated temperature for lower value of v. The derived matrix b(v, v') satisfies the condition of detailed balance. Some collision matrixes are depicted in fig.1. The dependence of the matrix on the tip temperature T_s may be noticed.

Probabilities of escape, $P_e(v)$ are shown in fig.2. The escape probability, Pe for the bound particle becomes small as the tip temperature decreases or as the field strength increases. The situation is reversed for the particle that hit the surface with larger nomal velocity. This may be understood as follows. Particles have some probability to collide with the metal atoms moving in the same direction and to loose necessary amount of

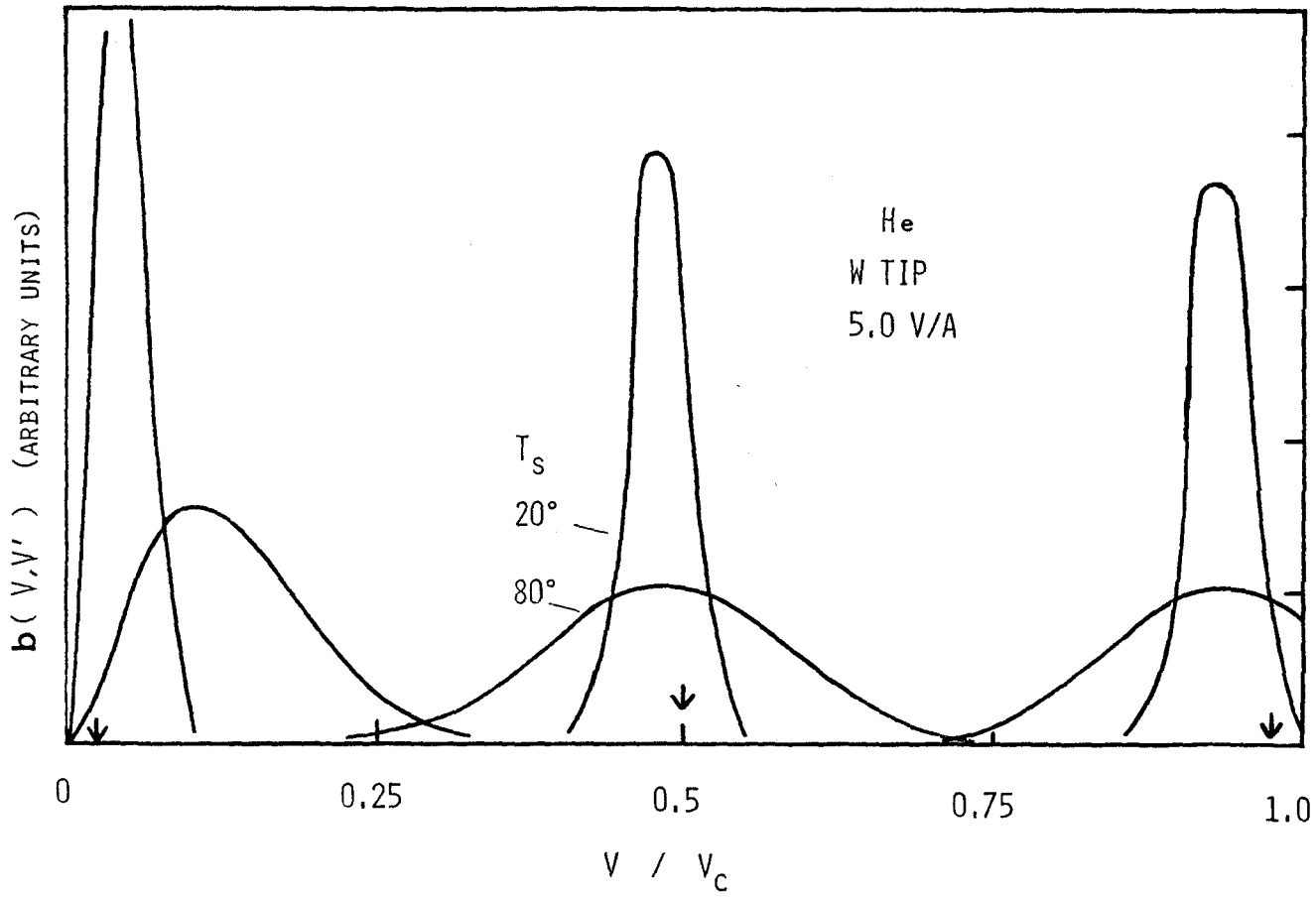

Fig. 5-1.

The collision matrix elements, b(v, v') for helium with a tungsten tip, at a field strength of 5.0 V/A and T_g = 80 K. The incident normal velocity v' for each curve is shown by the arrow. The value of v_c is 0.380 in $eV^{1/2}$ (see I for the unit of velocity).

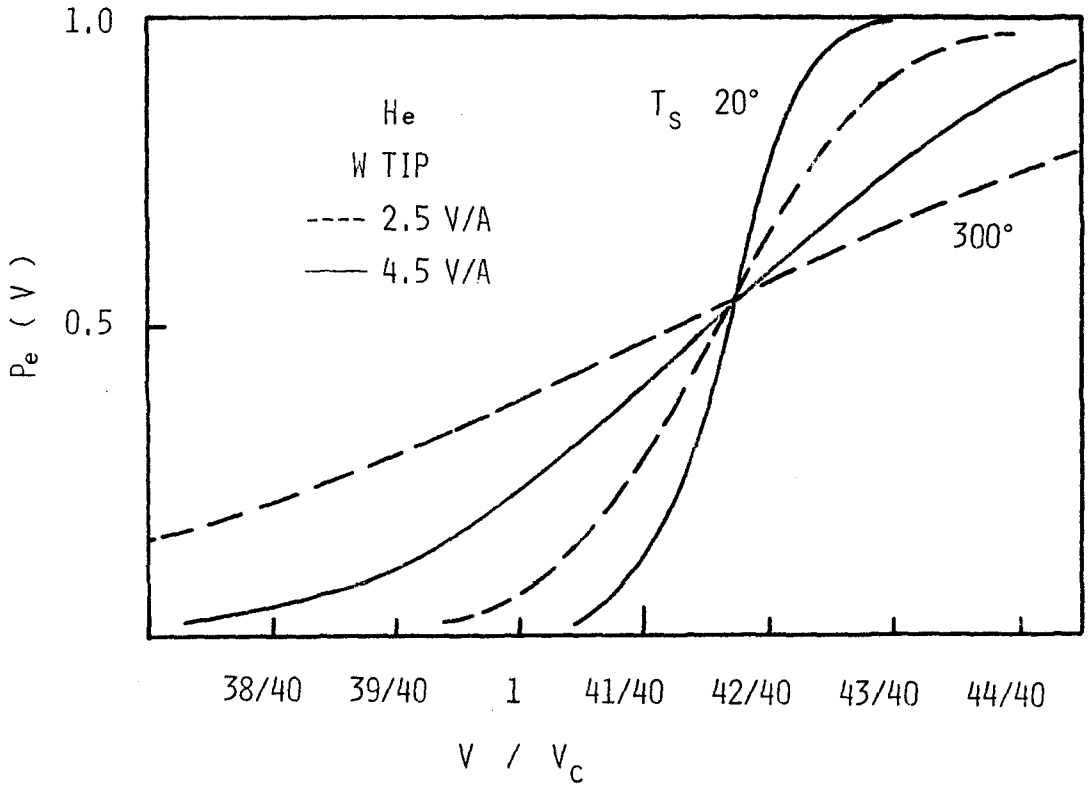

Fig. 5-2.

Probabilities of escape, $P_e(v)$ for helium with a tungsten tip at T_g = 80 K, and at F = 2.5 V/A (dashed curves) and at F = 4.5 V/A (solid curves). The values of v_c are 0.169 and 0.338 $eV^{1/2}$ for F = 2.5 V/A and 4.5 V/A, respectively.

velocity to be trapped, when the surface is high temperature.

As regards P_c , it changes only slightly when T_s is changed.

5.4 Results and Discussion

The balance equation (4) is the second kind Fredholm type integral equation. Following VE, it is replaced by matrix equation and solved by iteration. Some particle distributions for helium on tungsten are depicted in figs.3, 4 and 5. Figure 3 shows the dependence of the particle distributions on the tip temperature at very low field of 2.5 V/A. The curves and those found from Maxwell distributions fit together except for 300 K. At 300 K, the population of high-energy particles is lowered than that found from Maxwell distribution, because high-energy particles are easy to escape by thermal activation.

Shown in fig.6 are the ratios of N_t to the thermal equilibrium value of the supply function, $S_0 \exp(E_p/kT_s)$. S_0 and E_p are given by (4-7c) and (4-2c) respectively. For low F, e. g. 2.0 V/A, and for $T_s \geqq 80$ K, k_e is much greater than k_i. In this case, seen from fig.6, N_t is often nearly equal to $S_0 \exp(E_p/kT_s)$. Then,

$$I = 2k_i N_t \sim 2k_i S_0 \exp(E_p/kT_s) \ , \tag{22}$$

$$k_e \sim P_c S \exp(-E_p/kT_s)/2S_0 \ . \tag{23}$$

At 20 K and F = 2.0 V/A, k_e is comparable to k_i and the concentration of gas particles at the tip surface is much smaller than that in thermal equilibrium.

The structure of particle distribution for low temperature

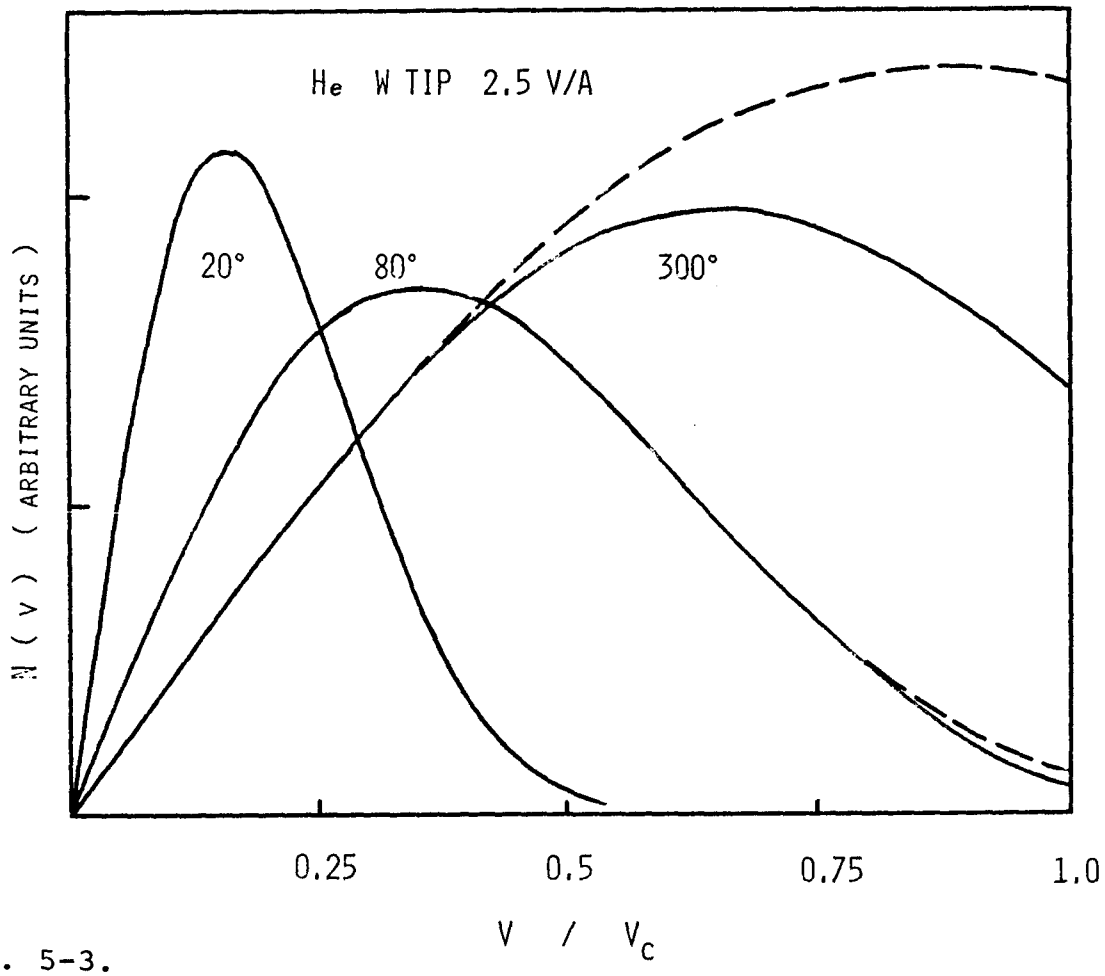

Fig. 5-3.

Particle distribution for helium with a tungsten tip under isothermal conditions, at a field strength of 2.5 V/A, from the present calculation, solid curves and the Maxwell distribution, dashed curves. The latter curves are normalized so that their lower velocity parts fit together with those of the former curves. The peak values of the solid curves (the values of v_c) are 1.3×10^8 (0.196), 5.3×10^4 (0.169) and 2.4×10^2 (0.131) in $PV/\sqrt{2\pi m}$ ($eV^{1/2}$) units for T equal to 20 K, 80 K and 300 K. Where P is the gas pressure and V its volume.

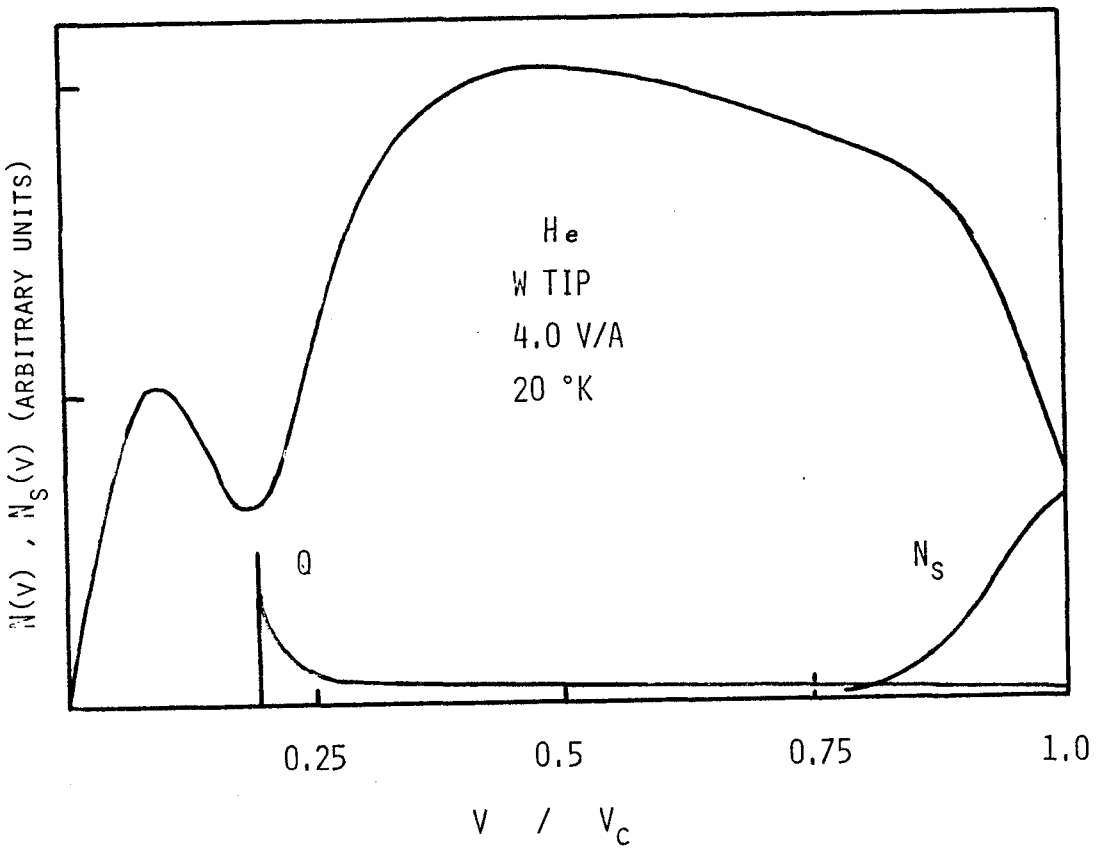

Fig. 5-4.

Particle distribution, N(v) together with $N_S(v)$ and Q(v), for helium with a tungsten tip at $T_S = T_g = 20$ K and F = 4.0 V/A. The peak value of Q(v) is 0.3. $v_c = 0.317$ $eV^{1/2}$.

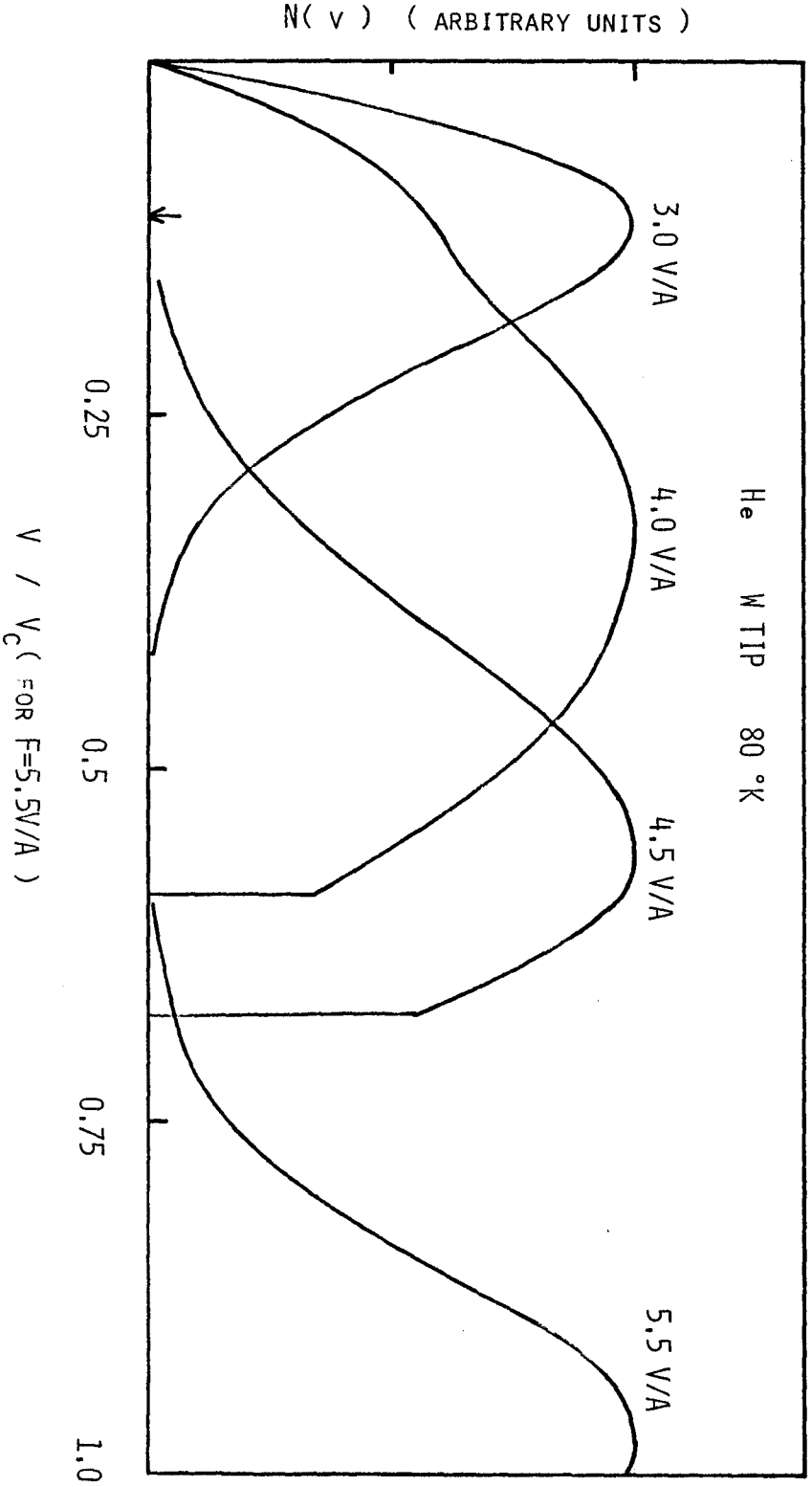

Fig. 5-5.
Particle distribution for helium with a tungsten tip at $T_s = T_g = 80$ K. The thermal velocity, v_{th} ($\sqrt{kT/m}$) is shown by an arrow. The value of v_c for F = 5.5 V/A is 0.423 $eV^{1/2}$. The peak values are 2.3×10^5, 4.4×10^4, 2.6×10^4 and 1.1×10^4 ($PV/\sqrt{2\pi m}$) for F equal to 3.0, 4.0, 4.4 and 5.5 (V/A).

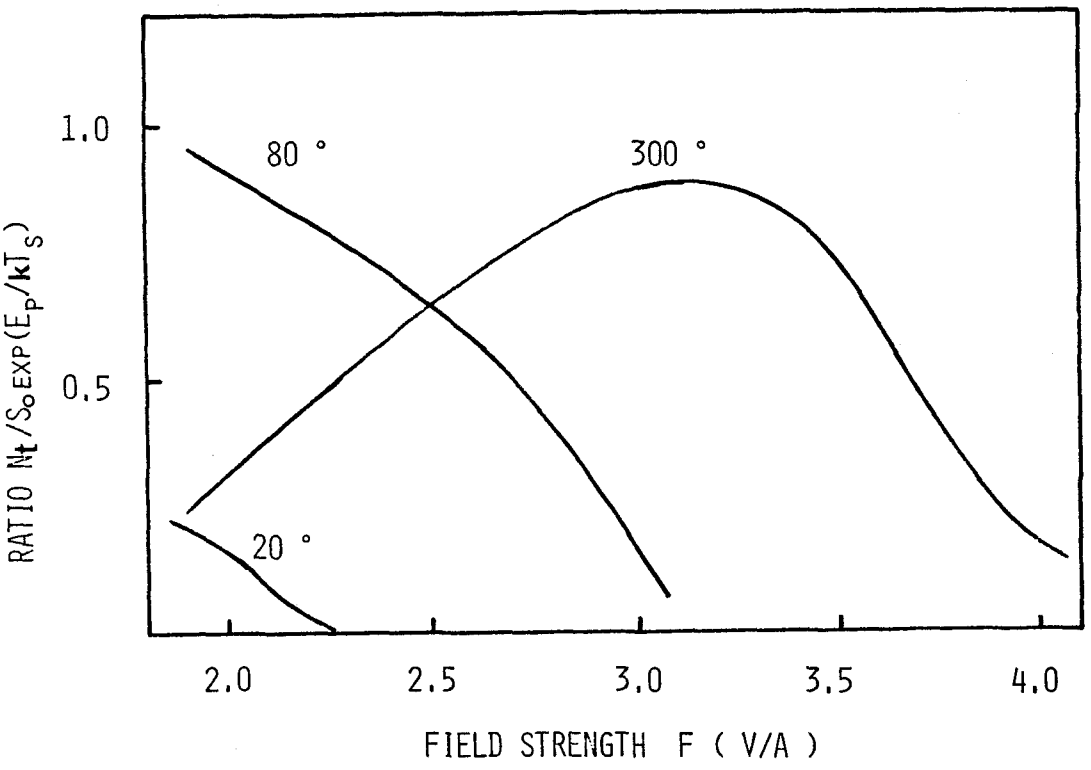

Fig. 5-6.

The ratio $N_t/S_0 \exp(E_p/kT_s)$, for helium with a tungsten tip, under isothermal conditions.

discussed by VE is seen from fig.4. It can be seen from fig.5 that the low-energy peak virtually disappears at 80 K. This has been also indicated by VE. It can be also seen from fig.5 that particles are ionized before they are well accomodated to the tip temperature for high field.

When T_s rises, k_e increases both by the increase of P_e for the bound particles and by the shift of the peak of the particle distribution to the larger velocity shown in fig.3. When field is increased, in spite of the decrease of P_e for the bound particles (see fig.2), k_e increases by the shift of the peak of the particle distribution to the larger velocity (see fig.5). The values of k_e, k_i and N_t for various temperatures and fields are collected in appendix 4.

5.4.1 Current-Voltage Characteristics

Logarithmic plots of the total ion current I versus the field strength F, for helium on tungsten, are given in fig.7. The curves exhibit most of the features observed experimentally[1~5,14] in the similar way to VE. The values of the slope of an almost straight high-field region and of the cut-off field strength[12] are in good agreement with those of VE.

The slopes of low-field region are 46, 34 and 31 at T equal to 20 K, 80 K and 300 K respectively in isothermal conditions. This increase of the slope with decreasing temperature is in good agreement with the experiment by Chen and Seidman[14]. They explained this temperature dependence of the slope of very low field region by the assumed expression of the ion current similar to eq.(22).

Anyway, for low field where $k_e \gg k_i$, ion current is expressed by

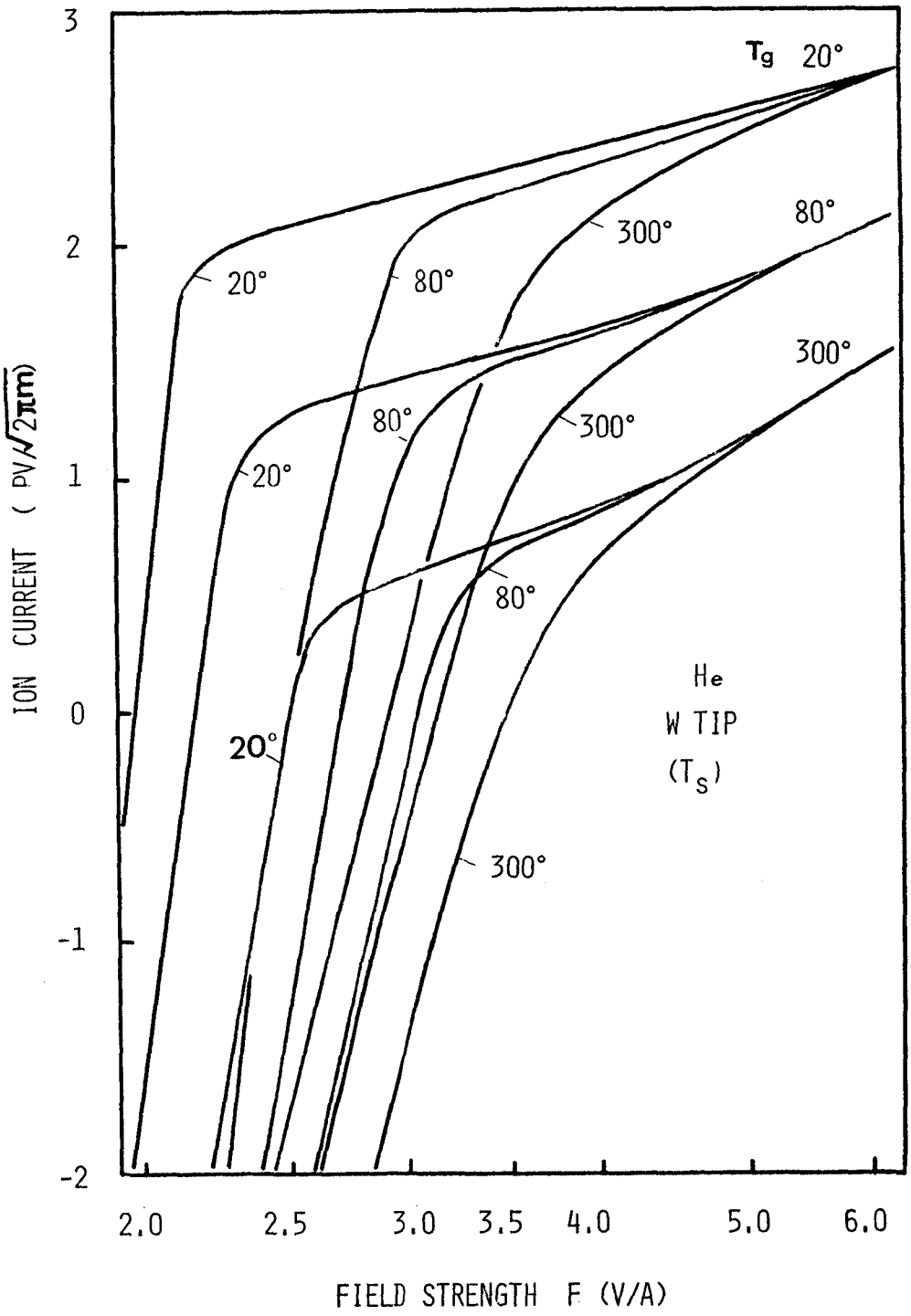

Fig. 5-7.

Logarithmic plot of the total ion current per unit tip surface versus the field strength for helium with a tungsten tip, under the same gas pressure.

$$I = k_i P_c S / k_e \quad . \tag{24}$$

On the other hand, in the straight high-field region, ion current must be expressed by eqs.(19) or (17) and (21).

In fig.8, the ratios of the ion current to the supply function, S, together with P_c, have been plotted. As has been shown in I, P_c increases when field strength increases.

As discussed by Tsong and Müller[5], the number of atoms escaping from the tip region without ionization is indeed comparable or larger than the ionized fraction under the usual experimental conditions. As VE has stressed, the straight high-field region is an intermediate region where the current does not equal the supply. At 20 K, k_e is much smaller than k_i for $F > 2.25$ V/A. Then,

$$I = P_c S \quad . \tag{25}$$

The curves I /S and P_c for T = 20 K in fig.8 fit together for F from 2.5 V/A to 4.0 V/A. For higher field, the contribution from free particles become large.

5.4.2 Temperature Effects

Tsong and Müller[5] have investigated the effects of the tip temperature on the ion current at a given field strength and gas temperature. Plots of the ion current versus the tip temperature, for helium on tungsten, are given in fig.9. The calculated curves for F = 3.25 V/A seem to fit with the experimental curves. The tip temperature dependence of the ion current is explained by the behaviour of k_e as a function of T_s discussed in this chapter. For low field, when T_s rises, ion current decreases rapidly by the rapid increase of k_e.

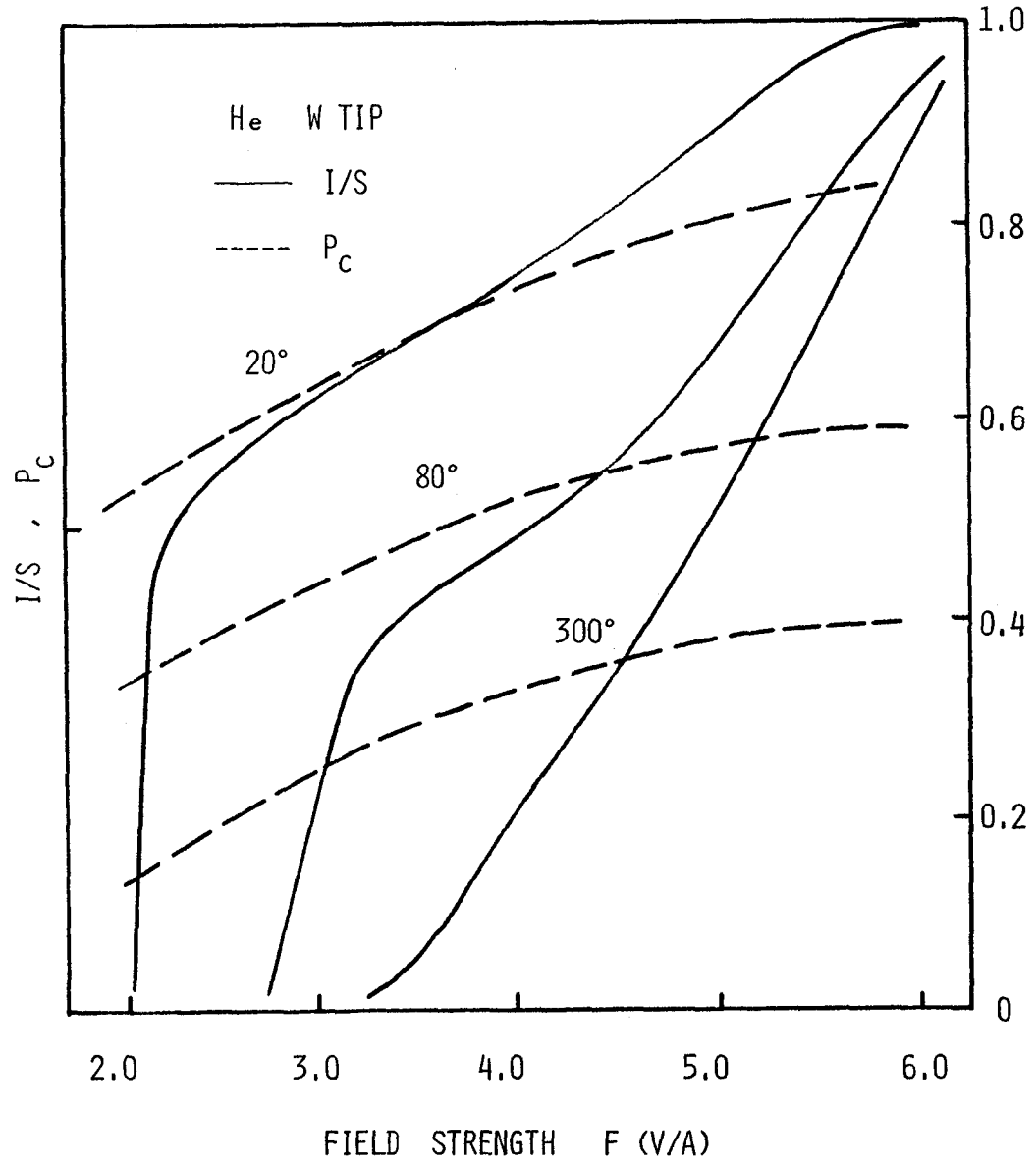

Fig. 5-8.

The ratios I/S (solid curves) and the capture probability P_c (dashed curves) versus field strength for helium with a tungsten tip.

For high field, on the other hand, when T_s rises, ion current decreases only slowly, in agreement with the experiment, by three reasons as follows. The increase of k_e with T_s becomes small as the shift of the peak of the distribution with T_s is less remarkable for high field. Next, k_i becomes larger than k_e for high field and ion current is proportional to $(k_i + k_e)^{-1}$ not to k_e^{-1}. Finally, the contribution to the ion current from free particle, which is insensitive to T_s , becomes large for high field.

It is observed experimentally that ion current with 78 K gas temperature decreases only slightly at T_s = 78 K. This effect is more remarkable for neon and hydrogen on tungsten at 3.8 V/A and 4.5 V/A respectively[5] . The calculations suggest that this may be explained as follows. For temperature and field strength in discussion, k_e is much smaller than k_i and so $(k_i + k_e)^{-1}$, and hence I decreases only slightly as k_e increases.

It can be seen from fig.7 that the shifts of the cut-off fields towards higher fields are caused mainly by the increase of T_s. This effect may be explained as follows. From the discussion of sec. 5.4.1, the cut-off may be considered as the field at which k_i becomes comparable to k_e. When T_s rises, k_e increases and then the cut-off field, where $k_i \sim k_e$, shifts towards higher fields.

The gas temperature has effects on I mainly through its effects on S and P_c. The total supply to the tip, S is proportional to T_g under the same gas pressure. Our calculation showed that P_c increases the number by $2 \sim 4$ times when T_g decreases from 300 K to 20 K. This dependence of P_c on T_g has been discussed in I.

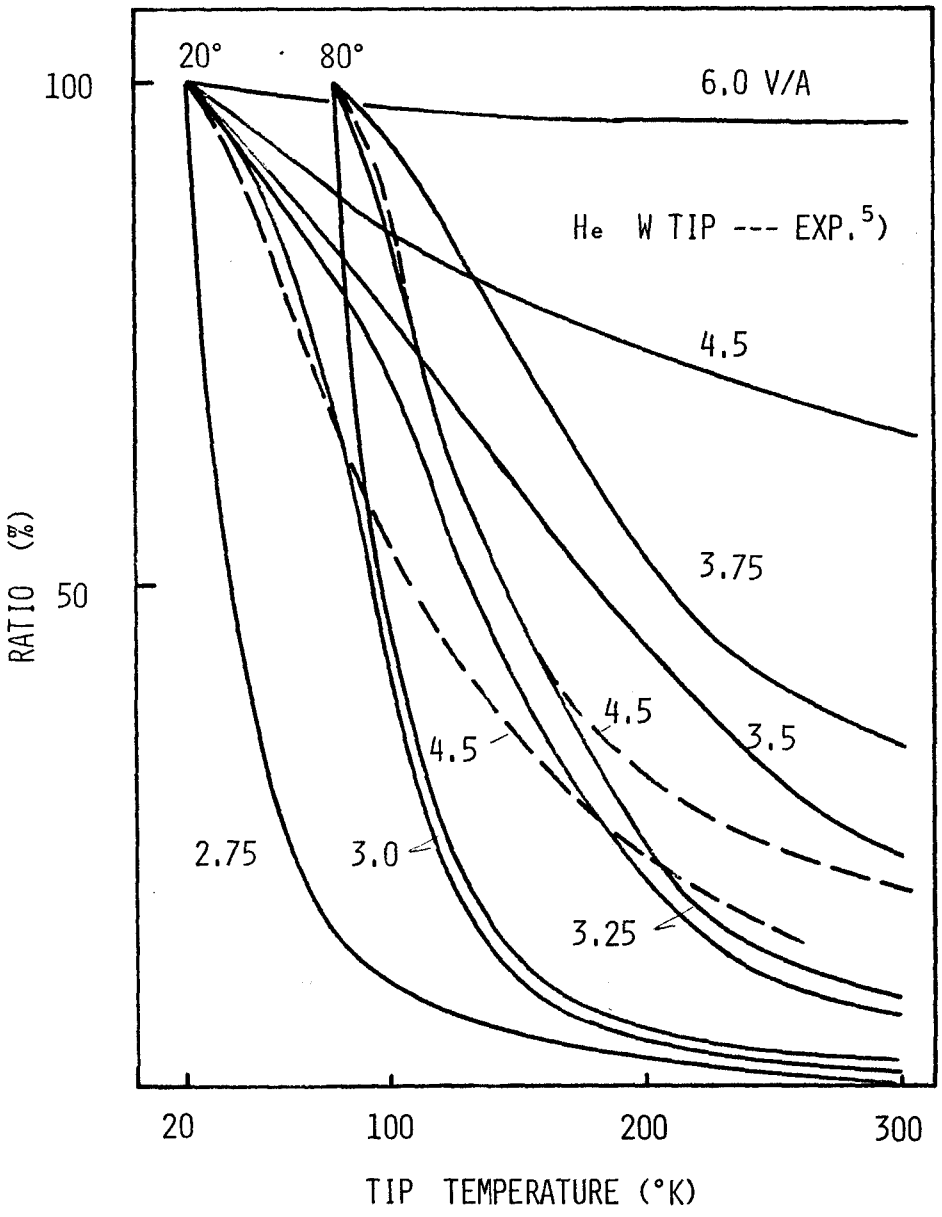

Fig. 5-9.

Relative ion current versus tip temperature for helium with a tungsten tip with 20 K and 80 K gas temperature. Solid lines are calculated curves for various field strength. Dashed lines are experimental curves at F = 4.5 V/A by Tsong and Müller[5] .

Ratios of ion current at two different temperatures under isothermal conditions are plotted as a function of field strength in fig.10. The curves exhibit most of the features observed experimentally[5] . However, the critical field strength where the value of the ratio increases abruptly is smaller by 0.5 V/A for I_{20}/I_{80} and 1.0 V/A for I_{80}/I_{300}.

5.4.3 The Effects of Field Adsorption on Ion Current

Tsong and Müller[15] have shown that the probability P_a that at any instant of time an inert-gas atom is field adsorbed[6] on the apex of the surface atom is given by

$$P_a = \left\{ 1 + (\nu C T_s / P_{gas} F) \exp(-H/kT_s) \right\}^{-1} . \qquad (26)$$

where H is the short-range binding energy and C is a constant which can be estimated from experimental conditions. For field adsorption of helium on tungsten, H is chosen as $(f_a - 1)E_p$ $= 1.399\ E_p$, where f_a is an enhancement factor, and C as $C(T_s/P_{gas}F) = 10^{-5}$sec at 20 K, 2mTorr and 4.5 V/A[15] . For P_{gas} = 2mTorr, the values of P_a for a variety of temperatures and fields have been collected in table 1. The field adsorption may have effects on I by changing the ionization probability[16,17] and by changing the gas-surface interaction. So, we calculated the ion current for the two cases where the ionization life time, τ (see eq. (1-14)) is assumed to be $\tau_1 = (1 - 0.9\ P_a)\tau$ and $\tau_2 = (1 + 9.0\ P_a)\tau$. Field ionization are enhanced and suppressed by a factor of ten by field adsorption in the case 1 and 2 respectively.

It is assumed that the change of the gas-surface interaction by field adsorption is taken into account for by

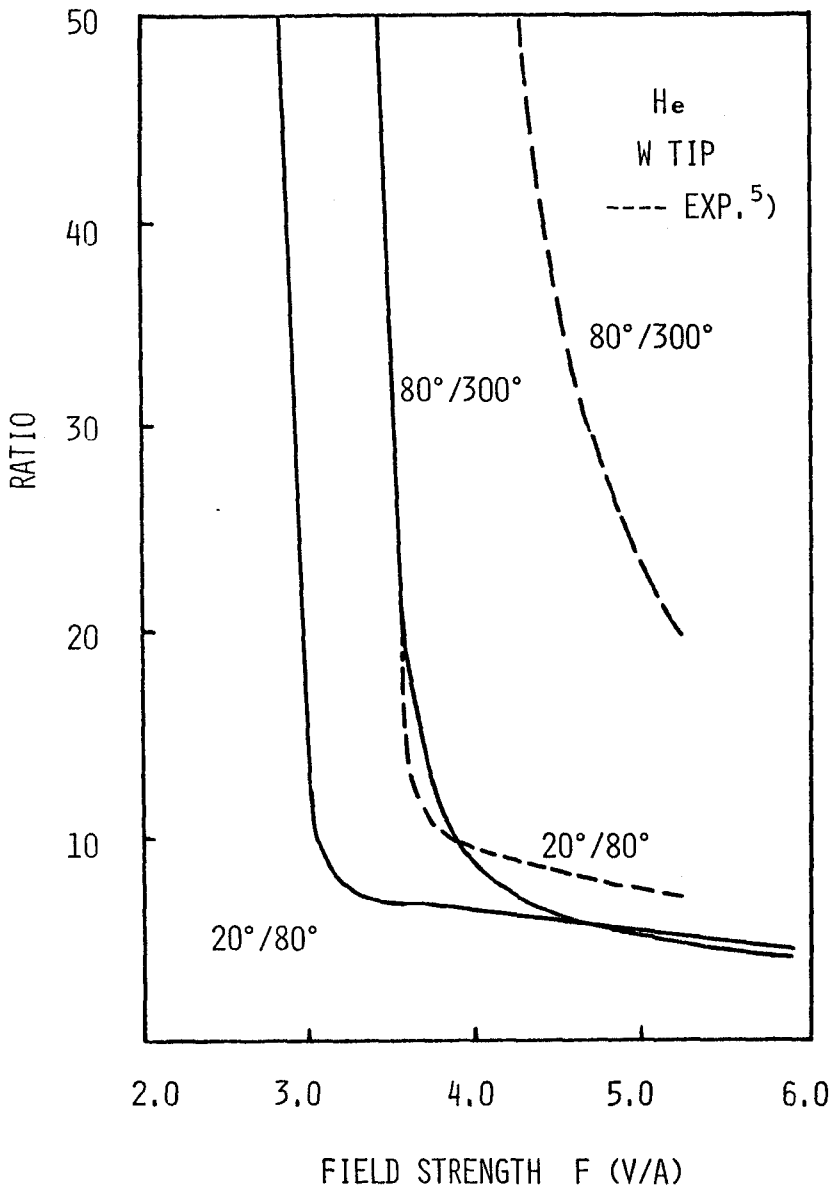

Fig. 5-10.

Ratio of ion current at two different temperatures under isothermal conditions versus field strength for helium with a tungsten tip. Solid lines are calculated curves and dashed lines are experimental curves by Tsong and Müller[5].

taking the mass ratio of a gas particle to a metal atom, μ as a function of P_a. Here μ is assumed to be $(1 + P_a)\mu$, for both cases. Then, the accomodation coefficient is increased by two times by field adsorption. The calculated results are shown in fig.11.

The curves exhibit many interesting features. 1) In the straight high-field region, ion currents are increased equally for both cases. The values of k_e (k_i) are 2.2×10^{-5} (4.0×10^{-3}), 4.7×10^{-6} (4.0×10^{-4}), 2.2×10^{-7} (4.0×10^{-5}), and 2.2×10^{-8} (4.0×10^{-6}) for τ equal to $\tau \times 10^{-1}$, τ , $\tau \times 10$ and $\tau \times 10^{2}$ at F = 3.0 V/A, T_s = 20 K and T_g = 80 K. These show that k_e strongly depends on k_i and $k_e \ll k_i$ for the field range in discussion. Then I is expressed by $P_c S$ and the shifts of I towards higher values are solely caused by the increase of P_c by field adsorption.

It may be noticed that, in general, some part of the straight high-field region is independent on the magnitudes of k_i , though narrow for higher tip temperature (see the curve for $T_s = T_g$ = 80 K in fig.11). Ion current, which is proportional to $k_i/(k_i + k_e)$ for the field region in discussion, is kept constant for the change of the ionization probability on account of the following change of k_e, as discussed above. 2) The enhancement and the suppression of the ion current due to those of the field ionization by field adsorption are seen in both the extremely low field region where $I = k_i P_c S/k_e$ and in the relatively high field region where contribution to I from free particles, $\langle Q \rangle_s S$ becomes large. 3) In the case 2, where field ionization is suppressed by field adsorption, the curve for T_s = 20 K and T_g = 80 K intersects with the curve for no

Table 5-1

Probability P_a for helium with a tungsten tip for 2mTorr.

F (V/A) \ T_s (°K)	20	80	300
2.0	0.98	3.6×10^{-7}	1.4×10^{-9}
2.5	1.0	1.2×10^{-5}	4.1×10^{-9}
3.0	1.0	7.3×10^{-4}	1.4×10^{-8}
3.5	1.0	8.7×10^{-2}	5.8×10^{-8}
4.0	1.0	0.96	2.5×10^{-7}
4.5	1.0	1.0	1.6×10^{-6}
5.0	1.0	1.0	1.3×10^{-5}

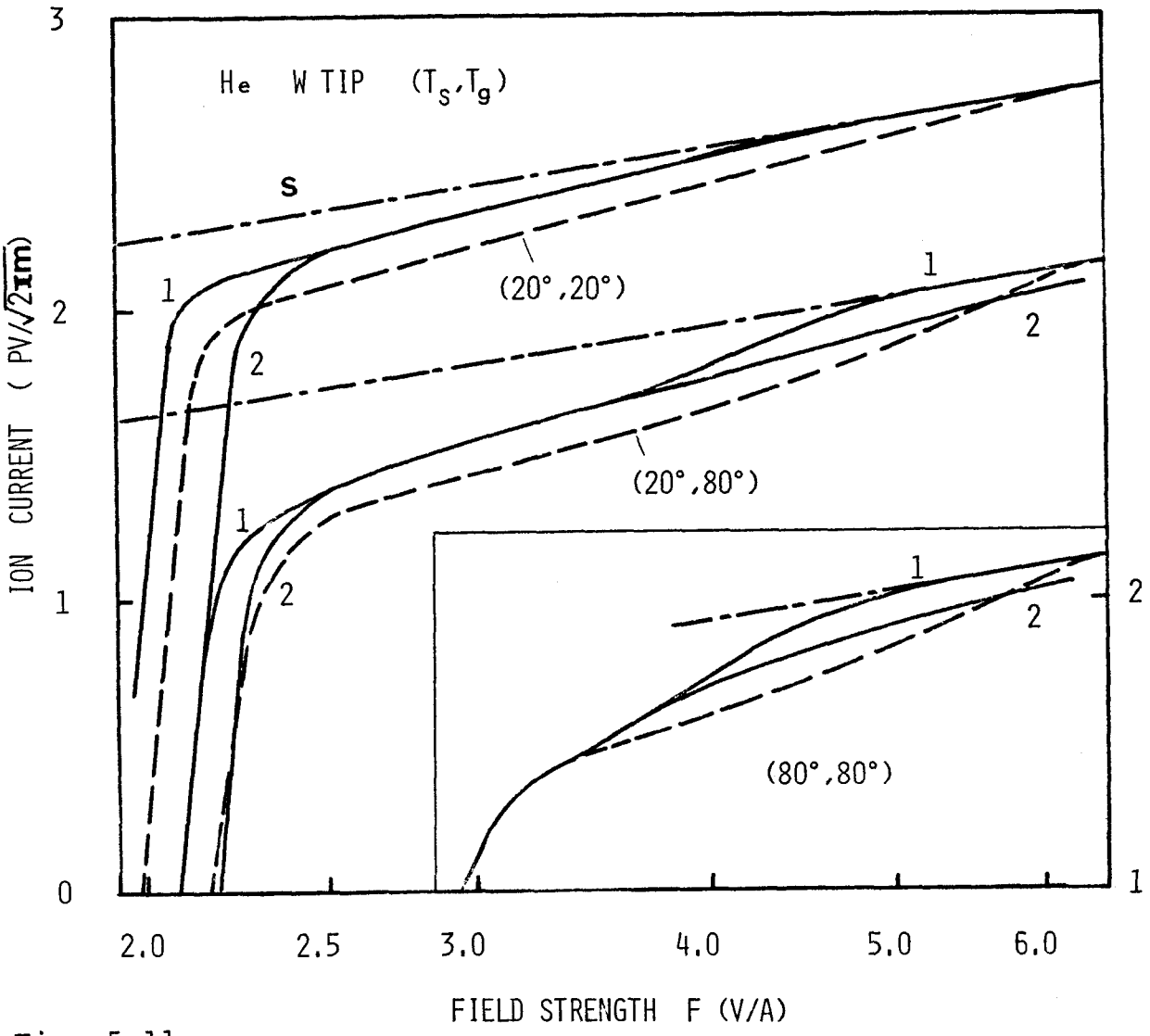

Fig. 5-11.

Logarithmic plot of the total ion current versus the field strength for helium with a tungsten tip. Solid lines 1 and 2 are calculated curves for the case 1 and 2, respectively. Dashed lines are the curves when no adsorption effect are considered. The total supplies are plotted also (dot-dash-lines).

adsorption.

This reversal of the values of ion current from field adsorbed surface and from no-adsorbed surface, when field is increased, suggests the mechanism to explain the unusual features of FIM image at 4.2 K[18] . At 4.2 K, the brightness of image spots in the same plane change as the field strength is varied. The metastable site atom A in fig.12 is imaged brighter than the atom B and C in the very high field region ($F \geq 5.7$ V/A). When the applied voltage is lowered the image brightness of the atom A is diminished and the images shown by the broken lines in fig.12 become brighter[18] . At 4.2 K, the probability of field adsorption P_a at site B or C may be larger than that at site A, because, to the former site adsorbed inert atoms are supplied by migration of them from the inner part of the (011) plane.

The field-adsorbed or physisorbed helium atom increases the time spent by an ionizable helium gas atom in the ionization zone by improving the accomodation as well as suppresses the ionization probability of the gas atom[16,17] . On the analogy of 3), the latter effect is expected to be more effective than the former effect at very high field and vice versa in the working-range of the field. Namely, at very high field the ionization life time of a gas particle, τ is so short that particles that are flying even in high speed are almost ionized in passing through the ionization zone once, and so, it does not matter for ion current generation whether the lost momentum of the particle is large or not. On the other hand, in the working-range of the field where the ionization life time is long, the change of the staying time of particles in the ionization zone by the field adsorption is more effective than

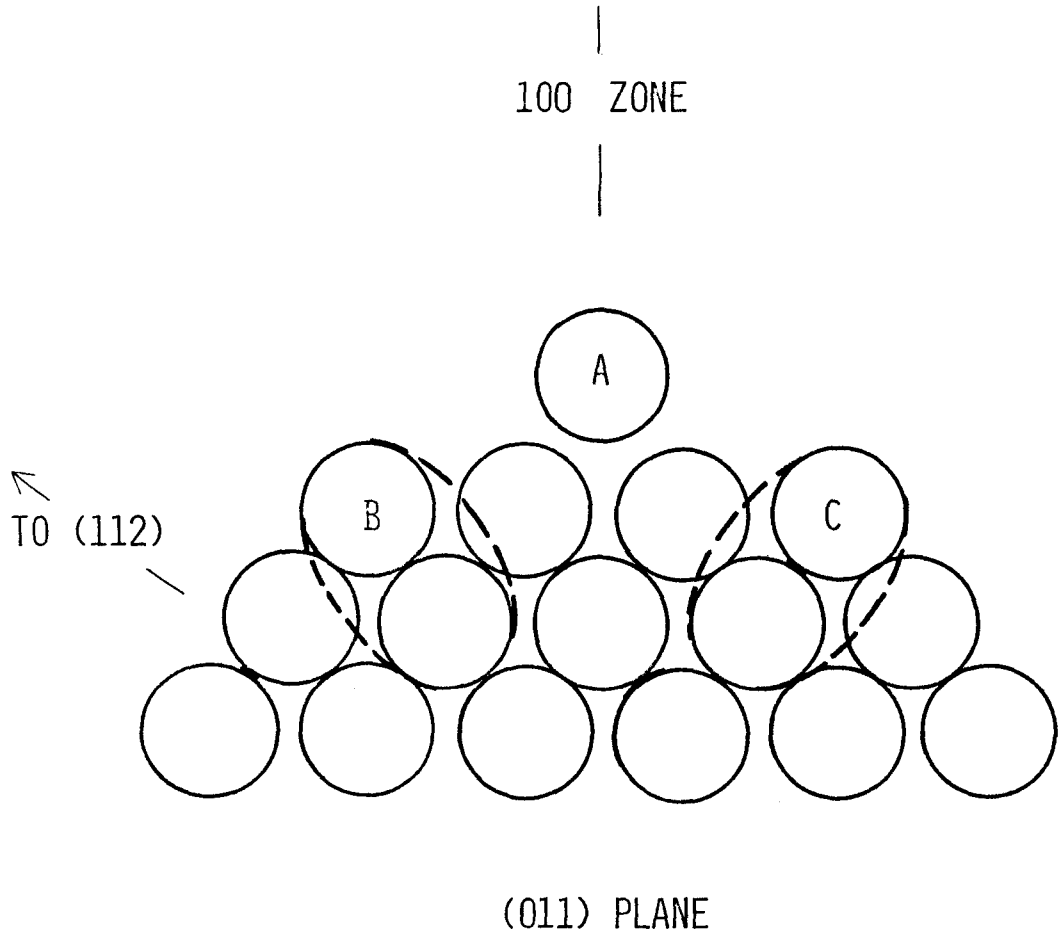

Fig. 5-12.

Schematic diagram of the ledge of the (011) plane of tungsten.

the change of the ionization probability itself.

Then, at very high field, the image of the atom A is brighter than that of B or C, because the ionization probability at A site is less suppressed by less adsorbed helium atoms than that at B or C site. When the applied field is lowered, the images of more adsorbed sites B and C become brighter than that of less adsorbed site A.

5.5 Conclusions

The rate constants for ionization, k_i and for escape, k_e are formulated as functionals of distribution function, N(v). The formula of the total ion current, I that is expressed by the rate constants, the total supply, S and the capture probability, P_c is derived. The formula coincides with that given by Southon[12] for $k_i \ll 1$. The behaviours of the ion current are analyzed by using these equilibrium properties of the system. In the very low field region, I is equal to $k_i P_c S/k_e$ and in straight high-field region, I is equal to $k_i P_c S/(k_i + k_e)$. In the latter region, there exists a part where I is independent of the values of k_i.

The effects of the tip temperature, T_s are discriminated from those of the gas temperature, T_g. The dependence of I on T_s is qualitatively explained by the T_s dependence of k_e. The gas temperature has also been shown to have considerable effects on the ion current, in agreement with the results of I.

It is shown that the ion current is indeed increased by the field adsorption of inert gas atoms even if the field ionization probability were suppressed[17]. Moreover, the proposed mechanisms that the ionization probability is decreased

and the staying time of a particle in the ionization zone is increased by the field adsorption of an inert gas atom enabled us to explain the experimentally observed anomalous features of field ion images at 4.2 K successfully.

CHAPTER 6

CONCLUSIONS

The Oppenheimer's method to calculate the transition probability between non-orthogonal states is applied to the field ionization in FIM, leading us to determine the probable choice of the initial and the final states and the perturbation potential.

Detailed calculation of the ionization probability using tight-binding states as metallic states has revealed the sensitive dependence of the ionization probability on the extention of the metal orbital outside the surface. It is also found how s- and d-state of the metal contribute to the field ion images. The consistent results of ion energy distribution with experiments has also been derived.

It has been shown by the simple one-dimensional calculations that the ionization probability is likely to be increased by the adsorption of species of low ionization energy such as chemisorption or metallic adsorption, without resonance in the transmission coefficient. On the other hand, the ionization probability is shown to be decreased by the adsorption of inert gas atoms in some cases. To corroborate the latter prediction the expression for the ionization probability through adsorbed inert gas atom is derived in the three-dimensional and many-body theoretical manners. The expression is examined to be reasonable in the absence of the adsorbate, and also in the orthogonal limit of the basis set. The calculation show that ionization probability for helium as imaging gas is indeed decreased by the field adsorption of helium and neon, although the degree of reduction for helium as

adsorbate is much higher than for neon.

With the aim of intermediating between the atomic description of field ionization processes suhc as the ionization probability and the gas-metal collision and the macroscopic properties of FIM such as ion current voltage characteristics, the extension of the theory of the ion current generation is undertaken.

The distributions of supply of particles at the tip surface as functions of velocity components have been derived. The author reveals the importance of cooling the ambient gas temperature which is likely to be a cause to increase the catching probability of the firstly incident particles to the emitter surface.

Based on the existing formula of the balance equation for the distribution of concentrated gas particles, the expression for the total ion current in terms of equilibrium quantities such as rate constants for ionization and for escape by thermally activated processes has been derived. Field ion current is computed versus other parameters of interest on the basis of the balance equation which is extended from one-dimensional model to the three-dimensional one. The computed properties of the FIM such as the field and temperature dependence of the total ion current, which agreed fairly well to the experimental observations, have been discussed physically in the light of the above mentioned expression for the field ion current. The present investigation enables us to discriminate between the effects of the gas temperature and the tip temperature, leading us to understand the detailed mechanisms of ion current generation.

It is confirmed that only a fraction of particles attracted to the tip by polarization contributes to the ion current, as suggested by the previous investigators.

Finally the experimental results that the ion current is enhanced by the field adsorption of inert gas atoms is qualitatively explained by the present treatment of the ion current generation, consistent with the theoretically expected suppression of the ionization probability in the previous chapter. Moreover, the proposed mechanisms that the ionization probability is decreased and the staying time of a particle in the ionization zone is increased by the field adsorption of an inert gas atom enabled us to explain the experimentally observed anomalous features of field ion images at 4.2 K successfully.

The procedures of the present work may shed new light on the understanding of the image formation mechanisms in FIM.

APPENDIX 1

THE POLARIZATION ENERGY OF ATOM AS POTENTIAL ENERGY

The total Hamiltonian of a valence atom under the electric field may be expressed as follows.

$$H_t = -\frac{\hbar^2}{2M}\nabla_R^2 - \frac{\hbar^2}{2m}\nabla_r^2 - \frac{e^2}{|\vec{R}-\vec{r}|} + e\vec{F}(\vec{r})\cdot\vec{r} - e\vec{F}(\vec{R})\cdot\vec{R}, \quad (1)$$

where $\vec{F}(\vec{r})$ is the field strength.

We apply the Born-Oppenheimer approximation. Then the eigen function of the total Hamiltonian $\Psi(r, R)$ may be decomposed as,

$$\Psi(r, R) = \phi_r(r, R)\cdot\phi_R(R) , \quad (2)$$

$$\left(-\frac{\hbar^2}{2m}\nabla_r^2 - \frac{e^2}{|\vec{R}-\vec{r}|} + e\vec{F}(r)\cdot\vec{r} - e\vec{F}(R)\cdot\vec{R}\right)\phi_r(r, R)$$

$$= U(R)\,\phi_r(r, R) \quad , \tag{3}$$

$$\left(-\frac{\hbar^2}{2M}\nabla_R^2 + U(R)\right)\phi_R(R) = E\,\phi_R(R) \quad . \tag{4}$$

Now, if F varies so slowly as F is constant in the range where $\phi_r(r, R)$ has remarkable magnitude,

$$(e\vec{F}(r)\cdot\vec{r} - e\vec{F}(R)\cdot\vec{R})\,\phi_r(r, R) \approx e\vec{F}(R)\cdot(\vec{r}-\vec{R})\,\phi_r(r, R). \tag{5}$$

Then, U(R) is calculated by the perturbation theory as

$$U(R) = W - \frac{1}{2}\alpha F(R)^2 \quad , \tag{6}$$

$$\left(-\frac{\hbar^2}{2m}\nabla_r^2 - \frac{e^2}{|\vec{R}-\vec{r}|}\right)\phi_r(r, R) = W\,\phi_r(r, R) \quad , \tag{7}$$

where α is the polarizability of an atom.

So, the motion of the ion core is described by the following equation.

$$\left(-\frac{\hbar^2}{2M}\nabla_R^2 + W - \frac{1}{2}\alpha F(R)^2\right)\phi_R(R) = E\,\phi_R(R) \quad . \tag{8}$$

This shows that the polarization energy of an atom acts as the potential energy of the atom.

However, we must remember, following Slater[1], that U(R) is really not just a potential energy but it also includes the kinetic energy of the electronic motion.

APPENDIX 2

DERIVATION OF THE TRANSITION MATRIX ELEMENT BETWEEN SLATER DETERMINANTAL STATES

Consider first the one body matrix elements $\widetilde{V}_{KHe}$ in eq.(3-17).

$$\widetilde{V}_{KHe} = \int \left\{ \phi_K(r) - \sum_{A'} \phi_{A'}(r) \langle A' | K \rangle - \phi_{He} \langle He | K \rangle \right\}^* \cdot$$

$$\left\{ \frac{p^2}{2m} + V_m(r) + V_{He}(r) + V_A(r) + eFz \right\} \cdot$$

$$\left\{ \phi_{He}(r) - \sum_{A'} \phi_{A'} \langle A' | He \rangle \right\} d\tau$$

$$= \langle K | \frac{p^2}{2m} + V_{He} | He \rangle + \langle K | eFz + V_A + V_m | He \rangle$$

$$- \sum_{A'} \langle K | \frac{p^2}{2m} + V_A | A' \rangle \langle A' | He \rangle$$

$$- \sum_{A'} \langle K | eFz + V_{He} + V_m | A' \rangle \langle A' | He \rangle$$

$$- \sum_{A'} \langle A' | \frac{p^2}{2m} + V_{He} | He \rangle \langle K | A' \rangle$$

$$- \sum_{A'} \langle A' | eFz + V_A + V_m | He \rangle \langle K | A' \rangle$$

$$- \langle He | \frac{p^2}{2m} + V_{He} | He \rangle \langle K | He \rangle$$

$$- \langle He | eFz + V_m + V_A | He \rangle \langle K | He \rangle$$

$$+ \sum_{A'A''} \langle A' | \frac{p^2}{2m} + V_A | A'' \rangle \langle A'' | He \rangle \langle K | A' \rangle$$

$$+ \sum_{A'A''} \langle A' | eFz + V_{He} + V_m | A'' \rangle \langle A'' | He \rangle \langle K | A' \rangle . \quad (1)$$

By introducing the two body matrix elements, some terms of eq.(1) cancel each other and such interaction potential as V_A are canceled.

Now consider $\widetilde{V}_{HeKHeHe}$.

$$\tilde{V}_{HeKHeHe} = V_{HeKHeHe} - V_{HeHeHeHe}\langle K \mid He\rangle$$

$$- \sum_{A'} V_{HeA'HeHe}\langle K|A'\rangle - \sum_{A'} V_{HeKA'He}\langle A'|He\rangle$$

$$+ \sum_{A'A''} V_{HeA'A''He}\langle K|A'\rangle\langle A''|He\rangle \quad . \qquad (2)$$

The first term of eq. (2) and the first term of eq. (1) together become the one matrix element of the Hartree-Fock Hamiltonian between ϕ_K and ϕ_{He} as

$$\langle K \left| \frac{p^2}{2m} + \frac{-2e^2}{|r - R_{He}|} \right| He\rangle + V_{HeKHeHe}$$

$$= \int \phi_K^* \left(\frac{p^2}{2m} + V_{HF,He} \right) \phi_{He}\, d\tau = E_{He}\langle K \mid He\rangle \quad , \qquad (3)$$

where

$$V_{HF,He} = \frac{-2e^2}{|r - R_{He}|} + \int \frac{\phi_{He}^*(r')\, e^2\, \phi_{He}(r')}{|r - r'|}\, d\tau' \quad . \qquad (4)$$

In the same manner, all the other V_{He} in eq.(1) may be rewritten as $V_{HF,He}$ together with the remaining four terms of eq. (2). Consequently, the first term and the 7th term in eq. (1) cancel each other.

Next consider $\sum_A \left(\sum_\sigma \tilde{V}_{A\sigma KHeA\sigma} - \tilde{V}_{AKAHe} \right)$.

$$\sum_A \left(\sum_\sigma \tilde{V}_{A\sigma KHeA\sigma} - \tilde{V}_{AKAHe} \right) = \sum_A \Big\{ 2\, V_{AKHeA} - V_{AKAHe} - \sum_{A'} \langle A'|He\rangle \cdot$$

$$(2\, V_{AKA'A} - V_{AKAA'}) - \sum_{A'} \langle K \mid A'\rangle\, 2\, V_{AA'HeA}$$

$$+ \sum_{A'} \langle K \mid A'\rangle V_{AA'AHe} - 2\langle K \mid He\rangle V_{AHeHeA} + \langle K|He\rangle V_{AHeAHe}$$

$$+ \sum_{A'A''} \langle A'|He\rangle \langle K \mid A''\rangle (2\, V_{AA''A'A} - V_{AA''AA'}) \Big\} \quad . \qquad (5)$$

The first term in eq. (5) and the term $\langle K|V_A|He\rangle$ which appears in the second term of eq. (1) cancel each other.

$$\sum_A 2\, V_{AKHeA} + \langle K|V_A|He\rangle$$

$$= \int \phi_K^*(r) \left\{ \sum_A \int \frac{2e^2}{|r-r'|} \phi_A^*(r')\, \phi_A(r')\, d\tau' \right\} \phi_{He}(r)\, d\tau$$

$$- \int \phi_K^*(r) \frac{z_A e^2}{|r-R_A|} \phi_{He}(r)\, d\tau \approx 0 \quad . \qquad (6)$$

In the same manner, by the 4th and the 6th term of eq. (5), the interaction V_A which appear in the 6th and 8th term in eq. (1) will vanish.

Now, the 3rd and the last term in eq. (5) are used to rewrite V_A in the 3rd and the 9th term of eq. (1) to $V_{HF,A}$ in the same manner as $V_{HF,He}$, and in consequence these two terms in eq. (1) cancel each other.

For example the 3rd term of eq. (5) and the 3rd term of eq. (1) together become

$$- \sum_{A'} \langle A'|He\rangle \int \phi_K^*(r) \left\{ \frac{p^2}{2m} + V_A(r) + 2 \sum_A \int \frac{\phi_A^*(r')\, e^2\, \phi_A(r')}{|r-r'|} d\tau' \right.$$

$$\left. - \sum_A \int d\tau' \frac{\phi_A^*(r')\, \phi_{A'}(r')\, e^2\, \phi_A(r)}{|r-r'|\, \phi_{A'}(r)} \right\} \phi_{A'}(r)\, d\tau$$

$$= - \sum_{A'} \langle A'|He\rangle \left\langle K \left| \frac{p^2}{2m} + V_{HF,A'} \right| A' \right\rangle$$

$$= - \sum_{A'} \langle A'|He\rangle \langle K|A'\rangle E_{A'} \qquad (7)$$

Finally, the role of the remaining terms of eq. (3-17) $\sum_{K'\sigma} \widetilde{V}_{KK'\sigma\, K'\sigma\, He} - \sum_{K'} V_{K'KK'He}$ may be to rewrite $eFz + V_m(r)$ in eq. (1) to $eFz\,\Theta(z) + U(r)$ where $U(r)$ is the Hartree-Fock potential of the metal defined below.

For example,

$$\langle K \mid U(r) \mid He \rangle$$

$$= \int \phi_K^*(r) \left\{ V_m(r) + \sum_{K'\sigma} \int \frac{\phi_{K'}^*(r')\, e^2 \phi_{K'}(r')}{|r - r'|} d\tau' \right.$$

$$\left. - \sum_{K'} \int \frac{\phi_{K'}^*(r')\, e^2\, \phi_{He}(r')\, \phi_{K'}(r)}{|r - r'|\, \phi_{He}(r)} d\tau' \right\} \phi_{He}(r)\, d\tau. \tag{8}$$

Finally one obtains the transition matrix elements M as eq. (3-19).

APPENDIX 3

THE COLLISION MATRIX

The scattering of a gas atom from a solid surface is called thermal scattering when the kinetic energy of the gas atom is a few tenths of an eV [2] and this is the case in the usual condition of FIM. This scattering is well explained by the simple classical model which assume the solid atom as a cube and so the velocity component parallel to the surface is conserved [3]. We base the collision matrix on this model.

The relation of the normal velocity components of the gas atom before and after the collision may be obtained from the velocity distribution of the free metal particles, assuming conservation of energy and momentum [4].

$$b(v_n' , v_t' , v_n , v_t)$$

$$= C\, \delta(v_t' - v_t)(v_n + v_n') \exp(-M((1 + \mu)v_n - (1 - \mu)v_n')^2/8kT_S), \tag{1}$$

where $\mu = m/M$ and C is the normalization constant determined by the following normalization condition.

$$\int_{-\infty}^{\infty} dv_t' \int_{-\infty}^{0} dv_n' \, b(v_n, v_t, v_n', v_t') = 1 \quad . \tag{2}$$

When gas atom is considered to collide with the metal atom of effective collision speed as Logan and Stickney[3] supposed, the collision matrix is given as,

$$b_{LS}(v_n', v_t', v_n, v_t)$$

$$= C_{LS} \, \delta(v_t' - v_t)(2\mu v_n / ((1+\mu)v_n' - (1-\mu)v_n))^{1/2} \cdot$$

$$\exp(-Mv_n((1+\mu)v_n' - (1-\mu)v_n)/4kT_S\mu) \, . \tag{3}$$

Both collision matrixs gives the average $v_n'_{av}$ as

$$v_n'_{av} = v(1-\mu)/(1+\mu) + 2kT_S\mu/(Mv_n(1+\mu)) \, . \tag{4}$$

Logan and Stickney called the collision characterized by (4) as representative collision. As $b_{LS}(v_n', v_t', v_n, v_t)$ shows very sharp peak at $v_n' = v_n'_{av}$, the results by using this matrix is almost equal to that based on the representative collision. The average accomodation coefficient obtained from eq. (4) resembles that of two dimensional classical hard sphere collision. In this connection, the classical hard sphere value of accomodation $4\mu(1+\mu)^{-2}$ is 0.083 in the case of a helium atom on tungsten.

We followed Van Eekelen (appendix 2 of the reference 4) to obtain the collision matrix that is used in the matrix equation in Chapter 5.

APPENDIX 4

Values of k_e, k_i, and N_t for helium with a tungsten tip.

F(V/A)	T_g(°K) \ T_s(°K)	20			80			300		
	20	76 -6	24 -7	58 +1*	55 -2	29 -7	82 +4	52 -1	26 -7	82 +3
2.0	80	17 -4	60 -7	40 +6	10 -1	49 -7	68 +3	67 -1	40 -7	11 +3
	300	16 -2	40 -7	48 +3	37 -1	41 -7	21 +2	14	39 -7	60 +4
	20	48 -6	19 -4	64 +7	88 -3	18 -4	70 +5	29 -1	12 -4	20 +4
2.5	80	26 -6	10 -4	19 +7	21 -2	12 -4	50 +4	37 -1	10 -4	30 +3
	300	11 -4	19 -4	63 +5	87 -2	17 -4	15 +3	62 -1	15 -4	23 +2
	20	72 -5	55 -3	29 +6	18 -3	72 -3	15 +6	15 -1	51 -3	47 +4
3.0	80	47 -5	40 -3	68 +5	34 -3	60 -3	22 +5	20 -1	48 -3	72 +3
	300	84 -5	51 -3	78 +4	18 -2	65 -3	98 +3	33 -1	55 -3	65 +2
	20	29 -4	43 -2	49 +5	68 -3	80 -2	22 +5	94 -2	66 -2	72 +4
3.5	80	42 -4	68 -2	52 +4	79 -3	96 -2	33 +4	12 -1	75 -2	12 +4
	300	49 -4	65 -1	86 +3	10 -2	93 -2	51 +3	19 -1	78 -2	13 +3
	20	15 -3	44 -1	59 +4	25 -2	45 -1	49 +4	14 -1	43 -1	31 +4
4.0	80	11 -3	35 -1	13 +4	22 -2	43 -1	94 +3	14 -1	41 -1	65 +3
	300	20 -3	50 -1	15 +3	28 -2	53 -1	13 +3	18 -1	50 -1	90 +2
	20	20 -3	12	25 +4	43 -2	12	22 +4	22 -1	12	15 +4
4.5	80	21 -3	13	40 +3	44 -2	13	38 +3	23 -1	13	30 +3
	300	31 -3	15	58 +2	48 -2	15	55 +2	25 -1	16	45 +2
	20	23 -3	29	11 +4	68 -2	29	98 +4	32 -1	30	76 +3
5.0	80	26 -3	31	18 +3	69 -2	31	17 +3	29 -1	32	15 +3
	300	38 -3	35	26 +2	73 -2	35	25 +2	32 -1	36	24 +2

* The values of k_e, k_i and N_t are arranged in order. For example, 76 -6 means 0.76×10^{-6}. N_t is in the units of $PV/\sqrt{2\pi m}$.

Acknowledgement

The author wishes to express his sincerest thanks and appreciation to Professor Shogo Nakamura for his kind advices and encouragement throughout this investigation.

The author would like to thank Professor Teruo Hanawa for his helps and fruitful advices to the present work.

The author wants to express his thanks to Professor Junkichi Nakai and Professor Katsumi Ura for their helps and suggestions during its completion.

Sincere thanks are also due to the members of the laboratory, in particular Mr. Toshiyuki Adachi and Mr. Satoshi Nishigaki for their interest and many discussions through this work. The same thanks are also extended to Miss Katsuko Yuzuriha for her help in preparing the manuscript.

The author's gratitude goes to Mrs. Fumiko Iwasaki for her sacrifice and patience throughout the course of this study.

Numerical computations were done at the Osaka University Computation Center.

REFERENCES

Chapter 1

1. E. W. Müller, Advances in Electronics and Electron Physics, 13, (1960) 83.
2. E. W. Müller and T. T. Tsong, Field-Ion Microscopy, Principles and Applications, Elsevier Publishing Co., New York, London, Amsterdam, 1969.
3. K. M. Bowkett and D. A. Smith, Field-Ion Microscopy, North-Holland Publishing Co., Amsterdam-London, 1970.
4. E. W. Müller, Quart. Rev. (London) 23, (1969) 177.
5. T. T. Tsong and E. W. Müller, Phys. Rev. Lett., 25, (1970) 911.
6. D. S. Boudreaux and P. H. Cutler, Phys. Rev., 149, (1966) 170.
7. S. P. Sharma, S. J. Fonash and G. L. Schrenk, Surface Sci., 23, (1970) 30.
8. C. B. Duke, Tunneling in Solids, Academic Press, New York, 1969.
9. P. H. Cutler and J. C. Davis, Surface Sci., 1, (1964) 194.
10. D. S. Boudreaux and P. H. Cutler, Surface Sci., 5, (1966) 230.
11. B. A. Lippman, Phys. Rev., 102, (1956) 264. See also M. H. Mittleman, Phys. Rev. 122, (1961) 1930.
12. E. W. Müller and T. T. Tsong, Field Ion Microscopy, Field Ionization and Field Evaporation, Pergamon Press, New York, 1974.
13. J. R. Oppenheimer, Phys. Rev., 31, (1928) 67.
14. T. E. Feuchtwang, Phys. Rev., B 10, (1974) 4121.
15. E. C. Kemble, The Fundamental Principles of Quantum Mechanics, McGraw-Hill Book Co., New York, 1937.

16. A. Messiah, Quantum Mechanics, North-Holland Publishing Co., Amsterdam, 1961.

17. E. W. Müller, Z. Physik 131, (1951) 136.

18. M. G. Inghram and R. J. Gomer, J. Chem. Phys., 22, (1954) 1279.

19. E. W. Müller and K. Bahadur, Phys. Rev., 102, (1956) 624.

20. T. T. Tsong and E. W. Müller, J. Chem. Phys., 41, (1964) 3279.

21. D. S. Boudreaux, Ph. D. Thesis, The Pennsylvania State University (unpublished).

22. S. J. Fonash and G. L. Schrenk, Phys. Rev., 180, (1969) 649.

23. S. P. Sharma and G. L. Schrenk, Phys. Rev., B 2, (1970) 598.

24. Z. Knor and E. W. Müller, Surface Sci., 10, (1968) 21.

25. T. Utsumi, 20th F. E. Symposium, University Park, Pa. August (1973).

26. E. W. Müller and T. Sakurai, 20th F. E. Symposium, University Park, Pa. August (1973).

27. W. Schmidt, T. H. Reisner and E. Krauts, Surface Sci., 26, (1971) 297.

28. K. D. Rendulic, Surface Sci., 28, (1971) 285, 34, (1973) 581.

29. S. B. McLane, E. W. Müller and S. V. Krishnaswamy, Surface Sci., 27, (1971) 367.

30. A. P. Janssen and J. P. Jones, Surface Sci., 33, (1972) 554.

31. M. E. Alferieff and C. B. Duke, J. Chem. Phys., 46, (1967) 938.

32. C. B. Duke and M. E. Alferieff, J. Chem. Phys., 46, (1967) 923.

33. A. J. Jason, R. D. Burns and M. G. Inghram, J. Chem. Phys., 47, (1965) 3742.

34. T. T. Tsong, Surface Sci., 28, (1972) 651.

35. D. A. Nolan and R. M. Herman, Phys. Rev., B 8, (1973) 4099.

36. J. C. Slater, Quantum Theory of Atomic Structure, McGraw-Hill, New York, 1960.

37. D. A. Nolan and R. M. Herman, Phys. Rev., B 10, (1974) 50.

38. M. J. Southon, Ph. D. Thesis, University of Cambridge (unpublished), 1963.

39. R. H. Good and E. W. Müller, in "Handbuch der Physik", Springer, Berlin, 21, (1956) 176.

40. H. A. M. Van Eekelen, Surface Sci., 21, (1970) 21.

41. E. W. Müller, J. Appl. Phys., 28, (1957) 1.

42. R. Gomer, Field Emission and Field Ionization, Harvard University Press, Cambridge, Mass., 1960.

Chapter 2

1. T. Sakurai, 1974, Ph. D. Thesis, The Pennsylvania State University (unpublished).

2. H. Iwasaki and S. Nakamura, Surface Sci., 43, (1974) 301.

3. J. R. Oppenheimer, Phys. Rev., 31, (1928) 67.

4. A. Messiah, Quantum Mechanics, North-Holland Publishing Co., Amsterdam, 1961.

5. D. S. Boudreaux and P. H. Cutler, Surface Sci., 5, (1966) 230.

6. D. S. Boudreaux and P. H. Cutler, Phys. Rev., 149, (1966) 170.

7. J. W. Gadzuk, Surface Sci., 6, (1966) 159.

8. H. Iwasaki and S. Nakamura, Surface Sci., 33, (1972) 525.

9. Z. Knor and E. W. Müller, Surface Sci., 10, (1968) 21.

10. T. T. Tsong and E. W. Müller, J. Chem. Phys., 41, (1964) 3279.

11. S. P. Sharma and G. L. Schrenk, Phys. Rev., B 2, (1970) 598.
12. J. W. Gadzuk, Phys. Rev., 182, (1969) 416.
13. L. P. Bouckaert, R. Smoluchowski and E. P. Wigner, Phys. Rev., 50, (1936) 58.
14. J. C. Slater, Phys. Rev., 36, (1930) 57.
15. J. Kudo, S. Nakamura and T. Kuroda, Japan. J. Appl. Phys., (1974) (to be published).
16. L. F. Mattheiss, Phys. Rev., 139, (1965) 236.
17. T. Utsumi, 20th F. E. Symposium, University Park, Pa. August (1973), private communication.
18. E. W. Müller and T. Sakurai, 20th F. E. Symposium, University Park, Pa. August (1973).

Chapter 3(section 3.1 is to be pubulished in Surface Sci.)

1. E. W. Müller and T. T. Tsong, Field-Ion Microscopy, Principles and Applications, Elsevier Publishing Co., New York, London, 1969.
2. C. B. Duke and M. E. Alferieff, J. Chem. Phys., 46, (1967) 923.
3. M. E. Alferieff and C. B. Duke, J. Chem. Phys., 46, (1967) 938.
4. A. J. Jason, R. D. Burns and M. G. Inghram, J. Chem. Phys., 47, (1967) 3742.
5. A. Messiah, Quantum Mechanics, North-Holland Publishing Co., Amsterdam, 1961.
6. T. Sakurai, T. T. Tsong and E. W. Müller, Phys. Rev., B 10, (1974) 4205.
7. T. T. Tsong, Surface Sci., 28, (1972) 651.
8. H. Iwasaki and S. Nakamura, Japan. J. Appl. Phys. Suppl.2, Pt.2, (1974) 43.

9. D. A. Nolan and R. M. Herman, Phys. Rev., B 10, (1974) 50.
10. S. B. McLane, E. W. Müller and S. V. Krishnaswamy, Surface Sci., 27, (1971) 367.
11. T. T. Tsong and E. W. Müller, Phys. Rev. Lett., 25, (1970) 911.
12. T. T. Tsong and E. W. Müller, J. Chem. Phys., 55, (1971) 2884.
13. E. W. Müller, Quart. Rev. (London) 23, (1969) 177.
14. W. Schmidt, Th. Reisner and E. Krauts, Surface Sci., 26, (1971) 297.
15. K. D. Rendulic, Surface Sci., 28, (1971) 285, Surface Sci., 34, (1973) 581.
16. A. P. Janssen and J. P. Jones, Surface Sci., 33, (1972) 554.
17. D. A. Nolan and R. M. Herman, Phys. Rev., B 8, (1973) 4099.
18. T. B. Grimley, J. Phys., C 3, (1970) 1934.

Chapter 4 (submitted to Surface Sci.)

1. E. W. Müller, Advances in Electronics and Electron Physics, 13, (1960) 83.
2. R. Gomer, Field Emission and Field Ionization, Harvard University Press, Cambridge, Mass., 1960.
3. M. J. Southon, Ph. D. Thesis, University of Cambridge (unpublished) 1963.
4. H. Iwasaki and S. Nakamura,submitted to Surface Sci..
5. H. A. M. Van Eekelen, Surface Sci., 21, (1970) 21.
6. R. M. Logan and R. E. Stickney, J. Chem. Phys., 44, (1966) 195.
7. T. T. Tsong and E. W. Müller, J. Appl. Phys., 37, (1966) 3065.

8. E. W. Müller, S. Nakamura, O. Nishikawa and S. B. McLane, J. Appl. Phys., 36, (1965) 2496.
9. F. O. Goodman, Surface Sci., 26, (1971) 364.

Chapter 5 (submitted to Surface Sci.)

1. E. W. Müller and K. Bahadur, Phys. Rev., 102, (1956) 624.
2. K. Bahadur, J. Sci. Ind. Res. (India) 19 b, (1960) 177.
3. M. J. Southon and D. G. Brandon, Phil. Mag., 8, (1963) 579.
4. U. Feldman and R. Gomer, J. Appl. Phys., 37, (1966) 2380.
5. T. T. Tsong and E. W. Müller, J. Appl. Phys., 37, (1966) 3065.
6. E. W. Müller, Quart. Rev. (London) 23, (1969) 177, Naturwis., 57, (1970) 222.
7. S. B. McLane, E. W. Müller and S. V. Krishnaswamy, Surface Sci., 27, (1971) 367.
8. E. W. Müller and T. T. Tsong, Field Ion Microscopy, Field Ionization and Field Evaporation (Pergamon Press, 1973).
9. H. Iwasaki and S. Nakamura, Surface Sci., preceding paper.
10. H. A. M. Van Eekelen, Surface Sci., 21, (1970) 21.
11. R. Gomer, Field Emission and Field Ionization (Harvard University Press, 1961).
12. M. J. Southon, Ph. D. Thesis, University of Cambridge (unpublished) 1963.
13. R. M. Logan and R. E. Stickney, J. Chem. Phys., 44, (1966) 195.
14. Y. C. Chen and D. N. Seidman, Surface Sci., 27, (1971) 231.
15. T. T. Tsong and E. W. Müller, J. Chem. Phys., 55, (1971) 2284.

16. D. A. Nolan and R. M. Herman, Phys. Rev., B 8, (1973) 4099, Phys. Rev., B 10, (1974) 50.

17. H. Iwasaki and S. Nakamura, Japan. J. Appl. Phys. Suppl.2, Pt.2, (1974) 43, Surface Sci. to be published.

18. T. Adachi and K. Ohnishi and S. Nakamura, Japan. J. Appl. Phys., 13, (1974) 549.

Appendixes

1. J. C. Slater, Quantum Theory of Molecules and Solids, Vol. 1, McGraw-Hill Book Co., New York, (1963).

2. F. O. Goodman, Surface Sci., 26, (1971) 364.

3. R. M. Logan and R. E. Stickney, J. Chem, Phys., 44, (1966) 195.

4. H. A. M. Van Eekelen, Surface Sci., 21, (1970) 21.

LIST OF PUBLICATIONS

1. H. Iwasaki and S. Nakamura, "Field Ionization Process in tne Field Ion Microscope," Surface Sci. 33, (1972) 525.

2. H. Iwasaki and S. Nakamura, "Ionization Probability Calculations in the Field Ion Microscope," Surface Sci. 43, (1974) 301.

3. H. Iwasaki and S. Nakamura, "Field Adsorption Effects in the Field Ionization Probability in the Field Ion Microscope," Japan. J. Appl. Phys. Suppl.2, Pt. 2, (1974) 43.

4. H. Iwasaki and S. Nakamura, "A Model Calculation of Field Ionization through Adsorbed Atoms in FIM," to be published in Surface Sci.

5. H. Iwasaki and S. Nakamura, "Ion Current Generation in the Field Ion Microscope; I Dynamic Approach," submitted to Surface Sci.

6. H. Iwasaki and S. Nakamura, "Ion Current Generation in the Field Ion Microscope: II Quasi-Static Approach," submitted to Surface Sci.